UNIVERSITÀ
DI PAVIA

PhD IN BIOMEDICAL SCIENCES

DEPARTMENT OF BIOLOGY AND BIOTECHNOLOGY

"LAZZARO SPALLANZANI"

Unveiling Ca^{2+} dynamics into a model of human cerebrovascular endothelial cell line: implications for neurovascular coupling

PhD Supervisors:

Prof. Francesco Moccia

Prof. Gerardo Rosario Biella

PhD Co-supervisors:

Dr. Giorgia Scarpellino

Prof. Egidio D'Angelo

PhD dissertation of

Valentina Brunetti

a.y. 2024/2025

INTRODUCTION 5
CHAPTER 1: NEUROVASCULAR UNIT 5
1.1 Concept of neurovascular unit 5
1.2 Cerebrovascular tree 5
1.3 Characteristics and functions of the Blood - Brain Barrier 6
1.3.1 The Human Cerebrovascular Endothelial Cell Line: hCMEC/D3 9
1.4 The role of microvascular endothelium in cerebral blood flow regulation 10
CHAPTER 2: Neurovascular coupling 13
2.1 Concept of Neurovascular Coupling 13
2.2 Molecular mechanism of neurovascular coupling 14
2.2.1 Neuronal and astrocytic signaling pathways 14
2.2.2 Endothelial signaling pathways 17
CHAPTER 3: Ca^{2+} signals in neurovascular coupling 19
3.1 Endothelial Ca^{2+} Signaling: From Local to Global Ca^{2+} Signals 19
3.2 Exploring the endothelial Ca^{2+} toolkit: the Ca^{2+} response to G_qPCRs 20
3.3 Exploring the endothelial Ca^{2+} toolkit: Ca^{2+} clearing mechanisms and the dual role of NCX 23
3.3.1 Na^{+}/Ca^{2+} exchanger (NCX) 23
3.3.2. Structure of NCX 24
3.3.3 Regulation of NCX 24
3.3.4 Role of NCX in endothelial cells 25
3.4 Endo-lysosomal Ca^{2+} signals in vascular endothelium 26
3.5 TRP channels 27
3.5.1 TRP taxonomy and functions 27
3.5.2 TRP channels in brain endothelial cells: TRPV4, TRPV3, and TRPA1 30
3.5.3 Transient Receptor Potential Mucolipin 1 (TRPML1) 31
3.5.3.1 TRPML1 structure 31
3.5.3.2 TRPML1 biophysical properties and gating mechanism 32
3.6 Regulation and role of the resting membrane potential in vascular endothelial cells 33
CHAPTER 4: A new milestone on current knowledge about intracellular Ca^{2+} signaling in cerebrovascular ECs: Ca^{2+} signals in hCMEC/D3 cells 34
4.1 Intracellular Ca^{2+} Signals Induce Acetylcholine-Dependent NO Production in hCMEC/D3 cells 34
4.2 NMDA Receptors in hCMEC/D3 cells: NO Release and Hemodynamic Response 35
4.3 GABA receptors induce Ca^{2+} signals and NO production in hCMEC/D3 cells 37
4.4 Purinergic receptors modulate ATP response in hCMEC/D3 cells 39

4.5 Histamine 1 Receptor induces intracellular Ca^{2+} oscillations and NO release in hCMEC/D3 cells 39
CHAPTER 5: AIMS OF THE THESIS 41
CHAPTER 6: METHODS 42
6.1 Cell culture 42
6.2 Solutions 42
6.3 Automated patch-clamp electrophysiology 43
6.4 Ca^{2+} imaging and NO imaging 43
6.5 Gene silencing 44
6.6 Western Blotting 45
6.7 Immunofluorescence 46
6.8 Statistical analysis 47
6.9 Chemicals 47
CHAPTER 7: RESULTS 48
PART 1: Evaluation of biophysical properties of the membrane 48
7.1 Measurement of the resting V_M of hCMEC/D3 cells by using the APC technology 48
7.2 Measurement of the resting membrane currents in hCMEC/D3 cells 49
PART 2: Evaluation of global Ca^{2+} dynamics in hCMEC/D3 cells: effects of extracellular Na^+ on NCX/H1R signaling pathway 50
7.3 Extracellular Na^+ reduction induces intracellular Ca^{2+} signals in hCMEC/D3 cells 50
7.4 Extracellular Ca^{2+} entry is necessary to trigger $0Na^+_o$-induced Ca^{2+} oscillations in hCMEC/D3 cells 53
7.5 $0Na^+_o$ –induced Ca^{2+} oscillations are triggered and sustained by $InsP_3$-dependent intracellular Ca^{2+} release in hCMEC/D3 cells. 54
7.6 SOCE sustains $0Na^+_o$-induced Ca^{2+} oscillations in hCMEC/D3 cells 57
7.7 $0Na^+_o$–induced Ca^{2+} oscillations are triggered by H1R in hCMEC/D3 cells 57
7.8 $0Na^+_o$–induced Ca^{2+} oscillations lead to NO release 59
PART 3: Evaluation of global Ca^{2+} dynamics in hCMEC/D3 cells: TRPML1 60
7. 9 Lysosomal TRPML1 contribution to global Ca^{2+} signaling in hCMEC/D3 cells 60
7.10 TRPML1-mediated global Ca^{2+} signals are sustained by lysosomal Ca^{2+} release and extracellular Ca^{2+} entry 62
7.11 ER Ca^{2+} release through $InsP_3Rs$ and SOCE contribute to TRPML1-mediated global Ca^{2+} signals in hCMEC/D3 cells 64
7.12 TRPML1 regulates ER Ca^{2+} load in hCMEC/D3 cells 66
7.13 TRPML1 mediates $PI(3,5)P_2$-evoked Ca^{2+} signals in hCMEC/D3 cells 67
7.14 TRPML1-mediated global Ca^{2+} signals lead to NO release in hCMEC/D3 cells 68
7.15 TRPML1 supports ATP-induced Ca^{2+} signaling and NO release in hCMEC/D3 cells 69
CHAPTER 8: DISCUSSION 71

PART 1: Evaluation of the biophysical properties of hCMEC/D3 cells 71
PART 2: Evaluation of global Ca^{2+} dynamics in hCMEC/D3 cells: NCX1 AND HR1 73
PART 3: Evaluation of global Ca^{2+} dynamics in hCMEC/D3 cells: TRPML1 79
CHAPTER 9: CONCLUSIONS 83
CHAPTER 10: BIBLIOGRAPHY 84

INTRODUCTION

CHAPTER 1: NEUROVASCULAR UNIT

1.1 Concept of neurovascular unit

The concept of neurovascular unit (NVU) was formally introduced and embraced by the scientific community at the first Stroke Progress Group meeting of the National Institute of Neurological Disorders and Stroke of the NIH in 2001. In the last years, the interest on neurovascular unit has grown because of its implications in healthy brain function, but also in presence of brain diseases, in particular neurodegenerative and aging conditions. This concept empathizes the close relationship between brain cells and vessels (Iadecola, 2017). The interest has come from a greater understanding of signaling at the microcirculation level, composed of endothelial cells (ECs), mural cells [comprising vascular smooth muscle cells (VSMCs) and pericytes (PCs)], and astrocytic end-feet. To better understand how all these components work together, it is mandatory to clarify how the brain vasculature works.

1.2 Cerebrovascular tree

Arising from the Circle of Willis, at the base of the brain, cerebral vessels form highly-interconnected network of pial arteries and arterioles which run on the brain surface (Iadecola, 2017; Schaeffer & Iadecola, 2021). Pial arteries are made of several layers of SMCs, which are separated from the endothelium by an elastic lamina (Roggendorf & Cervos-Navarro, 1977). The pial vessels are also densely innervated by nerve fibers originating from peripheral autonomic and sensory ganglia (Hamel, 2006; Iadecola, 2017).

Pial arteries dive into the brain substance, surrounded by the perivascular space, an extension of the subarachnoid space (Schaeffer & Iadecola, 2021). Penetrating arterioles, which are enriched with a thinner layer of SMCs, branch off pial arteries and enter the brain tissue, giving rise to parenchymal arterioles. At this level, the elastic lamina becomes less prominent, eventually becoming a single layer. The perivascular nerves are lacking and astrocytic end-feet encase arterioles (Iadecola, 2017). ECs extend protrusions through the basal lamina into SMCs (myoendothelial projections) enriched with gap junctions (Longden, Hill-Eubanks, & Nelson, 2016). In cerebral capillaries, SMCs are replaced by PCs, mural cells embedded into the endothelial basement membrane, covering approximately 30% of the vascular surface (Schaeffer & Iadecola, 2021). Capillaries exhibit a very wide and heterogeneous distribution, which depends on the brain's metabolic and energy demands. Capillaries are located at approximately 13 μm from neurons in order to support metabolic exchanges.

The arteriolar-capillary transitional zone (ACT) includes capillaries from the first to fourth order, originated from parenchymal arterioles. This zone is covered by PCs which begin at the end of the precapillary sphincter, which is a SMC ring located at the point where arterioles transition to capillaries (ACT) (Schaeffer & Iadecola, 2021). Both first order capillaries and pre-capillary sphincters play a role in the regulation of blood flow. They have been shown to dilate in response to somato-sensory stimulation, providing blood flow from parenchymal arterioles to capillary bed (Moccia, Negri, Faris, & Angelone, 2022) (**Figure 1**).

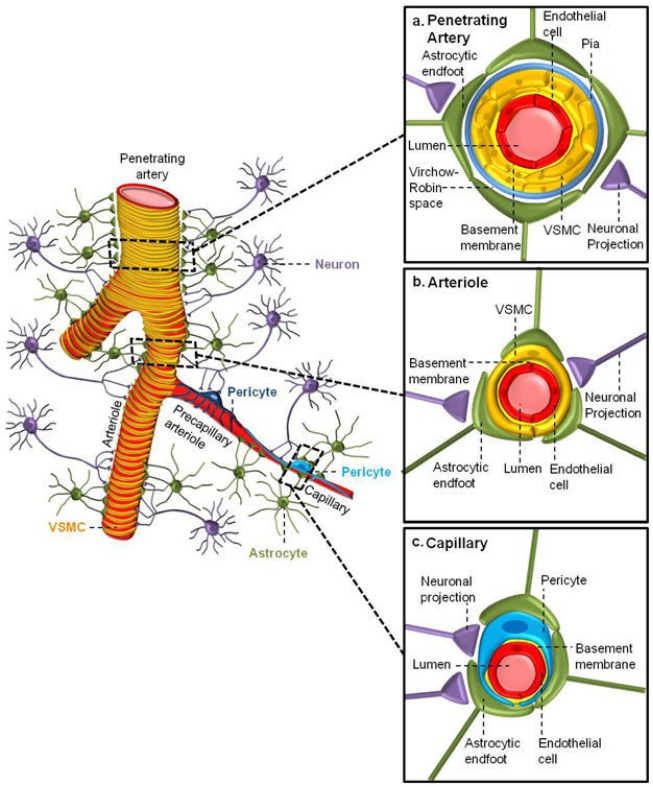

Figure 1. Schematic representation of the cerebral tree. Pial arteries run along the subarachnoid space and give rise to the intracerebral arteries that penetrate deep into the brain parenchyma. Along their path, they change their composition until they emerge as capillaries. The panels show the particular composition of intracerebral arteries and capillaries (Kisler, Nelson, Montagne, & Zlokovic, 2017).

1.3 Characteristics and functions of the Blood - Brain Barrier

The need for accurate and specific regulation of the environment and functions of the central nervous system (CNS) has led to the definition of a structure known as Blood - Brain Barrier (BBB) (Daneman & Prat, 2015). Its unique cellular characteristics describe the critical role that the BBB plays in regulating the homeostasis of the CNS, ensuring the proper performance of its functions and, at the same time, protecting it from the potential action of external agents that would compromise its integrity. As already explained in section 1.2, blood vessels are lined by cerebral ECs, which have unique properties that distinguish them from the ECs found in other tissues, and mural cells, which lay on the abluminal surface of the EC layer (Daneman & Prat, 2015) (**Figure 2**). ECs are derived from mesodermal embryos and form the inner walls of blood vessels. The ECs of cerebral capillaries

form a single layer of cells, which is very different from arteries and veins, where ECs form multiple layers. The specific characteristics of ECs, therefore, lead to the formation of continuous, non-fenestrated capillaries that perform the demanding tasks of maintaining ion balance and transporting nutrients (Daneman & Prat, 2015). As mentioned above, cerebral ECs differ from other types of ECs since they have tight junctions (TJ) and adherents' junctions (Keaney & Campbell, 2015). In addition, two types of transporters are expressed on their surface: efflux transporters, which transport hydrophilic molecules, and highly specific nutrient transporters. The BBB, therefore, only allows the passage of lipid-soluble molecules of approximately 180 Da. This highlights the need for transport mechanisms that allow the regulated passage of larger molecules, such as GLUT-1, which is essential for glucose transport; Mfsd2a, a brain-endothelium enriched receptor for the omega 3 fatty acid, docosahexaenoic acid; and transporters capable of regulating the entry and exit of harmful molecules, such as beta-amyloid peptide (β-amyloid or Aβ), the main molecule responsible for Alzheimer's disease (Keaney & Campbell, 2015). Another very important transporter is the sodium-dependent excitatory amino acid transporter 1 (EAAT1), which is essential for the removal of glutamate from the brain; maintaining glutamate clearance is in fact essential for protecting neurons from the excessive stimulation of glutamatergic receptors (Zlokovic, 2011). Additional characteristics that distinguish brain ECs are: the presence of a high number of mitochondria, which ensure continuous production of adenosine triphosphate (ATP) molecules in order to maintain the ion gradient necessary for all transport functions; the presence of a low level of leukocyte adhesion molecules, limiting the entrance of immune cells into the CNS (Daneman & Prat, 2015). The combination of all of the components cited above, allow the ECs to finely regulate the CNS homeostasis (Daneman & Prat, 2015). Given the cellular characteristics mentioned so far, any reduction or loss of each of these properties leads to an alteration in the established balance.

In fact, although the BBB is an extremely dynamic structure, capable of adapting to multiple physiological conditions, it has been shown that the loss of a single property can lead to the development of brain diseases such as Alzheimer's, stroke, and hypertension (Keaney & Campbell, 2015). Another fundamental component of the BBB is represented by mural cells. Mural cells include VSMCs and PCs. PCs sit on the surface of the microvascular ECs (Daneman & Prat, 2015) (**Figure 2**). Their long processes, which extend on the luminal surface of ECs, could often span multiple ECs bodies. The importance of PCs is due to their extension composition: they are made up with contractile proteins which have the ability to regulate the diameter of the capillaries.

Although PCs are sitting on the abluminal surface of the endothelium, most of them do not completely touch the ECs, because they are separated by a basement membrane (BM) they are embedded within (Daneman & Prat, 2015). As already known for CNS ECs, also CNS PCs are different from PCs in

other tissues. For example, they are derived from the neural crest and not from mesoderm like other PCs; in addition, CNS pericytes provide the highest degree of vascular coverage compared to other tissues. PCs play a key role in mediating angiogenesis, deposition of extracellular matrix, wound healing, infiltration of immune cells and also regulating the blood flow in response to neuronal activity (Daneman & Prat, 2015).

As stated above, PCs do not directly touch the ECs, but they face the BM. Around the vascular tube there are two BMs, an inner vascular BM and an outer parenchymal BM. The BM represents an extracellular matrix secreted by ECs and PCs and it is composed of different molecules. The importance of the BM is due to their role as an anchor for many signaling processes, and also because they provide an additional barrier for molecules and cells (Daneman & Prat, 2015).

Other important components of the BBB are astrocytes. Astrocytes are glial cell types, which extend polarized processes that enclose both neuronal processes and blood vessels. The end-feet process contains a lot of proteins including dystroglycan-dystrophin and aquaporin 4 (Daneman & Prat, 2015). Astrocytes are very important for the regulation of blood flow: they relay signals that regulate blood flow in response to neuronal activity. While PCs play a major role in BBB formation, astrocytes are not involved in BBB assembling, but they only regulate the structure once it is formed (Daneman & Prat, 2015).

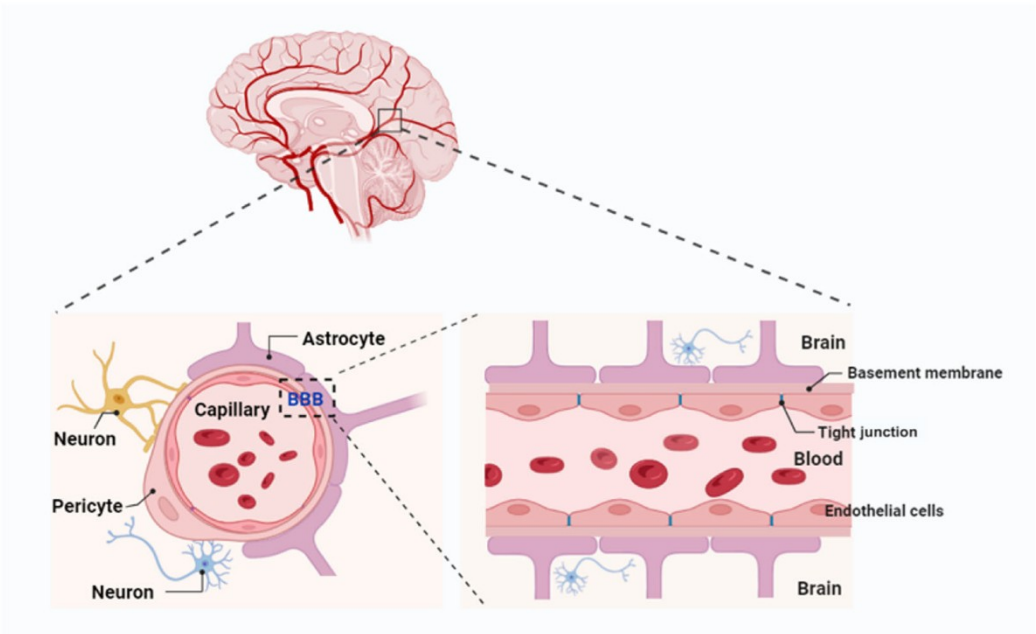

Figure 2. Composition of the BBB. BBB is composed of endothelial cells, which are connected through tight junctions, basal membrane, pericytes, which envelope the tube vessel and end-feet astrocytes (Ding, Kshirsagar, Agrawal, & Murry, 2025).

1.3.1 The Human Cerebrovascular Endothelial Cell Line: hCMEC/D3

The importance that the BBB has assumed in recent years has led to the development of several cell lines that can be used for its study and characterization. Many of these cell lines have been isolated from animals, as they are easier to obtain, such as bEND3 and bEND5. In contrast, obtaining freshly isolated human brain ECs or brain EC lines is much more difficult, as the amount of tissue available is limited. Although brain capillaries isolated from fresh human tissue represent a unique model of BBB, access to such tissue remains a major challenge (Hartz et al., 2018). Furthermore, several regulatory and safety considerations must be taken into account when working with human tissues, since they may pose serious risks, such as blood-borne pathogens and potential infection transmission. Another important aspect to be considered is the post-mortem interval (PMI) (Hartz et al., 2018); autopsies must be carried out within for 4 hours after patient's death, making strict control of the timing of the isolation procedure essential. A short PMI, ideally less than 4 hours, is crucial to ensure the availability and quality of capillaries after isolation. For all these reasons, in the last years, the induced pluripotent stem cell (iPSC) platform has opened new frontiers for scientific discovery and therapeutic development (Cerneckis, Cai, & Shi, 2024). iPSCs may represent a novel approach to study the human BBB and its endothelial component. These advanced models can be used to study drug toxicity, efficacy and pharmacokinetics, serving as an additional preclinical platform for drug screening. Importantly, iPSCs could therefore facilitate the study of human endothelium without the hurdles associated with isolating capillaries from fresh human brain samples (Cerneckis et al., 2024). Nevertheless, the robust generation of iPSC-derived human brain microvascular ECs continues to pose significant challenges and often exceeds the capacities of standard cellular physiology laboratories. A reliable alternative cellular model for studying the human BBB is represented by immortalized human ECs. One of the most widely employed models of the human BBB is the human cerebrovascular endothelial cell line, hCMEC/D3 cells (Helms et al., 2016). hCMEC/D3 cells were obtained from an hTERT/SV40-immortalized clone derived from vessels isolated from the temporal lobe and located within the healthy tissue excised during epilepsy surgery. In the first step after removal from the tissue, the cells were immortalized through transduction with a lentivirus vector containing a catalytic subunit of human telomerase (hTERT) and SV40 large T antigen. Following this, capillary ECs were isolated and the clones were characterized for human cerebral endothelium (Weksler, Romero, & Couraud, 2013). These cells, plated in culture on type I or type IV collagen, form a monolayer of cells, subject to contact inhibition. The cells express junction-associated IgG-like proteins such as PECAM-1 and JAM-A, TJs such as VE-adherin, claudin-3 and -5, and occludin, scaffold proteins such as beta-catenin and ZO-1 and -2, as well as the Par-3/Par-6/PKCz polarity complex. While most proteins present in intact vessels are expressed, certain proteins exhibit reduced

expression in the cell line (Helms et al., 2016; Weksler et al., 2013). For example, claudin-5 is expressed at lower levels than in naive cerebral microvessels. Therefore, this cellular model of the human BBB in its basic state acts as a barrier to large molecules, while it is relatively permeable to small solutes (Helms et al., 2016). hCMEC/D3 cells also express a high number of transporters, with approximately 44 transcripts detected. The main transporters include SLC2A1 (Glut-1), SLC7A5 (LAT-1), and SLC16 (MCT). Glut-1 appears to be expressed at levels comparable to those in intact vessels. Other transporters and receptors are expressed at very high levels, including MCT-1, the insulin receptor, and the transferrin receptor. Transcriptomic analysis has also identified 23 ABC efflux transporters, including P-gp, Mrp-4, and BCRP. Therefore, the hCMEC/D3 cell line represents a highly useful and accessible model, particularly suitable for studying drugs and brain responses to different stimuli (Helms et al., 2016; Kumabe et al., 2025)

1.4 The role of microvascular endothelium in cerebral blood flow regulation

Cerebrovascular tone is regulated by neuronal activity through the release of numerous vasoactive mediators that modulate the contractile activity of arteries/arterioles and capillaries. The main vasoactive mediator responsible for controlling cerebral blood flow (CBF) is the gasotransmitter nitric oxide (NO). The role played by astrocytes, PCs, and VSMCs in modulating CBF is well known; the situation is different for microvascular ECs, whose involvement in these mechanisms is not yet fully understood (Guerra et al., 2018; Moccia et al., 2022). Traditionally, it was believed that the vasorelaxant mediators responsible for the local increase in CBF were released exclusively by glutamatergic neurons and/or astrocytes located between active synapses and adjacent microvessels (Mapelli et al., 2017; Mishra et al., 2016). This model has been refuted by recent evidence showing that mouse cerebral ECs are able to sense neuronal activity and synaptic activation, initiating the hemodynamic response and propagating vasodilation to the vessels and surface of the upstream arterioles (Guerra et al., 2018; Hogan-Cann & Anderson, 2016; Longden et al., 2017). Unlike a few years ago, it is now clear that, as the first interface between blood and brain tissue, the endothelial monolayer maintains vascular tone and regulates CBF in response to increased neuronal activity (Longden et al., 2017; Longden & Nelson, 2015). The cerebral endothelium is capable of generating at least two powerful vasoactive mediators: NO and endothelium-dependent hyperpolarization (EDH) (Guerra et al., 2018). In the CNS, NO controls several key functions for cognitive processes, such as neurotransmission, synaptic plasticity, vascular tone regulation, gene transcription, and also produces post-translational modifications to proteins (Forstermann & Sessa, 2012). In mammals, NO can be generated by three different isoforms of the enzyme NO synthase (NOS): nNOS (neuronal), eNOS (endothelial), and iNOS (inducible). For all three isoforms, the canonical pathway for NO synthesis is via the oxidation of L-arginine with NO synthase oxidation (Forstermann & Sessa, 2012). NO

derived from nNOS is activated by the release of glutamate, which stimulates neuronal N-methyl-D-aspartate (NMDA) receptors, with subsequent entry of Ca^{2+} into the neuronal soma (Attwell et al., 2010). nNOS appears to be involved in functional hyperemia (Attwell et al., 2010). The activity of eNOS in the vascular endothelium is regulated by several mechanisms. For example, its enzymatic activity depends on the substrate L-arginine, the availability of various cofactors, including tetrahydrobiopterin (BH4), and it can be suppressed by endogenous inhibitors (Gaynullina, Tarasova, Shvetsova, Borzykh, & Schubert, 2022). A key mechanism of eNOS regulation is its dependence on intracellular Ca^{2+}, which can increase during neuronal activity. Further control over eNOS is exerted by transcriptional, post-transcriptional, post-translational, and post-translational modifications (Gaynullina et al., 2022). For example, eNOS can be phosphorylated at serine, threonine, and tyrosine residues, which, depending on whether the site is activating or inhibitory, modify eNOS activity (Gaynullina et al., 2022). The activity of eNOS in the endothelium can therefore be regulated by a balance between phosphorylation and dephosphorylation, under the activation of certain kinases, which mediate NO production as needed (Gaynullina et al., 2022). Furthermore, eNOS is able to interact with numerous proteins that modify its activity, such as caveolin-1, heat shock protein 90 (HSP90), endoglin, nitric oxide synthase trafficking (NOSTRIN), and nitric oxide synthase-interacting protein (NOSIP). The Ca^{2+}/calmodulin complex, which is essential for activating the enzyme following an increase in intracellular Ca^{2+} levels (Gaynullina et al., 2022). NO derived from ECs diffuses to VSMCs and induces relaxation via soluble guanylate cyclase, which acts as an NO acceptor and produces cyclic guanosine monophosphate (cGMP). The latter, in turn, activates protein kinase G (PKG), which phosphorylates the target serine and threonine residues in VSMCs, thereby modulating the ion signaling machinery driving VSMC contraction. For instance, PKG activates the high-conductance Ca^{2+}-activated K^+ channels (big conductance or BK_{Ca}), thereby promoting VSMC hyperpolarization (Gaynullina et al., 2022). The other main mediator of vasodilation generated by the cerebral endothelium is EDH. According to the canonical mechanism described in resistance microvessels, EDH is triggered by an increase in Ca^{2+} concentration ($[Ca^{2+}]_i$), which stimulates small- and intermediate-conductance Ca^{2+}-activated K^+ channels (respectively, SK_{Ca} and IK_{Ca} channels), which cause EC hyperpolarization. This hyperpolarization may propagate both to upstream ECs and to the overlying VSMCs, causing them to relax and consequently vasodilate, inhibiting voltage-dependent Ca^{2+} entry (Garland & Dora, 2017). This mechanism requires a tight regulation of both Ca^{2+}-permeable channels and Ca^{2+} signal decoders, such as SK_{Ca} and IK_{Ca}. To achieve this precise spatial arrangement, ECs form protrusions through the elastic lamina, which establish heterocellular coupling with adjacent VSMCs via myoendothelial junctions (Guerra et al., 2018). The endoplasmic reticulum (ER) also protrudes into the myoendothelial junctions, thus creating an intracellular Ca^{2+}

reservoir that is physically distant from the cytoplasmic cisternae, but sensitive to inositol-1,4,5-trisphosphate ($InsP_3$) and juxtaposed to IK_{Ca} channels, which are also located in endothelial protrusions (Garland & Dora, 2017). In contrast, SK_{Ca} channels are distributed along the entire plasma membrane of ECs. The main Ca^{2+} release channel of the ER consists of $InsP_3$ receptors ($InsP_3Rs$), which, in the ECs of resistance arterioles, generate repetitive and local Ca^{2+} release events, called Ca^{2+} pulsars, whose frequency can be increased by the action of extracellular vasoactive agonists, such as acetylcholine. In contrast, SK_{Ca} channels are distributed along the entire plasma membrane of ECs. K^+-dependent vasodilation can be increased by stimulation of endothelial inward rectifying K^+ (K_{IR}) channels or by activation of Na^+/K^+ ATPase on VSMCs (Guerra et al., 2018). In the cerebral microcirculation, endothelial SK_{Ca} and IK_{Ca} channels are mainly activated by Ca^{2+} influx mediated by Transient Receptor Potential (TRP) channels and are primarily located in intraparenchymal arterioles (Longden et al., 2017(Earley, 2011). Conversely, $K_{IR}2.1$ channels are the main mechanism responsible for EDH in response to neuronal activity at capillary level (Longden et al., 2017; Moccia et al., 2022). Mouse brain capillary ECs express $K_{IR}2.1$ channel, which can serve as "electrical amplifiers" that transform a local rise in external K^+ in a hyperpolarizing signal. The endothelial hyperpolarization is electrotonically conducted to the upstream ACT zone through inter-endothelial gap-junctions to induce pericyte relaxation and local vasodilation (Moccia et al., 2022). It should be noted that EDH does not cause vasodilation limited to the site of stimulation; it can propagate along the vascular endothelium until it reaches the main upstream arteries (more than 2 mm away). This phenomenon, called retrograde vasodilation, contributes to a reduction in vascular resistance and an increase in blood flow in activated areas of the brain (Guerra et al., 2018).

CHAPTER 2: Neurovascular coupling

2.1 Concept of Neurovascular Coupling

As already stated in paragraph 1.4, it is necessary to emphasize that the close connection between neuronal activity and CBF regulation reflects the brain's timely demand for O_2 and glucose, a demand that is limited to the areas activated during synaptic activity (Iadecola, 2017). CBF is highly sensitive to variations in these two components, while the physiological fluctuations in arterial pressure are unlikely to affect CBF. In fact, one of the first mechanisms by which the brain intervenes following changes in the blood pressure is the 'auto-regulation' system (also known as myogenic response), which ensures that CBF is constant despite fluctuations in the mean blood pressure within the 50-150 mmHg range (Guerra et al., 2018). There is also a second, much more specific mechanism, represented by functional hyperemia or neurovascular coupling (NVC), which allows blood flow to increase during the activation of specific regions of the brain (Moccia et al., 2022). NVC, or functional hyperemia, is the mechanism through which an increase in neuronal activity leads to a local increase in CBF in order to meet the metabolic demands of the brain (Guerra et al., 2018). Considerations regarding the specific energy needs of the brain have led to the definition of a "feedback" model whereby neuronal activity is guided by the metabolic and clearance needs of tissues (Iadecola, 2017) (**Figure 3**). CBF can be regulated directly by a feedback mechanism capable of detecting the concentration of respiratory gases and metabolites. For example, it is known that an increase in CO_2 and adenosine tensions or a decrease in O_2 tension causes an increase in CBF, inducing VSMC relaxation and consequent vasodilation of the microvessels supplying the active region. An alternative mechanism that has been proposed to explain the increase in CBF is the so-called "feedforward" mechanism, according to which neuronal activity releases signals that can dilate cerebral microvessels. In fact, it has been shown that neurons can directly stimulate vessels or activate astrocytes, which in turn release vasoactive mediators responsible for NVC. Furthermore, as discussed in paragraph 1.4, neuronal activity may directly stimulate microvascular ECs to produce vasorelaxing mediators. In both cases, the signaling cascade is initiated by synaptically-released neurotransmitters, particularly glutamate (Attwell et al., 2010; Iadecola, 2017). Despite the substantial differences between the two proposed mechanisms, it is now widely accepted that they are not mutually exclusive and may drive functional hyperemia at different times and in the different brain regions (Iadecola, 2017; Schaeffer & Iadecola, 2021; Zlokovic, 2011).

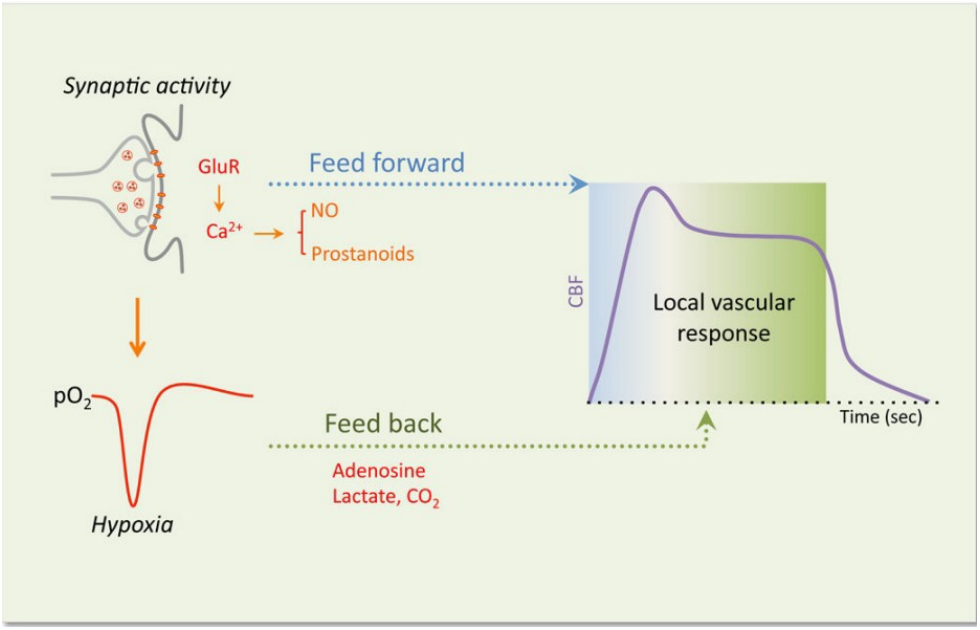

Figure 3. The feedforward and feedback mechanisms proposed to explain neurovascular coupling. NVC is primarily driven by non-metabolic feedforward mechanisms and metabolic feedback mechanisms. They substantially differ because they are mediated by two different metabolic pathways, but both converge on microvessels to increase CBF (Iadecola, 2017).

2.2 Molecular mechanism of neurovascular coupling

2.2.1 Neuronal and astrocytic signaling pathways

According to the canonical model, increased neuronal activity triggers the synaptic release of glutamate, which then activates two different signaling pathways, which are located on neurons and astrocytes, respectively.

An increase in $[Ca^{2+}]_i$ in the dendritic tree is the indispensable signal for inducing the synthesis and release of vasoactive mediators in response to neuronal activity (Guerra et al., 2018; Iadecola, 2017). Specifically, the process begins with the release of glutamate, which activates N-methyl-D-aspartate receptors (NMDARs) and α-amino-3-hydroxy-5-methyl-4-isoxazole propionic acid (AMPA) receptors, causing Ca^{2+} influx into neurons and recruitment of nNOS in the hippocampus and GABAergic interneurons. The production of NO, resulting from the activation of nNOS, induces VSMC relaxation via a soluble guanylate cyclase/PKG-dependent mechanism, thus promoting arteriolar vasodilation (Guerra et al., 2018; Tran, 2022). Studies conducted by Lecrux and his research group have shown that pyramidal neurons represent true "neurogenic hubs" because they release glutamate and prostaglandin E2. Studies on $COX2^{-/-}$ mice have shown a reduction in functional hyperemia, demonstrating the important role played by COX2-dependent prostanoids, such as prostaglandin E2 (PGE2) (Lecrux et al., 2011; Niwa, Araki, Morham, Ross, &

Iadecola, 2000). However, *in vivo* experimental evidence supports the involvement of PGE2 not only as a vasodilator but also as a vasoconstrictor (Tran, 2022). The vasodilatory role of NO may vary depending on the area of the brain involved (Iadecola, 2017). In the hippocampus and cortex, this gasotransmitter is the main mediator of vasodilation evoked by neuronal activity, while it plays a permissive role in the somatosensory cortex, where functional hyperemia is initiated by PGE2.

Intense synaptic activity also increases $[Ca^{2+}]_i$ in perisynaptic astrocytic processes, thereby activating phospholipase A2 (PLA2) and cleaving arachidonic acid (AA). The latter diffuses to adjacent VSMCs and is converted to 20-hydroxy-eicosatrienoic acid (20-HETE) by cytochrome P450 4A (Guerra et al., 2018). However, 20-HETE formation is inhibited by neuronal- or endothelial-derived NO, thus maintaining PGE2-dependent vasodilation (Guerra et al., 2018).

Several lines of controversy have emerged regarding the involvement of astrocytes in NVC. One of the primary points of contention concerns the polarity of the vascular response, as astrocyte activation in brain slice preparations has also been observed to induce vasoconstriction (Mulligan & MacVicar, 2004). Subsequent investigations into the mechanisms governing the balance between vasodilation and vasoconstriction demonstrated that the direction of the vascular response to astrocytic stimulation is influenced by both the basal arteriolar tone (Lia, Di Spiezio, Speggiorin, & Zonta, 2023) and the metabolic brain state. Specifically, a physiological myogenic tone of approximately 30%–40% favors vasodilation, whereas a reduced tone, such as that found in *ex vivo* brain slices lacking blood perfusion, tends to promote vasoconstriction in response to the same vasoactive stimuli, such as Group 1 metabotropic receptors (mGluR) activation or elevated extracellular K^+ concentration ($[K^+]_o$). Additionally, the enzymatic pathways responsible for the production of vasoactive metabolites from AA are modulated by oxygen availability, such that vascular responses are biased toward dilation under physiological oxygen levels, but shift toward constriction under hyperoxic conditions (Lia et al., 2023). Beyond its impact on AA metabolism, oxygenation also influences NVC through its regulation of glycolytic activity. The increase in oxygen consumption associated with neuronal activity enhances anaerobic glycolysis. This metabolic shift leads to elevated production and extracellular release of lactate, which in turn reduces prostaglandin clearance through competition at the prostaglandin/lactate transporter (Lia et al., 2023). As a result, prostaglandin-mediated vasodilation is potentiated. Currently, the diminished production of ATP under these conditions increases the availability of adenosine, a potent vasodilator, further contributing to the overall vasodilatory response.

Glutamate is able to increase $[Ca^{2+}]_i$ in astrocytes by binding to mGluR1 and mGluR5, which are coupled to G_q proteins and activate PLCβ. PLCβ catalyzes the production of $InsP_3$, which induces the release of Ca^{2+} from the ER by binding to $InsP_3Rs$ (Guerra et al., 2018). Surprisingly, mGluR1

and mGluR5 are weakly expressed in adult astrocytes, although NVC is not affected. Therefore, the mechanism by which neuronal activity can increase the $[Ca^{2+}]_i$ in perisynaptic astrocytes has not yet been fully clarified (Iadecola, 2017). Alternative signal transduction pathways have been proposed to explain astrocyte involvement in NVC. For example, neuronal activity releases the neuromodulator ATP and activates the G_q protein-coupled purinergic receptors (P2Y), which mediate the synthesis of $InsP_3$ and, therefore, ER Ca^{2+} release (Guerra et al., 2018). Recent studies have suggested that astrocytes contribute to capillary, but not arteriole-mediated regulation of CBF in the somatosensory cortex (SSCx) (Mishra et al., 2016). Capillary vasodilation was shown to require astrocytic Ca^{2+} signaling mediated by P2X1 purinergic receptors, which subsequently activates AA synthesis via COX-1, leading to the production of PGE_2 and its action on EP4 receptors. Notably, the involvement of this purinergic signaling cascade in capillary vasodilation was confirmed *in vivo* following sensory stimulation (Lia et al., 2023; Mishra et al., 2016). The apparent discrepancy with earlier findings implicating mGluRs in astrocytic responses to neuronal activity may be attributed to developmental shifts in receptor expression profiles within astrocytes. Conversely, vasodilatory responses observed in arterioles were independent of the astrocyte-mediated pathways described above and instead relied on the activation of NMDARs and NOS, indicating a predominant role for NO in the regulation of arteriolar tone (Lia et al., 2023).

In addition, astrocytes are able to sense transmural pressure through the mechanosensitive channel, TRPV4, which is located in astrocytic peduncles and can be activated by a local increase in blood pressure (Kim et al., 2015). The initial hemodynamic response may, therefore, activate TRPV4 channels, resulting in an increase in astrocyte $[Ca^{2+}]_i$ and recruiting PLA2 (Guerra et al., 2018). Most studies have focused on the contribution of the excitatory system to NVC, which is unlikely to represent the sole driver of the hemodynamic response (Gascoigne, Serdyukova, & Aksenov, 2021). Therefore, the involvement of the inhibitory GABAergic system in the regulation of CBF has also been considered. Multiple studies have demonstrated that GABAergic interneurons are critical for the full manifestation of the hemodynamic response, both in the presence of chemical or electrical stimulation, during epileptiform discharges, and in response to sensory as well as optogenetic stimulation (Gascoigne et al., 2021). This evidence can be demonstrated by observing the presence of GABA receptors on the abluminal surface of arterioles, onto which the axonal terminals of GABAergic interneurons project (Gascoigne et al., 2021; Kocharyan, Fernandes, Tong, Vaucher, & Hamel, 2008). GABAergic projections are therefore able to induce arteriolar vasodilation through VSMC hyperpolarization, improving hemodynamic response (Gascoigne et al., 2021). These findings suggest that the GABAergic response can maintain O_2 tension in the

active brain areas by acting on two levels: first, by reducing O_2 demand, and second, by increasing O_2 supply through NVC (Gascoigne et al., 2021) (**Figure 4**).

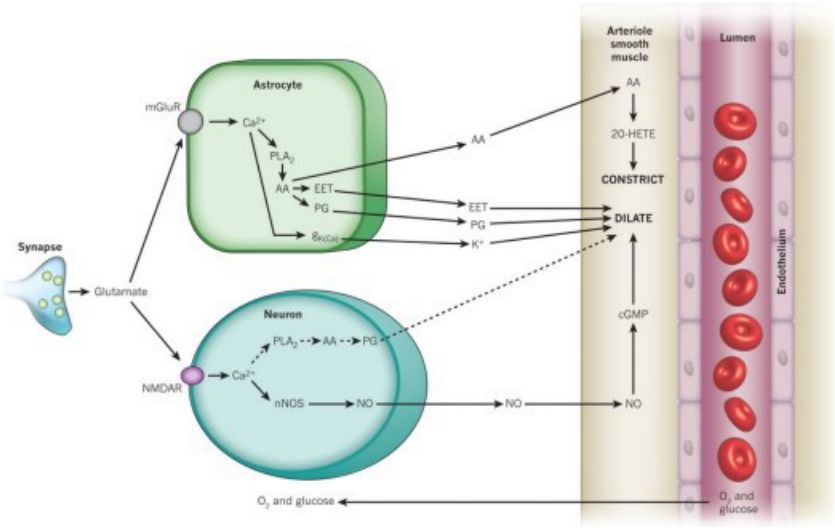

Figure 4. Main signaling pathways involved in the regulation of NVC by neurons and astrocytes. The release of glutamate activates neuronal AMPA and NMDA receptors followed by Ca^{2+} influx and nNOS activation. The resulting production of NO and PGE2 acts on VSMCs and PCs (Attwell et al., 2010). Intense synaptic activity also increases $[Ca^{2+}]_i$ in perisynaptic astrocytic processes, thereby activating PLA2 and cleaving AA.

2.2.2 Endothelial signaling pathways

NVC or functional hyperemia represents the process that translates the neuronal activity in a rapid increase in CBF, leading to a dilation of penetrating arterioles and pial arteries (Longden et al., 2017). Since this process is so important for providing the brain with O_2 and nutrients, it must be able to guarantee a long-lasting and fast transmission of vasodilatory signals from the deep of the cortex to the brain's surface (Longden et al., 2017). For a long time, it has been generally recognized that the vasodilator mediators released during NVC from neurons and astrocytes primarily target VSMCs of parenchymal arterioles, although they cannot directly interact with most neurons due to their limited distribution. The situation within the capillary bed is markedly different, as it forms a net that delves into the deepest regions of the brain. In fact, neurons are closely apposed to ECs. This anatomical arrangement lead to the concept formulated in (Longden et al., 2017), according to which capillaries represent "sensors" of neuronal activity and are able to propagate the vasodilatory signal to upstream parenchymal arterioles. A major role in this process is played by the $K_{IR}2.1$ channel in capillary ECs. Retrograde transmission of the vasoactive signal consists of in the propagation of endothelial hyperpolarization from the capillary bed to the upstream arterioles, where it is transmitted

electrotonically to the VSMCs via the myoendothelial projections (Longden et al., 2017). The $K_{IR}2.1$ channel is suitable for the perception of neuronal activity: it exhibits a strongly inward rectifying current-voltage relationship, meaning that the channel does not conduct to membrane potentials (V_M) more depolarized than the equilibrium potential of K^+ (E_K=-80 mV) due to the obstruction of the channel pore by cytosolic Mg^{2+} and polyamines. However, the $K_{IR}2.1$ channel conducts a modest outward K^+ current at potentials between E_K and the resting potential of cerebral ECs (V_M=-30/-40 mV). The outward K^+ current through $K_{IR}2.1$ increases following a modest increase in $[K^+]_o$, thereby promoting EC hyperpolarization. In other words, their V_M becomes more negative than the resting value of -30/-40 mV. The Nelson group has shown that the local increase in $[K^+]_o$ resulting from neuronal activity (approximately 10 mM) can activate $K_{IR}2.1$ channels located on the abluminal membrane of adjacent cerebral capillaries in the mouse brain (Jackson, 2017; Longden et al., 2017; Moccia et al., 2022). The resulting K^+ efflux causes local hyperpolarization, which is then propagated electrotonically to the upstream intraparenchymal arterioles through interendothelial communicating junctions. Herein, the endothelial hyperpolarization can be transmitted to adjacent VSMCs, which relax due to the reduction in Ca^{2+} influx through voltage-dependent L-type channels, causing an increase in CBF to the downstream capillaries (**Figure 5**). In addition, endothelial hyperpolarization initiated by the $K_{IR}2.1$ channel can be potentiated by adenosine, which is released by neurons and astrocytes and causes the activation of additional ATP-dependent K^+ channels, which are also located in the capillary endothelium (Moccia et al., 2022). $K_{IR}2.1$ activation requires the interaction with phosphatidylinositol-4,5-bisphosphate (PIP_2), a minor phospholipid component of the plasma membrane. PIP_2 is hydrolyzed to diacylglycerol (DAG) and $InsP_3$ following activation of the enzyme PLCβ by multiple agonists of G_q-Protein Coupled Receptors (G_qPCRs), including acetylcholine, glutamate, and PGE2. PIP_2 hydrolysis following extracellular stimulation inhibits the $K_{IR}2.1$ channel, thereby restoring the endothelial resting V_M. PIP_2 also inhibits the Ca^{2+}-permeable cation channel, TRPV4, which is activated by PIP_2 hydrolysis (Harraz, Longden, Hill-Eubanks, & Nelson, 2018) (Harraz et al., 2018). Therefore, G_qPCRs-dependent PIP_2 depletion could be necessary to repolarize (via $K_{IR}2.1$ channel inhibition) the endothelial V_M after the onset of the vasorelaxing hyperpolarizing signal. Or it could be required to prevent the propagation of the electrical signal further down the activated capillary bed by depolarizing the endothelial membrane (via TRPV4 activation) (Harraz et al., 2018). In addition, extracellular Ca^{2+} entry through TRPV4, which in turn stimulates the release of Ca^{2+} from the ER by activating $InsP_3Rs$ through the Ca^{2+}-induced Ca^{2+} release mechanism (CICR) (Longden et al., 2021). Notably, $InsP_3$- and TRPV4-driven endothelial Ca^{2+} signals were shown to induce robust NO release at the ACT zone, thereby causing relaxation of contractile pericytes located at capillary bifurcation and permitting the perfusion only of the branch experiencing Ca^{2+} activity

and, therefore, neuronal activity (Longden et al., 2021). These findings, although preliminary, suggest that endothelial Ca^{2+} signaling at the BBB plays a crucial role in the NO-dependent control of CBF.

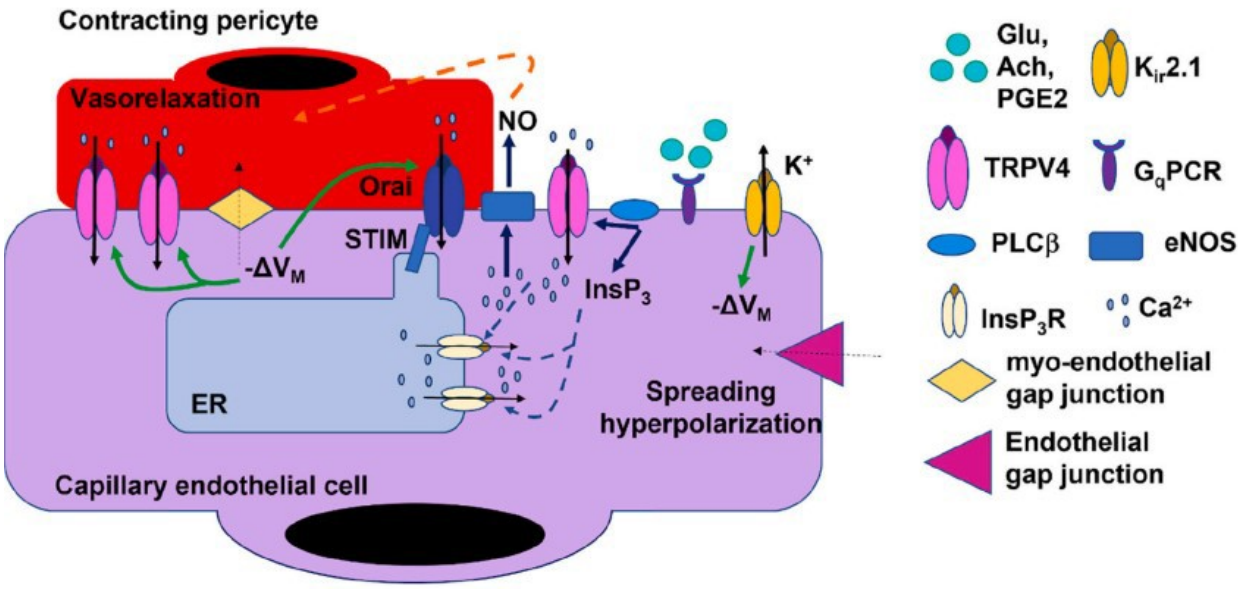

Figure 5. Endothelial ion channels involved in the regulation of CBF.

The image provides a general overview of the channels and elements involved in the vasodilation mechanism starting from the capillary endothelium (Moccia et al., 2022).

CHAPTER 3: Ca^{2+} signals in neurovascular coupling

3.1 Endothelial Ca^{2+} Signaling: From Local to Global Ca^{2+} Signals

The endothelium is now generally recognized as a dynamic element, which plays a key role in regulating the passage of substances between the blood and tissues, in coagulation, and in other highly complex processes, such as angiogenesis. Furthermore, brain capillary ECs are able to perceive neuronal activity, thereby playing a key role in NVC. There are still many issues to be clarified regarding how endothelial Ca^{2+} signals contribute to translating neuronal activity into vasodilatory signals in brain.

In ECs, increases in $[Ca^{2+}]_i$ arise in response to neurohumoral agonist, e.g. acetylcholine and ATP, to inflammatory mediators, e.g. histamine and bradykinin, to growth factors, e.g. vascular endothelial growth factor (VEGF) and angiopoietins, and to reactive oxygen species (ROS) (Moccia, Brunetti, Soda, Berra-Romani, & Scarpellino, 2023). Moreover, intracellular Ca^{2+} waves at the BBB could be elicited by neurotransmitters, such as glutamate and GABA (Moccia, Brunetti, Soda, Berra-Romani, et al., 2023), and by physical stimuli, including shear stress (Lim & Harraz, 2024). With the advent of fluorescent Ca^{2+} indicators and Genetically encoded Ca^{2+} indicators (GECIs), as well as of new

and advanced high-resolution imaging methods, it has been possible to identify how the complex of ion channels and receptors works in synergy to activate different types of Ca^{2+} signals, each of which is responsible for a specific regulatory function (Moccia, Brunetti, Soda, Berra-Romani, et al., 2023). The first studies carried out on ECs, using the ratiometric dye, Fura-2, showed that Ca^{2+} responses to different agonists or growth factors consisted of a transient, biphasic, monotonic, or oscillatory increase in $[Ca^{2+}]_i$, which is often not limited to the whole cytoplasm, but also spreads to neighboring ECs. However, high-speed Ca^{2+} imaging of ECs loaded with non-ratiometric Ca^{2+} indicators (e.g., Fluo-3, Fluo-4 and Cal520) or expressing GECIs have clarified that the Ca^{2+} signals underlying vascular responses comprise a broad mosaic of Ca^{2+} responses that often remain spatially localized (Moccia, Brunetti, Soda, Berra-Romani, et al., 2023). These Ca^{2+} microdomains are mediated by the opening of Ca^{2+}-permeable channels located on the ER membrane or plasma membrane, and it is believed that some of these may be coupled to Ca^{2+}-dependent effectors in such a way as to regulate various functions (Moccia, Brunetti, Soda, Berra-Romani, et al., 2023).

3.2 Exploring the endothelial Ca^{2+} toolkit: the Ca^{2+} response to G_qPCRs

It is important to highlight that much of our current understanding of the role of the endothelium in NVC comes from studies conducted in mice and rats, while knowledge in humans remains limited (Moccia et al., 2022). For instance, it is unknown whether human brain microvascular endothelial cells express $K_{IR}2.1$ channels and an extracellular K^+-dependent inward rectifier K^+ current. However, the hCMEC/D3 cell line, expresses functional NMDARs that may signal both in an ionotropic and a metabotropic mode in response to glutamate (Negri, Faris, Maniezzi, et al., 2021). This finding is relevant since mouse cerebral capillary ECs lack the main NMDARs subunit, i.e., GluN1. It turns out that human and mouse cerebrovascular ECs might exploit two distinct arrays of ion channels and membrane receptors to generate vasomediators in response to neuronal activity. The main features of Ca^{2+} signaling in capillary ECs have recently been revealed, particularly after the development of mouse lines that selectively express GECIs in vascular ECs (Garcia & Longden, 2020). Recently, cadherin 5 (Cdh5) has been used as a promoter for the expression of the Ca^{2+} indicator GCaMP8. The GCaMP8 mouse line expresses the GECI throughout the endothelial monolayer in a cell-specific manner, thereby allowing the first characterization of Ca^{2+} signals in capillary ECs. Due to the use of this transgenic line, it has been possible to ascertain that capillary ECs are different from those located in other areas of the vascular tree (Garcia & Longden, 2020). A recent investigation revealed that synaptic activity can also trigger endothelial Ca^{2+} waves in the mouse brain microvasculature (Longden et al., 2021; Moccia, Brunetti, Soda, Berra-Romani, et al., 2023). In vivo imaging in anesthetized transgenic mice selectively expressing GCaMP8 in ECs revealed a hierarchy of $InsP_3$-dependent Ca^{2+} signals, ranging from small, subsecond protoevents, caused by Ca^{2+} mobilization

through a limited number of $InsP_3Rs$, to high-magnitude, persistent (up to ~1 min) composite Ca^{2+} events sustained by large clusters of $InsP_3Rs$ (Moccia, Brunetti, Soda, Berra-Romani, et al., 2023). These frequent $InsP_3$-dependent local Ca^{2+} release events were sustained by TRPV4 activation upon PLCβ-dependent hydrolysis of PIP_2 (Longden et al., 2021; Moccia, Brunetti, Soda, Berra-Romani, et al., 2023). Somatosensory stimulation induced an increase in the amplitude and duration of these subcellular Ca^{2+} events and increased the prevalence of endothelial Ca^{2+} activity at the arteriole–capillary transitional zone. The agonist responsible for G_qPCR activation has not been identified (Longden et al., 2021; Moccia, Brunetti, Soda, Berra-Romani, et al., 2023), but it could be the synaptically released excitatory neurotransmitter glutamate. As discussed below, glutamate can bind to mGluR1 and mGluR5 to induce intracellular Ca^{2+} oscillations in cultured cerebrovascular ECs (Moccia, Brunetti, Soda, Berra-Romani, et al., 2023).

A recent investigation mined a publicly available RNA-seq dataset to explore the ion signaling machinery in mouse brain capillary ECs (Garcia and Longden, 2020). As outlined in **Figure 6**, the major Ca^{2+}-permeable channels expressed in cECs are $InsP_3Rs$ (Garcia & Longden, 2020). $InsP_3Rs$ are ubiquitously expressed in the membranes of the ER/SR. $InsP_3Rs$ release Ca^{2+} from the ER lumen into the cytoplasm, generating Ca^{2+} signals in response to various stimuli. $InsP_3$-dependent Ca^{2+} signals control a wide range of cellular functions. $InsP_3Rs$ opening is linked to the PLC pathway, which mediates the formation of $InsP_3$. $InsP_3Rs$ release Ca^{2+} from the ER only when they bind to both $InsP_3$ and Ca^{2+}, which therefore serve as co- agonists. PLC-derived $InsP_3$ primes $InsP_3Rs$ to be activated by local Ca^{2+} such that, in the presence of permissive $InsP_3$ concentrations, a spatially restricted Ca^{2+} pulse can be regeneratively propagated via CICR (Moccia, Brunetti, Soda, Berra-Romani, et al., 2023). In accord, $InsP_3Rs$ are clustered in the ER membrane, so that the activation of a single receptor may easily triggers CICR through the nearby $InsP_3Rs$ (Baker, Fan, Arige, Yule, & Serysheva, 2023). Each of the three $InsP_3R$ genes are expressed, while the ryanodine receptor (RyR) genes are absent, in mouse brain capillary ECs (Garcia & Longden, 2020). Another highly expressed Ca^{2+}-permeable channel is Orai, which is encoded by the *Orai1* and *Orai3* genes in mouse brain capillary ECs. The Orai protein contributes to SOCE at the plasma membrane. STIM (Stromal Interaction molecule 1), which is located on the ER membrane, is also involved in the SOCE mechanism. Specifically, the STIM1 and STIM2 isoforms, which are both expressed in mouse brain capillary ECs, are transmembrane ER proteins that serve as sensors of the ER Ca^{2+} reservoir through a lumenal EF-hand motif with low affinity for Ca^{2+} (Garcia & Longden, 2020). When Ca^{2+} levels drop, Ca^{2+} unbinding from this domain causes STIM oligomerization, leading to a conformational change: this causes STIM proteins to bind to the carboxy-terminal portion of Orai, which is located on the plasma membrane. This interaction, in turn, activates Orai, which mediates Ca^{2+} influx. The

incoming Ca^{2+} is immediately recaptured by Sarco-Endoplasmic Reticulum Ca^{2+}-ATPase (SERCA) to restore the ER Ca^{2+} pool (Garcia & Longden, 2020), but can also recruit a number of endothelial Ca^{2+}-dependent effectors, such as eNOS (Moccia et al., 2023). In addition to $InsP_3Rs$ and SOCE, mouse brain capillary ECs express other components of the endothelial Ca^{2+} toolkit, such as Ca^{2+}-transporting systems, lysosomal Two Pore Channels (TPCs), and many members of the TRP super-family of non-selective cation channels. In the next paragraphs, we mainly focus on the mechanisms investigated in the present thesis, namely: NCX and TRPML1.

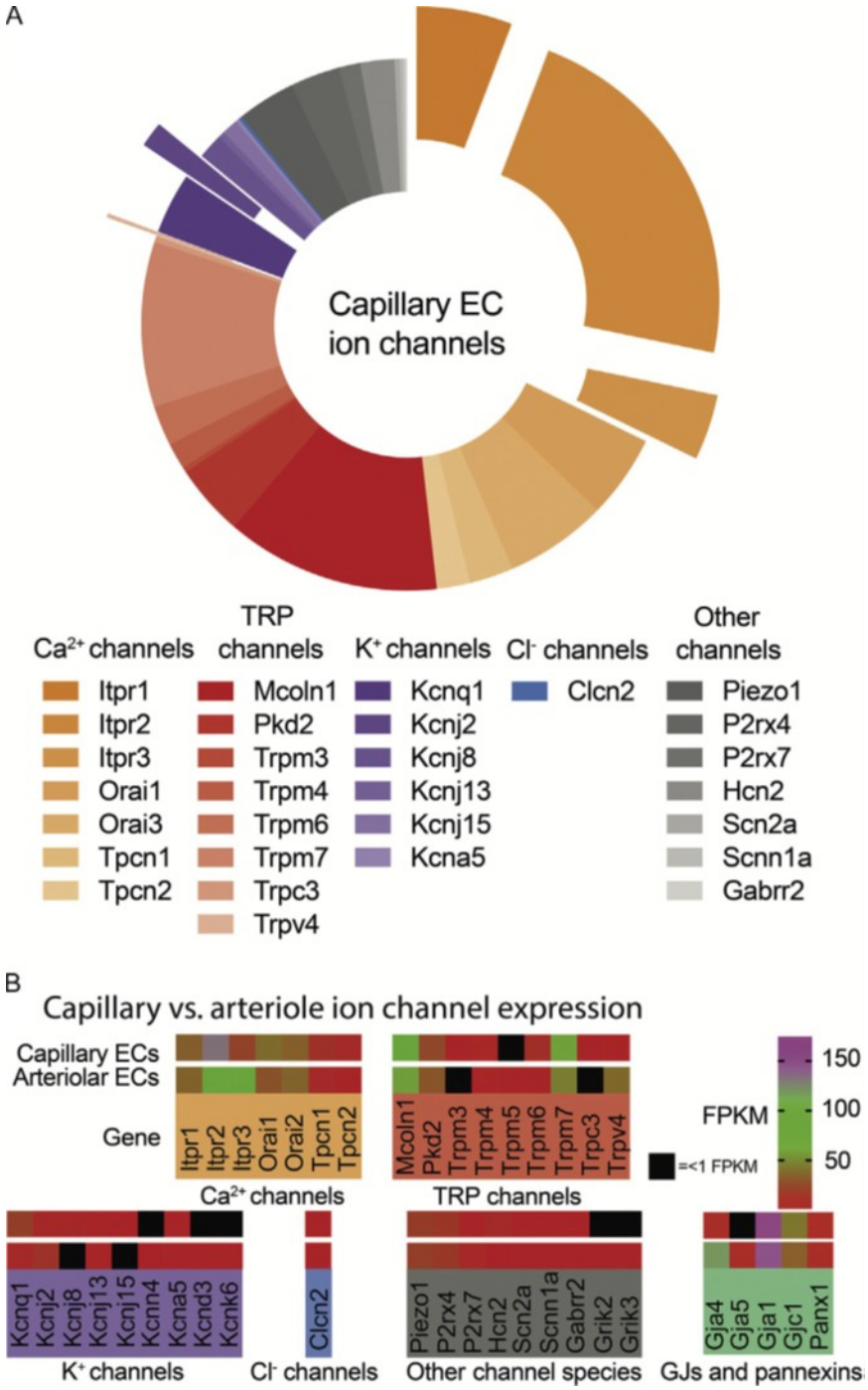

Figure 6. Capillary EC ion channel expression. RNA-Seq data from Vanlandewijck et al. (2018) and He et al. (2018) and reproduced in (Garcia & Longden, 2020), showing the relative expression of ion channel genes.

(Garcia & Longden, 2020).

3.3 Exploring the endothelial Ca^{2+} toolkit: Ca^{2+} clearing mechanisms and the dual role of NCX

Intracellular Ca^{2+} signals are of fundamental importance for a myriad of endothelial functions. However, an excessive increase in $[Ca^{2+}]_i$ can be harmful and lead to endothelial dysfunction (Negri, Faris, & Moccia, 2021b) (M. Wang, Preckel, Zuurbier, & Weber, 2025). Therefore, ECs are equipped with a repertoire of Ca^{2+}-transporting proteins that allow the Ca^{2+} concentration to be regulated in a controlled manner. These systems include: Plasma Membrane Ca^{2+} ATPase (PMCA), Na^+/Ca^{2+} exchanger (NCX), SERCA, and mitochondrial Ca^{2+} uniporter (MCU) (Moccia, Brunetti, Soda, Berra-Romani, et al., 2023). The concerted interaction among these Ca^{2+}-clearing mechanisms drives the rapid return of the $[Ca^{2+}]_i$ to pre-stimulation levels after agonist removal (Moccia, Brunetti, Soda, Berra-Romani, et al., 2023). However, the NCX is sensitive to the transmembrane Na^+ gradient and, therefore, it can also mediate Ca^{2+} entry following a sudden increase in the sub-membrane Na^+ concentration.

3.3.1 Na^+/Ca^{2+} exchanger (NCX)

The NCX protein was first isolated by exploiting a Ca^{2+} uptake assay in reconstituted liposomes (Nicoll, Ottolia, Goldhaber, & Philipson, 2013). The procedure identified a 120 kDa protein as the NCX, which then migrated as a 160 kDa band under non-reducing conditions and retained its function after proteolytic truncation. In accord, proteolysis reduced the size to 70 kDa although the functional exchange activity was retained (Nicoll et al., 2013). Only a small amount of protein could be isolated, but it proved to be very useful for the production of anti-NCX polyclonal antibodies. These antibodies enabled the cloning of the first NCX isoform (NCX1) via screening of a λ-phage expression library. Functional expression in Xenopus oocytes confirmed Na^+-dependent Ca^{2+} uptake, thereby establishing its identity. Subsequent cloning efforts identified two additional isoforms, NCX2 (Z. Li et al., 1994) and NCX3 (Nicoll et al., 1996). At the same time, a lot of splicing variants were identified (Nicoll et al., 2013).

DNA sequencing revealed a frame of 970 amino acids with a cleaved 32-residue leader peptide, which are not present in the mature form. The analysis suggested the presence of 12 transmembrane segments (TMSs), while experimental analysis revealed only 9 TMSs (Nicoll et al., 2013). A large loop was found between the N-and C- terminal groups. It contains a calmodulin-like binding domain and a 20 amino acid peptide with a sequence known as the exchanger inhibitory peptide (XIP), which acts as an autoinhibitory module (Nicoll et al., 2013). Mutations in the XIP region affect the Na^+-dependent inactivation. Alternative splicing within this intracellular loop yields tissue-specific NCX variants through inclusion of six short exons (A–F), with exons A and B being mutually exclusive.

These variants confer distinct regulatory properties, though the physiological relevance remains partially understood (Nicoll et al., 2013).

3.3.2. Structure of NCX

As shown in **Figure 7,** a model for the NCX1 with 9 TMSs and a large intracellular loop has been described (Nicoll et al., 2013). The two α repeats (alpha-1 and alpha-2) represent two regions of intramolecular homology. Alpha-1 spans portions of TMSs 2 and 3 while alpha-2 encompasses a portion of TMS7 and a portion of a reentrant loop between TMSs 7 and 8 (Nicoll et al., 2013). Intramolecular homology could mean that the NCX gene evolved from a duplication event and, because only the alpha repeats have retained intramolecular homology, this suggests their critical role in ion translocation. This aspect was confirmed through several mutational experiments, in which mutations within the alpha repeats significantly impaired ion translocation (Nicoll et al., 2013).

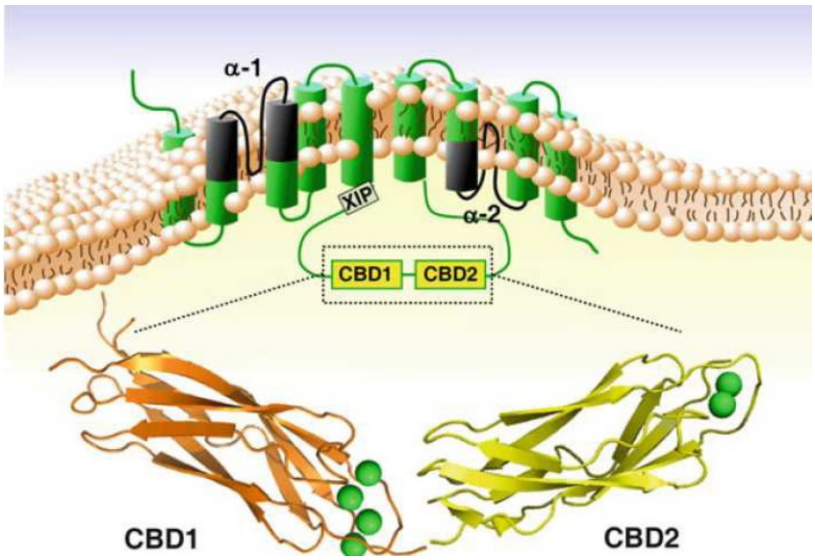

Figure 7. Two-dimensional model of the NCX1.
9 TMS domains on the extracellular surface.
The alpha repeat regions (alpha-1 and alpha-2), critical for ion transport are depicted in black. The XIP region is involved in autoregulation and binds PIP_2. The two Ca^{2+}-binding domains (CBD1 and CBD2) regulate the ion exchange activity. The structures of CBD1 and CBD2 are known and are shown as ribbon diagrams as determined by X-ray crystallography. Green balls represent bound Ca^{2+} *(Nicoll et al., 2013).*

3.3.3 Regulation of NCX

The main regulatory mechanisms of NCX1 are mediated by Na^+ and Ca^{2+} (Nicoll et al., 2013). In recent years, the regulation by Na^+ has been studied, but its exact physiological role is still unclear. It has been suggested that Na^+ regulation is involved in the effects exerted by PIP_2 has on the exchange activity. The Ca^{2+}-dependent regulation of NCX has been extensively studied through patch clamp experiments on large portions of membrane derived from oocytes. It has been shown that having Na^+ and Ca^{2+} on opposite sides of the membrane is not sufficient *per se* to initiate ion exchange (Nicoll et al., 2013). A low concentration of Ca^{2+} should be added to Na^+ in order to bind to a regulatory site

and activate the NCX activity. Subsequent experiments identified the binding site for Ca^{2+}: specifically, Ca^{2+} regulation was abolished by eliminating the large intracellular loop, which contains a region of about 140 amino acids that binds Ca^{2+} with high affinity. This was confirmed by mutating specific amino acids of the sequence, which eliminated Ca^{2+} binding. A second binding region for Ca^{2+} adjoining the Ca^{2+}-binding domain 1 (CBD1) region was identified and, therefore, termed CBD2. CBD1 plays the main role in regulating the Ca^{2+} affinity for the Ca^{2+}-dependent regulation, while the exact role of CBD2 is not yet fully understood (Nicoll et al., 2013).

3.3.4 Role of NCX in endothelial cells

One of the main differences between neurons and endothelium is the isoform they express: in fact, NCX1 is the main isoform detected in vascular endothelium. In vascular ECs, NCX may operate in either the forward (Ca^{2+} out) or the reverse (Ca^{2+} in) mode depending on the transmembrane Na^+ gradient. Therefore, NCX may contribute to clear cytosolic Ca^{2+} following an increase in $[Ca^{2+}]_i$ (Moreno-Salgado et al., 2023) or to prolong Ca^{2+} entry in response to a sustained influx of Na^+ that promotes Na^+ accumulation beneath the plasma membrane (Moccia et al., 2011). For instance, removal of $[Na^+]_o$ causes the NCX to switch into the reverse-mode and induced an increase in $[Ca^{2+}]_i$, which disappeared in the absence of extracellular Ca^{2+}, and in the presence of benzamil, which blocks both modes of NCX, and KB-R 7943, a selective inhibitor of the reverse-mode (Berra-Romani et al., 2010). The endothelial NCX plays a role in the regulation of vascular tone (Schneider et al., 2002) and angiogenesis (Andrikopoulos et al., 2011). For instance, the reverse mode of NCX1 can drive eNOS activation and NO production (Schneider et al., 2002). Specifically, the reverse mode of NCX1 could increase the concentration of Ca^{2+} beneath the plasmalemma and promote the formation of the Ca^{2+}/calmodulin complex in porcine aortic ECs. The subsequent binding of the Ca^{2+}/calmodulin complex to eNOS displaces caveolin-1, which forms a direct inhibitory complex, thus promoting NO synthesis (Schneider et al., 2002).

Furthermore, Andrikopoulos et al. showed that the Ca^{2+} influx through reverse mode NCX plays a key role in thrombin- (Andrikopoulos et al., 2015) and VEGF-induced angiogenesis (Andrikopoulos et al., 2011). A recent study also suggests that the NCX can be switched into the reverse mode by a reduction in extracellular Na^+ concentration $[Na^+]_o$ in rat middle cerebral artery (Klapczynska, Aleksandrowicz, & Kozniewska, 2023). Ca^{2+} entry through the reverse NCX mode stimulates the NO/cGMP signaling pathway, which leads to vasodilation and increase in CBF (Klapczynska et al., 2023).

3.4 Endo-lysosomal Ca^{2+} signals in vascular endothelium

The endo-lysosomal system comprises a multitude of acidic organelles enriched with H^+ and Ca^{2+}: lysosomes, lysosome-related organelles, secretory vesicles, vacuoles, and the Golgi apparatus (Negri, Faris, & Moccia, 2021a). The endo-lysosomal system, which includes lysosomes and endosomes, has emerged as one of the main regulators of intracellular Ca^{2+} dynamics. For instance, early endosomes (EEs), which primarily serve as the recycling organelle of the cell, contain Ca^{2+} concentrations in the millimolar range, but these concentrations quickly decrease (to 2-3 μM) due to progressive acidification, causing the release of Ca^{2+} through TRP Mucolipin 3 (TRPML3), which is expressed on their surface. The late endosomes (LEs), matured form EEs, have a much more acidic intraluminal pH (4.8-6.0) due to the activity of the vacuolar H-ATPase (v-ATPase). In addition, LEs undergo a progressive increase in Ca^{2+} concentration compared to EEs (Negri, Faris, et al., 2021a). Lysosomes are generally considered to be a highly acidic compartment, with a pH of 4.5-5.0, responsible for the degradation and recycling of damaged macromolecules and organelles. The extremely acidic lumen of lysosomes is derived from the presence of increased v-ATPase activity and a negative resting V_M (-20 mV/-40 mV) (Negri, Faris, et al., 2021a). Lysosomes contain a free $[Ca^{2+}]_i$ of around 500-600 μM and for this reason they represent the second largest Ca^{2+} reserve in the cell, after the ER. Although they occupy a relatively small space in the cell, lysosomes have been shown to be capable of mediating an increase in intracellular Ca^{2+} concentration, which can then propagate in Ca^{2+} waves when in contact with the ER (Faris et al., 2019; Morgan, 2016). Since extracellular Ca^{2+} contributes little to lysosomal refilling, lysosomes require an exchanger or pump to transport Ca^{2+} from the cytosolic lumen into the lysosomal lumen. Lysosomal refilling can also be carried out through the mobilization of Ca^{2+} from the ER, involving $InsP_3Rs$ and SOCE. Lysosomal uptake requires ATP and an H^+ gradient.

Given the need to maintain an adequate Ca^{2+} pool and an extremely acidic environment in order to perform normal functions, lysosomes have specific channels and transporters dedicated to Ca^{2+} entry

or release: TPCs, TRPML1, TRPM2 and TRPA1, P2X4 and CaV2.1 (**Figure 8**). As widely discussed in Chapter 4, previous work has shown that TPCs support neurotransmitters-induced Ca^{2+} signals in the hCMEC/D3 cell line. Herein, we focused our attention on TRPML1, which will be object of my thesis project.

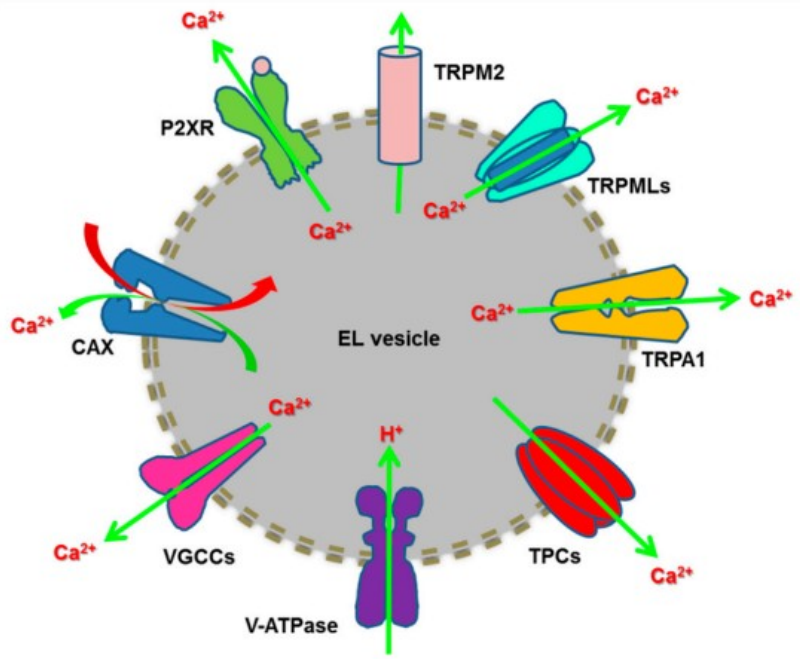

Figure 8. The EL Ca^{2+} signal machinery. The refilling of ER Ca^{2+} stores is driven by the proton gradient via ATPase and carried out by the Ca^{2+}/H^{+} exchanger (CAX) in non-placental mammalian cells. Ca^{2+} release is mediated by a number of Ca^{2+}-permeable channels, including TPC1-2, TRPML1-3, TRPM2, TRPA1, ionotropic P2X4 receptors, and voltage-dependent VGCCs (Negri, Faris, et al., 2021a).

3.5 TRP channels

3.5.1 TRP taxonomy and functions

TRP channels are a large and functionally versatile family of non-selective cation channels responsible for cell interaction with the surrounding microenvironment. The discovery and characterization of the TRP superfamily dates back to studies conducted on *Drosophila melanogaster* mutants (Montell & Rubin, 1989), whose photoreceptors were unable to maintain a prolonged depolarization following light stimulation and, under intense light conditions, behaved as if they were blind (Cosens & Manning, 1969). Subsequently, an impressive number of studies have demonstrated the expression and remarkable range of functions performed by these channels in mammals as well. In particular, 28 TRP channel isoforms have been discovered in mammals, divided into six subfamilies based on sequence homology: TRP Canonical (TRPC1-7), TRP Vanilloid (TRPV1-6), TRP Melastatin (TRPM1-8), TRP Ankyrin 1 (TRPA1), TRP Mucolipin (TRPML1-3), and TRP Polycystin (TRPP) (Earley & Brayden, 2015; Gees, Colsoul, & Nilius, 2010; Thakore & Earley, 2019) (**Figure 9**).

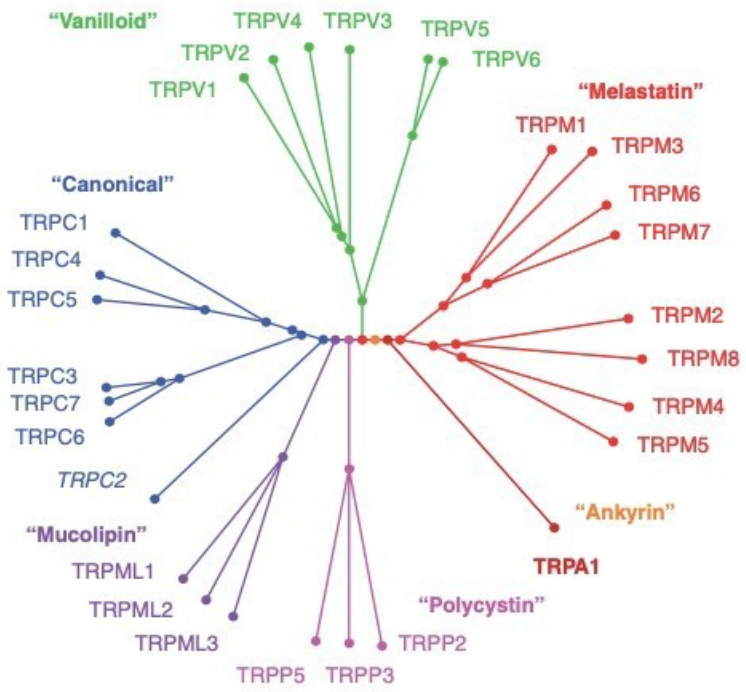

Figure 9. Phylogenetic tree of the mammalian TRP channel superfamily. TRPC, TRPM, TRPV, TRPA1, TRPP, and TRPML are the only subfamilies identified in mammals (Gees et al., 2010).

The TRPP subfamily consists of eight members, although only TRPP2, TRPP3, and TRPP5 exhibit the molecular architecture and function of an ion channel (Gees et al., 2010). Furthermore, TRPC2, which plays a crucial role in the acrosome reaction and pheromone detection in mice, is only a pseudogene in humans (Gees, Colsoul et al. 2010).

The molecular architecture of TRP channels comprises six transmembrane α-helix segments (S1-6) with a loop containing the P region that delimits the selectivity filter between S5 and S6 (Gees et al., 2010). In addition, the N-terminal and C-terminal ends face the intracellular environment and can differ greatly in length and perform different functions, such as providing regulatory domains for cytosolic kinases and other cellular/cytoskeletal proteins, as well as serving as binding sites for Ca^{2+}-dependent sensors (Negri, Faris, Berra-Romani, Guerra, & Moccia, 2019). This structure is very reminiscent of that described in voltage-dependent K^+ channels, although TRP channels do not have a voltage sensor in S4. The TRP domain includes two highly conserved sequences, known as TRP-box 1 and TRP-box 2 (Venkatachalam & Montell, 2007). The first consists of three variants of the Glu-Trp-Lys-Phe-Ala-Arg motif and provides the binding site for phosphatidylinositol phosphates, such as PIP_2 (Birnbaumer, 2009), or is involved in subunit assembly (Venkatachalam & Montell, 2007). TRP-box 2, on the other hand, is a proline-rich amino acid sequence that varies between the different TRPC and TRPM subunits, while it is absent in TRPV channels (Venkatachalam & Montell,

2007). TRPC, TRPV, and TRPA1 channels also share multiple ankyrin repeat domains (ARDs). Coiled-coil (CC) domains, which mediate subunit assembly and channel function, have been detected at the N-terminal end of TRPC and TRPM. These domains can also support the physical association between TRPC channels and STIM1 (Lee et al., 2014). In addition, the C-terminal end of TRPM2 is characterized by a NUDIX phosphohydrolase domain, which is involved in channel opening and responsible for ADPR binding. TRPM6 and TRPM7 channels also consist of functional enzyme domains, which can catalyze specific cellular reactions. Finally, TRPV3, TRPC4, and TRPC5 have a PDZ domain at the C-terminal end that allows them to interact with adjacent proteins (Gees et al., 2010). TRP channels have a tetrameric structure, and most of their subunits assemble preferentially to form homotetramers (Negri, Faris, Berra-Romani, et al., 2019). However, TRP channels can also form heterotetramers, combining with subunits belonging to the same subfamily or to different subfamilies (Negri, Faris, Berra-Romani, et al., 2019). For example, TRPC1 can assemble into functional heterotetramers with TRPC3, TRPC4, or TRPC5 (Smani et al., 2018). Any two members of the TRPV1-4 subunits can also assemble into heterotetrameric channels, located only at the plasma membrane (Cheng, Yang, Takanishi, & Zheng, 2007). Several studies have demonstrated the existence of heterotetramers consisting of TRP subunits belonging to different subfamilies, including: TRPC1/TRPV4, TRPV4/TRPC6, and TRPC1/TRPV6 (Negri, Faris, Berra-Romani, et al., 2019).

TRP channels are permeable to both monovalent (Na^+ and K^+) and divalent (Ca^{2+} and Mg^{2+}) cations, and their relative permeability to Na^+ and Ca^{2+} (P_{Ca}/P_{Na}) varies widely between different subunits. For example, TRPV5 and TRPV6 show a P_{Ca}/P_{Na} >100, while TRPM4 and TRPM5 are impermeable to Ca^{2+} (P_{Ca}/P_{Na} < 0.01) (Gees et al., 2010). The P_{Ca}/P_{Na} of the remaining TRP channels ranges from 0.5 (TRPM2) to 20 (TRPV1) (Gees et al., 2010). However, TRPM6 and TRPM7 are more permeable to Mg^{2+}, while TRPV1, TRPML1, and TRPP3 show high permeability to H^+ ions.

TRP channels are polymodal cellular sensors that can be controlled by a plethora of chemical, physical, thermal, mechanical, and nociceptive stimuli. For example, TRPV1-V4 and TRPM3 are activated by high temperatures, while TRPM8, TRPA1, and TRPC5 are sensitive to low temperatures (Nilius & Voets, 2007; Zimmermann et al., 2011). The TRPC2, TRPC3, TRPC6, and TRPC7 channels require the presence of PLC, and particularly the production of DAG. TRPM6 and TRPM7, which are permeable to magnesium ions (Mg^{2+}), are activated following a decrease in intracellular Mg^{2+} concentration (Voets et al., 2004). Furthermore, an increase in $[Ca^{2+}]_i$ is necessary to activate several TRP channels, including TRPM4 (Launay et al., 2002), TRPM5 (Liu & Liman, 2003), TRPM2 (Du, Xie, & Yue, 2009), and TRPA1 (Zurborg, Yurgionas, Jira, Caspani, & Heppenstall, 2007). TRPM2 can be activated by multiple stimuli, including ADP ribose (ADPR) and oxidative stress. TRP channels are involved in multiple physiological functions, such as sensory functions, including

temperature and taste detection and nociception, homeostatic functions, such as Ca^{2+} and Mg^{2+} reabsorption and osmoregulation, muscle contraction, and vasomotor control (Gees et al., 2010).

3.5.2 TRP channels in brain endothelial cells: TRPV4, TRPV3, and TRPA1

Several TRP channels have been detected in mouse brain microvascular ECs, including TRPC1, TRPM2, TRPV3, TRPV4, and TRPA1 (Zuccolo et al., 2017). Herein, we focus on TRPV4, TRPV3, and TRPA1, which contribute to regulate NVC in the mouse brain microcirculation.

TRPV4 channels represent a major Ca^{2+} influx pathway that controls endothelial Ca^{2+} signaling mechanisms and promotes endothelium-dependent vasodilation (Y. L. Chen & Sonkusare, 2020; Sonkusare et al., 2012). TRPV4 is a polymodal non-selective cation channel that can integrate an array of chemical and physical cues. These include, but are not limited to, PLA2-dependent generation of AA and EET acids, PLC-dependent depletion of PIP_2 or formation of $InsP_3$ and DAG, shear stress, mechanical stretch and decrease in intravascular pressure (Moccia, Brunetti, Soda, Berra-Romani, et al., 2023). Moreover, the activity of TRPV4 seems to be increased in such conditions characterized by elevated capillary permeability (Y. L. Chen & Sonkusare, 2020). The role of endothelial TRPV4 at the mouse BBB has been anticipated in chapters 2.2.2 and 3.2. Briefly, in the arterial ECs, TRPV4 channels are coupled with IK_{Ca}/SK_{Ca} channels or eNOS, thereby leading to VSMC relaxation and vasodilation (Moccia, Brunetti, Soda, Berra-Romani, et al., 2023). TRPV4-eNOS or TRPV4-IK/SK channel coupling is known to occur at MEPs. In the capillaries, however, there are no VSMCs surrounding the ECs. Furthermore, IK_{Ca}/SK_{Ca} channel currents were not observed in capillary ECs (Longden et al., 2017). Conversely, brain capillary ECs express eNOS, which can therefore be associated with TRPV4 channels (Longden et al., 2021). Harraz *et al.* showed that TRPV4 channels in mouse brain capillary ECs are tonically inhibited by basal levels of PIP_2 (Harraz et al., 2018). Neurotransmitter-induced activation of G_qPCR reduced PIP_2 levels and disinhibited TRPV4 channels, simultaneously reducing inwardly rectifying $K_{IR}2.1$ channel activity (Harraz et al., 2018). Additionally, TRPV4-mediated Ca^{2+} entry supports $InsP_3$-dependent ER Ca^{2+} release, thereby further promoting eNOS activation (Longden et al., 2021).

EDH in cerebral arteries may also be elicited by Ca^{2+} influx through carvacrol-activated TRPV3 channels, which could be activated by IK_{Ca} and SK_{Ca} (Pires et al., 2015). This study, however, neither clarified the physiological agonist of TRPV3 channels nor assessed whether they are located at MEPs. Conversely, TRPA1 channels are enriched at MEGJs in rat cerebral parenchymal arteries and may induce EDH both in isolated vessels (Sullivan et al., 2015) and *in vivo*. TRPA1 was found to be physiologically activated by superoxide anions generated by the reactive oxygen species-generating enzyme NADPH oxidase isoform 2 (NOX2), which colocalizes with TRPA1 in cerebral endothelium, but not in other vascular districts. It has been suggested that active neurons release ROS that can

peroxidize membrane lipids and thereby generate metabolites, e.g., 4-HNE, in the proximity of brain capillaries (Thakore et al., 2021). ROS-derived metabolites, in turn, gate TRPA1 and induce the Ca^{2+}-dependent opening of adjacent pannexin 1 (Panx1) channel, which release ATP into the extracellular milieu. The local elevation in extracellular ATP directly activates the Ca^{2+}-permeable P_2X receptors on neighboring endothelial cells, thus triggering a slow Ca^{2+} wave that spreads from the distant capillaries to the post-arteriole transitional segment (Thakore et al., 2021). Herein, endothelial cells express SK_{Ca}/IK_{Ca} channels. This fast electrical signal is locally amplified by $K_{IR}2.1$ channels and is electrotonically transmitted via MEGJs to overlying VSMCs to deactivate voltage-gated L-type Ca^{2+} channels and induce vasodilation (Thakore et al., 2021).

3.5.3 Transient Receptor Potential Mucolipin 1 (TRPML1)

As already stated in paragraph 3.4.1, the TRPML subfamily consists of three members, TRPML1, TRPML2, and TRPML3, which share approximately 75% amino acid sequence identity (Thakore, Pritchard, et al., 2020). TRPML1 has been named after a channelopathy known as mucolipidosis type IV, a disease which affects lysosomal storage, caused by a mutation in *MCOLN1*, the gene encoding for TRPML1 and localized on chromosome 1. The disease is characterized by psychomotor retardation, neurodegeneration, cornel opacities, elevated blood gastrin levels and achlorhydra (Negri, Faris, et al., 2021a). As mentioned above, TRPML1 is ubiquitously expressed and primarily localized to the late endo-lysosomal compartment, where the acidic luminal environment facilitates its activation (Negri, Faris, et al., 2021a). TRPML1 can also be trafficked to the plasma membrane, either via the biosynthetic pathway from the Golgi apparatus or through lysosomal exocytosis.

3.5.3.1 TRPML1 structure

TRPML1 consists of four subunits each comprising six transmembrane α-elices and presenting cytosolic amino- and carboxy-terminal tails. TRPML1 has also a characteristic extracellular loop between TM5 and TM6, which lines the selectivity filter of the channel pore; TRPML1 proteins exhibits a large N-glycosylated intraluminal loop connecting TM1 and TM2 and multiple cytosolic domains (Negri, Faris, et al., 2021a). The N-terminal di-leucine (L15L) promotes trafficking from the trans-Golgi network (TGN) to early endosomes and then to lysosomes via a mechanism involving Adaptor Protein Complex 1 (AP-1). The C-terminal di-leucine (L577L), on the other hand, interacts with AP-2 to facilitate recycling from the plasma membrane back to the LEL compartment (Di Paola, Scotto-Rosato, & Medina, 2018). Additionally, the C565CC palmitoylation motif supports TRPML1 recycling by promoting interaction between the C-terminal endocytic motif and AP-2. The R200P201 site in the luminal loop is susceptible to proteolytic cleavage by cathepsin B (CTSB), which

inactivates the channel by generating multiple protein forms, likely a regulatory mechanism to limit channel activity duration.

The cytosolic regions of TRPML1 are also primary sites for post-translational modifications and interactions with regulatory proteins. For example, Protein Kinase A (PKA) phosphorylates S557 and S559 in the C-terminal cytosolic domain, reducing channel conductance. Due to the significant distance between these serine residues and the pore region, phosphorylation may influence channel activity by disrupting protein-protein interactions or channel multimerization (Di Paola et al., 2018). Protein Kinase D (PKD) also phosphorylates TRPML1 in its C-terminal region, and this modification appears crucial for trafficking from the Golgi to lysosomes (Di Paola et al., 2018) (**Figure 10**).

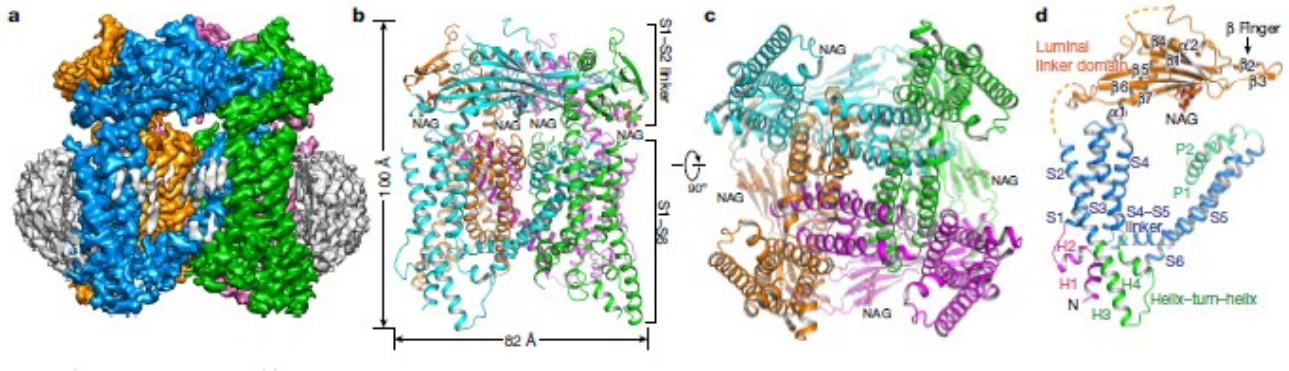

Figure 10. Overall structure of TRPML1. **a**, Side view of a 3D reconstruction of TRPML1 in a nanodisc (grey belt). Channel subunits are coloured individually, with lipid density in grey. **b**, Side view of a cartoon representation of the TRPML1 structure. *N*-acetylglucosamine (NAG) molecules are rendered as sticks. **c**, Cytosolic view of the channel. **d**, Structure of a single subunit in the same orientation as the cyancoloured subunit in **b** (Q. Chen et al., 2017).

3.5.3.2 TRPML1 biophysical properties and gating mechanism

TRPML1 is permeable to Ca^{2+}, Na^{+}, Fe^{2+}, Zn^{2+}, Mg^{2+}, and K^{+}, while it is not permeable to H^{+}. Nevertheless, TRPML1 is sensitive to changes in lysosomal pH. Patch clamp recording revealed that TRPML1 exhibits an inward-rectifying I/V relationship, meaning it favors Ca^{2+} flow toward the cytosol (Dong et al., 2008). Functionally, TRPML1 is activated by $PI(3,5)P_2$, a phosphoinositide enriched in endosomal and lysosomal membranes that binds to the N-terminal cytosolic region near TM1 (Faris, Shekha, Montagna, Guerra, & Moccia, 2018; Yuan et al., 2024). $PI(3,5)P_2$ is synthesized from PI(3)P via the phosphatidylinositol-3-phosphate 5-kinase PIKfyve (Fab1), a 240 kDa enzyme that phosphorylates PI3P at the D-5 position (Dong et al., 2010). PIKfyve is essential for preserving

endolysosomal morphology, and its activity can be enhanced by regulatory proteins such as Vac14 and Vac7, or its product can be converted into PI(5)P by the myotubularin (MTM/MTMR) PI3 phosphatase family (Dong et al., 2010). Mutations in enzymes responsible for $PI(3,5)P_2$ metabolism or its regulators are linked to neurodegenerative disorders such as amyotrophic lateral sclerosis (ALS) and Charcot-Marie-Tooth disease. Conversely, PIKfyve activity is suppressed by $PI(4,5)P_2$, which is more abundant in plasma membrane (Negri, Faris, et al., 2021a). TRPML1 is also physiologically gated by ROS (Negri, Faris, et al., 2021a). In the last years, several synthetic agonists have been developed to stimulate TRPML1-mediated Ca^{2+} release from the EL: ML-SA1 is able to force TRPML1 into an open conformation by interacting with a hydrophobic pocket located in proximity to the TM5-TM6 gate (Negri, Faris, et al., 2021a). Several endogenous modulators can also regulate TRPML1 activity. For example, Ca^{2+} release mediated by TRPML1 is inhibited upon phosphorylation by mammalian target of rapamycin (mTOR), PKA and high lysosomal concentrations of adenosine and sphingomyelin (Negri, Faris, et al., 2021a).

3.6 Regulation and role of the resting membrane potential in vascular endothelial cells

The membrane potential (V_M) plays a critical role in the regulation of endothelial-dependent functions (Voets, Droogmans, & Nilius, 1996). As aforementioned, EDH is critical for the regulation of vascular resistance and is emerging as a main determinant of CBF. In addition, Ca^{2+} entry in vascular endothelial cells may be modulated by any change in V_M according to the following general rule: hyperpolarization increases the driving-force pushing Ca^{2+} into the cytosol, while depolarization reduces Ca^{2+} influx across the plasmalemma (Moccia, Berra-Romani, and Tanzi, 2012). The Nilius group identified the different conductances that contribute to maintaining the endothelial V_M by using bovine pulmonary arterial ECs as a cellular model: an inwardly rectifying K^+ current, a volume-sensitive Cl^- current, and a non-selective cation current. These findings were then confirmed in guinea pig coronary ECs (von Beckerath, Dittrich, Klieber, & Daut, 1996). It was therefore concluded that the resting V_M of vascular endothelial cells scatters between -90 mV and +5 mV. A subsequent investigation reported that low and high concentrations of hydrogen peroxide (H_2O_2), respectively, inhibit and enhance the inward rectifier K^+ current in human umbilical vein endothelial cells (Bychkov et al., 1999). Intriguingly, electrophysiological recordings conducted on the naïve endothelium of rat small pulmonary arteries revealed that the resting ionic conductances change during postnatal development. At birth, the membrane was predominantly permeable to K^+, with a resting potential of -70 mV. Over the following 22 days of development, a Cl^- conductance emerged, thereby depolarizing the V_M to -45 mV (Olschewski et al., 2001).

CHAPTER 4: A new milestone on current knowledge about intracellular Ca^{2+} signaling in cerebrovascular ECs: Ca^{2+} signals in hCMEC/D3 cells

The establishment of the hCMEC/D3 cell line provided a novel cellular model that was not only suitable for investigating how synaptic activity fine-tunes the human BBB permeability, but also for studying how neuronal activity induces changes in the $[Ca^{2+}]_i$ and promotes Ca^{2+}-dependent NO release.

4.1 Intracellular Ca^{2+} Signals Induce Acetylcholine-Dependent NO Production in hCMEC/D3 cells

The cerebral cortex receives extensive cholinergic innervation originating from the basal forebrain. Cholinergic neurons in this region project to arterioles and intraparenchymal capillaries, thereby modulating CBF. Accordingly, activation of basal forebrain neurons promotes arteriolar vasodilation and enhances cerebral perfusion (Guerra et al., 2018; Hamel, 2004; Lecrux & Hamel, 2016). Acetylcholine mediates vasodilation primarily via the activation of M5 muscarinic acetylcholine receptors (M5-mAChRs), which are coupled to G_q proteins and initiate a signaling cascade that activates eNOS, culminating in NO release from the cerebral endothelium. This mechanism has been observed in both murine and porcine models (Elhusseiny & Hamel, 2000). Multiple studies have demonstrated that acetylcholine-induced NO production is associated with $[Ca^{2+}]_i$ oscillations in ECs across various vascular beds (Boittin et al., 2013; Guerra et al., 2018). Consistent with these findings, acetylcholine induces Ca^{2+} oscillations in the murine cerebrovascular endothelial cell line, bEND5. These oscillations arise from rhythmic Ca^{2+} release from the ER via $InsP_3Rs$ and are sustained by SOCE (Zuccolo et al., 2017). This same study also demonstrated that the oscillatory Ca^{2+} signals triggered by acetylcholine result in significant NO production, which depends on both ER-derived Ca^{2+} release and SOCE activation. By contrast, acetylcholine was found to elicit a biphasic $[Ca^{2+}]_i$ response in hCMEC/D3 cells (Zuccolo et al., 2018). Our laboratory also demonstrated that this response is mediated by M5-mAChRs. The initial phase of Ca^{2+} release is dependent on $InsP_3Rs$ in the ER and TPCs in endolysosomal vesicles, whereas the sustained plateau phase is maintained by SOCE activation (Zuccolo et al., 2018). The distinct Ca^{2+} signaling profiles elicited by acetylcholine in these two ECs lines likely reflect differences in their expression patterns of Ca^{2+}-permeable ion channels (Guerra et al., 2018). In hCMEC/D3 cells, only the $InsP_3R3$ isoform has been detected, whereas $InsP_3R1$ and $InsP_3R2$ are absent (Guerra et al., 2018). Conversely, bEND5 cells express $InsP_3R1$ and $InsP_3R2$, but not $InsP_3R3$ (Zuccolo et al., 2017). Among these isoforms, $InsP_3R2$ exhibits the highest sensitivity to $InsP_3$ and is a key mediator of CICR, making it the principal driver of oscillatory Ca^{2+} activity. In contrast, $InsP_3R3$ tends to suppress oscillatory behavior and instead favors

biphasic Ca^{2+} responses (Mikoshiba, 2007). Therefore, albeit the signaling machinery shaping the Ca^{2+} response to acetylcholine is roughly the same, subtle differences in the molecular mechanisms account for the diverse Ca^{2+} signatures generated by human *vs.* mouse brain microvascular ECs.

4.2 NMDA Receptors in hCMEC/D3 cells: NO Release and Hemodynamic Response

NMDA receptors are heteromeric ion channels composed of combinations of seven subunits: GluN1, GluN2A–D, and GluN3A–B. These receptors exhibit a relatively high single-channel conductance (~50 pS) and are permeable to Na^+, K^+, and Ca^{2+}. NMDA receptors possess multiple extracellular binding sites for modulatory ligands, including Mg^{2+}, glycine, and D-serine, which regulate receptor activity. A defining feature of NMDA receptors, distinguishing them from other ionotropic glutamate receptors, is their voltage-dependent activation. However, this voltage sensitivity does not arise from intrinsic channel gating but rather from the voltage-dependent binding of extracellular Mg^{2+} near the channel pore, which obstructs ion flux. Hyperpolarization of the membrane promotes this Mg^{2+}-mediated block, whereas depolarization relieves it, allowing current to pass through the channel (Lu et al., 2017). In neurons, NMDA receptors typically assemble as diheteromeric or triheteromeric complexes consisting of two obligatory GluN1 subunits and either two GluN2 subunits or a combination of GluN2 and GluN3 subunits. The precise subunit composition determines the receptor's biophysical and pharmacological characteristics. GluN1 is essential for receptor assembly and trafficking to the plasma membrane, while GluN2 and GluN3 subunits confer distinct functional properties (Brunetti et al., 2024) (Guerra et al., 2018). The extracellular domains of GluN1 and GluN3 contain binding sites for the co-agonists, glycine or D-serine, whereas glutamate primarily binds to GluN2 subunits (Lu et al., 2019). Among the GluN2 isoforms, GluN2A and GluN2B confer high Ca^{2+} permeability, elevated single-channel conductance, and pronounced Mg^{2+} sensitivity at negative membrane potentials (Wyllie, Livesey, & Hardingham, 2013). In contrast, GluN2C and GluN2D subunits are associated with reduced Ca^{2+} permeability and attenuated Mg^{2+} block (Brunetti et al., 2024).

Emerging evidence indicates that NMDA receptors can also signal through a non-canonical, metabotropic mechanism that is independent from ion conduction. This signaling mode is initiated by ligand-induced conformational changes within the intracellular domain of the receptor, which subsequently activate downstream intracellular signaling cascades. In neurons, metabotropic NMDA receptor signaling has been implicated in various cellular processes, including both spontaneous and activity-dependent neurotransmitter release, as well as in the induction of long-term depression (LTD) (Brunetti et al., 2024; Park, Stein, & Zito, 2022). Similarly, in rat cortical astrocytes, NMDA receptor signal in a flux-independent manner to stimulate the release of Ca^{2+} from the ER via $InsP_3$ signaling pathway, involving both $InsP_3Rs$ and RyRs (Guerra et al., 2018). Recent studies have shown that

NMDA receptors are also abundantly expressed in cerebral ECs, where they may be activated by glutamate released from neurons and possibly astrocytes during neuronal activity (Lu et al., 2017).

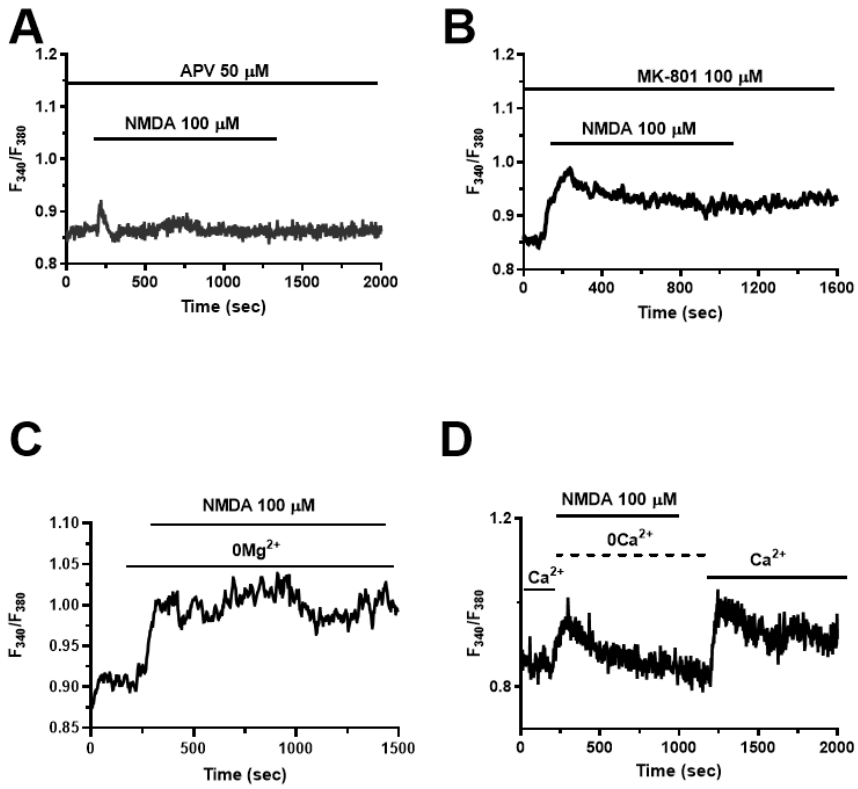

Figure 11. NMDAR receptors trigger metabotropic Ca^{2+} signals in hCMEC/D3 cells. (**A**), pretreatment with APV (50 μM, 30 min), a competitive antagonist at the glutamate binding site, markedly reduced the NMDA-induced Ca^{2+} signal. In panel (**B**), pretreatment with MK-801 (100 μM), a non-competitive pore blocker, did not affect the Ca^{2+} response to NMDA. Panel (**C**) shows that removal of extracellular Mg^{2+}, which would relieve the voltage-dependent block, did not enhance the Ca^{2+} signal. Finally, in panel (**D**), in the absence of extracellular Ca^{2+}, the initial Ca^{2+} peak was unchanged, although the duration of the response was shortened. The removal of the agonist followed by re-addition of extracellular Ca^{2+} resulted in a secondary Ca^{2+} increase, indicative of SOCE activation (Negri, Faris, Maniezzi, et al., 2021).

NMDA receptors have been detected in both human and murine microvasculatures, where they participate in the regulation of the BBB, leukocyte adhesion, glucose uptake, cysteine-induced mitochondrial toxicity, and glutamate-induced oxidative stress. Furthermore, endothelial NMDA receptors appear to play a significant role in neurovascular coupling (Brunetti et al., 2024; Guerra et

al., 2018). Recent evidence has demonstrated that glutamate can activate endothelial NMDA receptors, resulting in NO release and consequent arteriolar vasodilation. Although NO release following NMDA receptor activation requires an increase in $[Ca^{2+}]_i$, the underlying mechanism has only recently been elucidated.

A series of studies conducted in our laboratory initially demonstrated that glutamate trigger Ca^{2+} signaling in hCMEC/D3 cells (Zuccolo, Laforenza, et al., 2019) as well as in the murine bEND5 cell line (Zuccolo, Kheder, et al., 2019). These Ca^{2+} signals are mediated by Group 1 mGluRs, specifically mGluR1 and mGluR5. The Ca^{2+} response to glutamate initiate by Ca^{2+} release from the ER via the $InsP_3$ pathway and from acidic endolysosomal vesicles via TPCs activated by NAADP (Negri, Faris, Pellavio, et al., 2019). More recently, our group provided evidence that hCMEC/D3 cells also express the GluN1, GluN2C, and GluN3B subunits, although no detectable transmembrane current was elicited upon NMDA receptor stimulation (Negri, Faris, Pellavio, et al., 2019). Nonetheless, NMDA application induced an increase in $[Ca^{2+}]_i$, that was generated by intracellular Ca^{2+} release via $InsP_3Rs$ and TPCs and sustained by SOCE (Negri, Faris, Maniezzi, et al., 2021)(**Figure 11**). NMDA-induced Ca^{2+} signals were sensitive to APV, which blocks the agonist-binding site, but not MK-801, which obstructs the ion-conduction pathway; furthermore, the Ca^{2+} response to NMDA was sensitive to the genetic silencing of GluN1, which is the obligatory subunit to assemble a functional NMDA receptor (Negri et al., 2021). These findings suggest that NMDA receptors signal in a flux-independent manner in hCMEC/D3 cells (Brunetti et al., 2024; Park et al., 2022). Unexpectedly, NMDA-induced Ca^{2+} signals were also inhibited by the pharmacological and genetic blockade of mGluR1 and mGluR5 (Negri et al., 2021). Therefore, the flux-independent signaling mode of endothelial NMDA receptors requires the functional interaction with Group1 1 mGluRs. Importantly, NDMA receptors were found to support glutamate-induced intracellular Ca^{2+} release and NO production and, therefore, they were proposed to also play a critical role in NVC in the human brain microcirculation (Negri et al., 2021).

4.3 GABA receptors induce Ca^{2+} signals and NO production in hCMEC/D3 cells

GABA receptors named upon their sensitivity to γ-aminobutyric acid (GABA), the principal inhibitory neurotransmitter in the CNS. Beyond its role in maintaining the excitatory–inhibitory balance via inhibition of glutamatergic pyramidal neurons, GABA is also essential for generating oscillatory activity within neuronal networks. GABA inhibits neuronal activity primarily through the activation of ionotropic $GABA_A$ receptors, which are permeable to chloride ions (Cl^-). Activation of these receptors leads to membrane hyperpolarization, thereby reducing neuronal excitability (Chebib & Johnston, 1999). $GABA_A$ receptors are pentameric ligand-operated channels that are composed of three distinct subunits arranged in a 2α:2β:1γ stechiometry. Inhibitory GABAergic transmission is also mediated by metabotropic $GABA_B$ receptors, which are coupled to $G_{i/o}$ proteins and are widely

expressed in the CNS. These receptors function as obligate heterodimers, composed of $GABA_{B1}$ and $GABA_{B2}$ subunits. $GABA_B$ receptors mediate slow inhibitory postsynaptic potentials by activating $G_{i/o}$-regulated inwardly rectifying K^+ channels (GIRK), thereby promoting K^+ efflux and membrane hyperpolarization (Gascoigne et al., 2021). Recent studies have further suggested that $GABA_B$ receptors can also mediate increases in $[Ca^{2+}]_i$ in rat cortical neurons and mouse hippocampal granule cells. This signaling pathway involves the activation of $G_{i/o}$ proteins, which stimulate PLCβ, leading to hydrolysis of PIP_2 into $InsP_3$ and DAG. $InsP_3$ then activates IP_3Rs, resulting in ER Ca^{2+} release and depleting the ER Ca^{2+} stores, which activates SOCE and prolongs $GABA_B$ receptor-mediated Ca^{2+} signaling (Gascoigne et al., 2021). GABAergic signaling has also been observed in non-neuronal components of the NVU, including astrocytes and the cerebrovascular endothelium (Choi & Vasudevan, 2018; Mariotti, Losi, Sessolo, Marcon, & Carmignoto, 2016). Cortical blood vessels, along with perivascular astrocytes, receive GABAergic input from GABAergic interneurons (Kocharyan et al., 2008). Moreover, it has been well established that, during brain development, cerebral microcirculation guides the migration of GABAergic neurons from the dorsal to the basal telencephalon. Consequently, GABAergic neurons are capable of establishing bidirectional communication with the cerebral endothelium to coordinate neurovascular interactions (S. Li et al., 2018). The murine cerebral endothelium expresses multiple $GABA_A$ receptor subunits, including α1, α2, α6, β1, β2, β3, γ1, γ2, and γ3 (Shastry, Moning, Tyagi, Steed, & Tyagi, 2005), while functional evidence supports the expression of $GABA_B$ receptors (Shastry et al., 2005).

The growing interest in endothelial GABA receptors stems from the diverse functions they are proposed to fulfill within the NVU. Studies in the murine brain have demonstrated that the β3 subunit of $GABA_A$ receptors regulates cerebral angiogenesis, guides interneuron migration during embryonic development, and modulates CBF (Agrud et al., 2022). Preliminary evidence also showed that muscimol, a selective $GABA_A$ receptor agonist, induces an inward Cl^- current along with a transient increase in $[Ca^{2+}]_i$ in murine cerebrovascular ECs. Recent studies have highlighted that $GABA_A$ receptors may also exert metabotropic effects, whereby receptor activation stimulates intracellular Ca^{2+} release via the $InsP_3$ signaling pathway. During my bachelor's degree thesis, our research group demonstrated for the first time that both ionotropic $GABA_A$ receptors and metabotropic $GABA_B$ receptors mediate the Ca^{2+} response to GABA in the human brain microvascular endothelial cell line, hCMEC/D3 (Negri et al., 2022). By contrast, planar patch-clamp recordings failed to detect GABA-induced Cl^- currents (Negri et al., 2022). It was further shown that the $GABA_A$ receptors signal via a flux-independent mechanism to promote an increase in $[Ca^{2+}]_i$ through the functional interplay with $GABA_B$ receptors. The metabotropic Ca^{2+} response is shaped by ER Ca^{2+} release through IP_3Rs, lysosomal Ca^{2+} mobilization through TPCs, and SOCE activation (Negri et al., 2022), and is likely to

drive GABA-dependent endothelial activation in the brain microcirculation. These findings support a role for GABA receptors in sensing neuronal activity at the level of the human cerebral endothelium and contribute to a better understanding of their involvement at the NVU.

4.4 Purinergic receptors modulate ATP response in hCMEC/D3 cells

Purinergic signaling has been recognized as a critical regulatory system for the proper functioning of the NVU, contributing to the control of vasodilation and playing key roles in inflammatory responses (Bintig et al., 2012). Bintig et al., investigated the expression profile of purinergic receptors in the hCMEC/D3 cell line. Transcript analysis revealed the presence of the $P2Y_2$, $P2Y_6$, and $P2Y_{11}$ receptor subtypes, as well as $P2X_4$, $P2X_5$, and $P2X_7$, at the mRNA level. Functionally, purinergic stimulation of hCMEC/D3 cells induced intracellular Ca^{2+} signaling exclusively via the $P2Y_2$ receptor, which mediated calcium release from intracellular stores. This $P2Y_2$-dependent signaling pattern was similarly observed in primary cultured rat BBB ECs (Bintig et al., 2012). These findings demonstrate that the human BBB ECs exhibit a purinergic receptor repertoire comparable to that of their rat counterparts (Bintig et al., 2012). Moreover, liposomes functionalized with an ApoE-derived peptide (mApoE) and phosphatidic acid (PA) (referred to as mApoE-PA-LIP) were studied to clarify whether they could influence ATP-dependent Ca^{2+} dynamics in cultured hCMEC/D3 (Forcaia et al., 2021). Pre-treatment with mApoE-PA-LIP significantly increased both the duration and the area under the curve (A.U.C.) of ATP-evoked Ca^{2+} waves in hCMEC/D3 cells and astrocytes. Notably, mApoE-PA-LIP enhanced ATP-induced intracellular Ca^{2+} signaling even under $0Ca^{2+}_o$, suggesting that the observed increase in intracellular Ca^{2+} response is primarily attributable to release from intracellular stores (Forcaia et al., 2021). Furthermore, inhibition of SERCA activity using cyclopiazonic acid (CPA) abolished ATP-induced Ca^{2+} waves, indicating that $P2Y_2$ receptors predominantly mediate the mApoE-PA-LIP-induced enhancement of Ca^{2+} signaling (Forcaia et al., 2021). These findings support the conclusion that mApoE-PA-LIP modulate ATP-evoked intracellular Ca^{2+} dynamics via $InsP_3$-dependent ER Ca^{2+} release. As P2Y receptors are considered promising pharmacological targets for the treatment of cognitive dysfunction and exhibit neuroprotective roles in neuroinflammatory conditions, the ability of mApoE-PA-LIP to potentiate purinergic signaling may help mitigate Aβ-induced vasoconstriction and CBF reduction (Forcaia et al., 2021).

4.5 Histamine 1 Receptor induces intracellular Ca^{2+} oscillations and NO release in hCMEC/D3 cells

Histamine is a biogenic amine involved in numerous physiological and pathological processes, including inflammation, vascular permeability, gastric acid secretion, and vascular tone regulation (Panula, 2021). Histamine is produced in the brain by a group of tuberomamillary neurons in the posterior hypothalamus and mast cells in different parts of the brain (Panula, 2021). It is now

established that the 41 histaminergic TMN system regulates multiple functions within the central nervous system, such as neuronal excitability and synaptic plasticity, sleep and wakefulness, cognition, feeding and energy balance, while histamine dysfunction has been reported in sleep and motor disorders, Alzheimer's disease, schizophrenia, multiple sclerosis and addictive behaviors (1-3). Histamine released by tuberomamillary neurons exerts its action through at least three types of G-protein coupled histamine receptors (HRs), namely H1Rs, H2Rs and H3Rs, which are widely expressed in neuronal and glial cells. Conversely, H4Rs has been mainly described in peripheral tissues, such as leukocytes and bone marrow. Notably, H1Rs and H2Rs were also found in the vascular wall of human cerebral circulation, which is consistent with the innervation of cerebral blood vessels by histaminergic fibers. Early investigations revealed that histamine induces vasodilation in human cerebral, meningeal and temporal arteries via endothelial H1Rs which result in the downstream production of NO, the most powerful vasorelaxing agent in cerebral circulation. A recent investigation revealed that H1Rs mediate histamine-induced intracellular Ca^{2+} oscillations in the hCMEC/D3 cell line (Berra-Romani et al., 2019). Similar to GABA, the oscillatory Ca^{2+} response to histamine is shaped by ER Ca^{2+} release through $InsP_3Rs$, lysosomal Ca^{2+} mobilization through TPCs, and SOCE activation. Furthermore, histamine-induced intracellular Ca^{2+} spikes lead to robust NO release (Berra-Romani et al., 2019), which is likely to modulate the hemodynamic response to neuronal activity in the human brain microcirculation.

CHAPTER 5: AIMS OF THE THESIS

In the Thesis, we aim to provide further insights into the mechanisms shaping intracellular Ca^{2+} dynamics and NO release in hCMEC/D3 cells. We first explored the ionic bases of their resting V_M, which may change in response to neuronal activity and thereby modulate the driving-force for Ca^{2+} entry. Then, we assessed the Ca^{2+} response to a reduction in $[Na^+]_o$, which can occur during intense neuronal activity or brain disorders. Finally, we demonstrated that the lysosomal TRPML1 channel can be activated by $PI(3,5)P_2$ to promote inter-organellar Ca^{2+} cross-talk and ER Ca^{2+} refilling, which is critical to sustaining neurotransmitters-induced Ca^{2+} signals at the human BBB. The physiological relevance of $[Na^+]_o$-induced and TRPML1-mediated Ca^{2+} signals was evaluated by measuring Ca^{2+}-dependent NO release.

CHAPTER 6: METHODS

6.1 Cell culture

The human cerebral microvascular endothelial cells (hCMEC/D3) (Cat. #CLU512-A) were purchased from Cedarlane Labs (Burlington, Ontario, Canada). hCMEC/D3 were cultured with EBM-2 medium (Cat. #190860, Lonza, Basel, Switzerland) supplemented with 5% Fetal Bovine Serum (Cat. #124830, Gibco - Thermo Fisher Scientific, Waltham, Massachusetts, USA), 1% Chemically Defined Lipid Concentrate (Cat. #11905031, Life Technologies, Carlsbad, California, USA), 5 µg/mL Ascorbic Acid (Cat. #A4544, Merck KGaA, Darmstadt, Germany), 1 ng/mL human Basic Fibroblast Growth Factor (bFGF; Cat. #F0291, Merck KGaA, Darmstadt, Germany, 10 mM HEPES (Cat. #ECM0180D, Euroclone S.p.A, Milan, Italy) and 1.4 ng/mL Hydrocortisone (Cat. #H0135, Merck KGaA, Darmstadt, Germany). The cells were seeded at a concentration of 20,000 cells/cm^2 and grown in tissue culture flasks coated with 150 µg/mL rat tail Collagen type 1 (Cat. #C3867, Merck KGaA, Darmstadt, Germany) then were cultured at 37°C, 5% CO_2 saturated humidity incubator.

6.2 Solutions

Ca^{2+} and NO imaging experiments were conducted in extracellular physiological salt solution (PSS), composed of 150 mM NaCl, 6 mM KCl, 1.5 mM $CaCl_2$, 1 mM $MgCl_2$, 10 mM Glucose, 10 mM HEPES. In the Na^+-free solution ($0Na^+$), the extracellular Na^+ was substituted with 150 mM NMDG (Cat. #66930, Merck KGaA, Darmstadt, Germany) or choline chloride (Cat. #C1879, Merck KGaA, Darmstadt, Germany). In experiments requiring the removal of extracellular Ca^{2+} ($0Ca^{2+}_o$), Ca^{2+} was substituted with 2 mM NaCl (in PSS) or 2 mM NMDG or choline chloride (in $0Na^+_o$), and 0.5 mM EGTA was added. Solutions were titrated to pH 7.4 with NaOH. Finally, an osmolality of 300-310 mOsm/L was measured with an osmometer (Wescor 5500, Logan, Utah, USA).

Electrophysiology recordings were conducted using the following solutions in **Table 1** and **Table 2**.

Table 1
Intracellular solutions (in mM).

Solution	NaCl	KCl	EGTA	K-Fluoride	Cs-Fluoride	Cs-Chloride
1	10	50	20	60	0	0
2	10	0	20	0	60	50

All solutions also contained 10 mM Hepes and were titrated to pH 7.2 with, respectively, KOH and CsOH.

Table 2
Extracellular solutions (in mM).

Solution	NaCl	$CaCl_2$	Na-gluconate	NMDG-Cl
PSS	140	2	0	0
$0Na^+$	0	2	0	150
40 mM Cl^-	33	2	107	0

All solutions also contained 10 mM Hepes, 1 mM $MgCl_2$, 10 mM Glucose, 4 mM KCl and were titrated to pH 7.2 with KOH and NaOH.

6.3 Automated patch-clamp electrophysiology

The bioelectrical activity of hCMEC/D3 cells was measured by using the Port-a-Patch planar patch-clamp system (Nanion Technologies,Munich, Germany) in the whole-cell configuration at room temperature (22 ◦C), according to Nanion's standard procedure for the Port-a-Patch. Cultured hCMEC/D3 cells (2–3 days after plating) were detached with Detachin and suspended at a cell density of 1–5 × 106 cells/mL in external recording solution (**Table 1**). Suspended cells were placed on the NPC© chip surface, and the whole cell configuration was achieved. The successful rate of gigaseals recordings was around 70 % by paying attention to replacing the NPC© chip surface after each attempt or recording and to change the recording electrode every month. The internal recording solutions were either K^+ or Cs^+ based (**Table 1**: solutions 1 and 2, respectively) and were deposited in recording chips, having resistances of 3–5 MΩ. Whole-cell membrane potentials and currents were recorded by using an EPC-10 patch-clamp amplifier (HEKA, Munich, Germany) and the PatchMaster software (HEKA, Munich, Germany). Immediately after the whole-cell configuration was established, the cell capacitance (CM) and the series resistances (8.0 ± 0.2 MΩ, 4.6–9.9 MΩ; n=57) were measured. During records, these two parameters were measured, and if exceeding % with respect to the initial value, the experiment was discontinued (Berra-Romani et al., 2023). Liquid junction potential and capacitive currents were cancelled using the automatic compensation of the EPC-10. Data were filtered at 10 kHz and sampled at 5 kHz. In the current-clamp mode, the resting V_M was measured immediately after having obtained the whole-cell configuration at zero pA holding current. In the voltage-clamp mode, the holding potential was maintained at - 80 mV and the current-to-voltage (I-V) relationship was measured by using the following voltage-protocol: 2.5 sec lasting steps ranging from - 140 mV to + 70 mV and spaced by 10 mV. Each recording lasted for no longer than 20 minutes.

6.4 Ca^{2+} imaging and NO imaging

hCMEC/D3 cells were plated on glass Collagen type I-coated coverslips at a density of 5,000 cells/cm^2 and maintained in a 37°C, 5% CO_2 saturated humidity incubator for 24-48 hours. Then, the cells were loaded with the ratiometric Ca^{2+}-fluorophore Fura-2 acetoxymethyl ester (2 µM Fura-2/AM; Thermo Fisher Scientific, Waltham, Massachusetts, USA) in PSS for 30 minutes at 37 °C and

5% CO_2 (De Bock et al., 2013). Cells were observed by an upright epifluorescence Axiolab microscope (Carl Zeiss, Oberkochen, Germany) with a Zeiss ×40 Achroplan objective (water-immersion, 2.0 mm working distance, 0.9 numerical aperture). For ratiometric Ca^{2+} measurements, every 3 seconds cells were excited alternately at 340 and 380 nm, and the emitted light was detected at 510 nm. The excitation filters were mounted on a filter wheel (Lambda 10, Sutter Instrument, Novato, California, USA). Custom software, working in the LINUX environment, was used to drive the camera (Extended-ISIS Camera, Photonic Science, Millham, UK) and the filter wheel, and to measure and plot online the fluorescence. For each experiment, from 10 up to 40 "regions of interest" (ROIs) have been selected, corresponding to single cells in the chosen image field. Each ROI was identified by a number. Since cell borders were not clearly identifiable, a ROI may not include the whole cell or may include part of an adjacent cell. Adjacent ROIs never superimposed. $[Ca^{2+}]_i$ was monitored by measuring, for each ROI, the ratio of the mean fluorescence emitted at 510 nm when exciting alternatively at 340 and 380 nm (F_{340}/F_{380}). An increase in $[Ca^{2+}]_i$ causes an increase in the ratio. The experiments were performed at room temperature (23 °C).

The evaluation of NO release in hCMEC/D3 cells was performed loading the cells with the Amino-5'-methylamino-2',7'-difluoroscein diacetate (1 μM, DAf-FM DA) for 60 min in PSS at 37°C as illustrated in (Negri et al., 2022). The NO signals were measured with the same setup described above for Ca^{2+}, but with a different filter set, i.e., excitation at 480 nm and emission at 535 nm wavelength (emission intensity denoted as NOi (F_{535}/F_0). The changes in DAF-FM fluorescence evoked by extracellular stimulation were recorded and plotted online every 5 s.

The cellular production of NO was reported as relative fluorescence (F/F_0) of DAF-FM DA, where F is the fluorescence intensity obtained during recordings and F_0 is the basal fluorescence intensity.

6.5 Gene silencing

Genetic deletion of SLC8A1 gene, which encodes for NCX, and HRH1, which encodes for H1R, were carried by using a similar approach to that described in (Qi, Lin, Hu, & Wei, 2023). hCMEC/D3 were transiently transfected with the siRNA targeting NCX (siRNA ID 109333, 100 nM final concentration) purchased from Thermo Fisher Scientific (Waltham, Massachusetts, USA) or with the siRNA targeting H1R (siRNA sc-35563, 100 nM final concentration) purchased from Santa Cruz Biotechnology (Dallas, Texas, USA) by using the Lipofectamine™ RNAiMAX Transfection Reagent (Thermo Fisher Scientific, Waltham, Massachusetts, USA) protocol in Opti-MEM™ I Reduced Serum Medium (Thermo Fisher Scientific, Waltham, MA, USA), according to manufacturer's instructions. 4 hours after transfection, the siRNA-lipid complex was removed and fresh culture media containing was added to the cells. Cells were then kept in incubator at 37 °C and 5% CO_2 and allowed to grow according to the protocol to be used.

Genetic deletion of MCOLN1, which encodes for TRPML1, was carried by using a similar approach to that described in (Berra-Romani et al., 2023; Negri et al., 2020). Cells were transiently transfected with the esiRNA targeting TRPML1 (EHU062561, MISSION® esiRNA, 100 nM final concentration) purchased from Merck (Merck KGaA, Darmstadt, Germany) by using the Lipofectamine™ RNAiMAX Transfection Reagent (Thermo Fisher Scientific, Waltham, MA, United States) protocol in Opti-MEM™ I Reduced Serum Medium (Thermo Fisher Scientific, Waltham, MA, United States), according to manufacturer's instructions. 4 h after transfection, the esiRNA-Lipofectamin complex was eliminated and fresh culture media containing 5% FBS was added to the cells. Cells were then kept in incubator at 37°C and 5% CO2 and allowed to grow according to the protocol to be used. The effectiveness of silencing was determined by immunoblotting and the silenced hCMEC/D3 cells were used 48 h after transfection.

6.6 Western Blotting

hCMEC/D3 cells were seeded on a 6-well culture plate and grown to a confluency of 70%–80% (37°C, 5% CO_2). According to the protocol described above, cells were then silenced for the candidate gene and after 48h scraped with RIPA buffer (Pierce® RIPA Buffer, Thermo Fisher Scientific, Waltham, Massachusetts, USA) and protease inhibitor cocktail (Halt™ Protease Inhibitor Cocktail, 1:100, Thermo Fisher Scientific, Waltham, Massachusetts, USA). Lysates were centrifuged at 4 °C for 15 min at 13,000× g. Protein concentrations were determined by using a Bicinchoninic Acid (BCA) kit (Merck KGaA, Darmstadt, Germany) following the manufacturer's instructions. 20 µg of lysates were resuspended in SDS loading buffer, heated 30 min at 37 °C and then separated on 4%–15% Mini-PROTEAN TGX Precast Protein Gels Bio-Rad (BioRad, Hercules, California, USA). Then, the proteins were transferred out of the gel on to the PVDF Membrane (Trans-Blot Turbo Transfer Pack, Bio-Rad, Hercules, California, USA) with the Trans-Blot Turbo Transfer apparatus (BioRad, Hercules, California, USA). Membranes were blocked by incubation for 1 hour at room temperature in TBST (20 mM Tris, 150 mM NaCl, 0.1% Tween 20, pH 7.6) 5% BSA solution and then incubated in agitation overnight at 4 °C with primary antibodies: anti-NCX monoclonal antibody (Cat. #MA3-926, Thermo Fisher Scientific, Waltham, Massachusetts, USA), 1:200 in TBST 5% BSA 0.02% sodium azide; anti-H1R (Cat. #sc-35563, Santa Cruz, Dallas, Texas, USA), 1:500 in TBST 5% BSA 0.02% sodium azide; anti-Vinculin (Cat. #FNab09800, Fine Test, Wuhan, Hubei, China), 1:2,000 in TBST 5% BSA 0.02% sodium azide; anti-β-Actin-Peroxidase antibody (Cat. #A385416, Merck KGaA, Darmstadt, Germany), 1:1,000 in TBST 5% BSA 0.02% sodium azide. Membranes were then washed with TBST and incubated with the appropriate HPR–conjugated antibody (anti-mouse Cat. #31430,1:20,000 in TBST 5% BSA; Thermo Fisher Scientific, Waltham, Massachusetts,

United States). Protein expression was evaluated by using Fiji (ImageJ software, Wayne Rasband, NIH, Bethesda, Maryland, USA,).

For the TRML1 western blot, cells were seeded on a 6-well culture plate, grown to a confluency of 70%–80%, and then silenced or not, according to the protocol described below. For cell lysis, plates were kept on ice and cells were washed twice in ice-cold PBS, scraped with RIPA buffer (Pierce® RIPA Buffer, Thermo Fisher Scientific, Waltham, MA, United States) and protease inhibitor cocktail (Halt™ Protease Inhibitor Cocktail, 1:100, Thermo Fisher Scientific, Waltham, MA, United States). Lysates were vortexed and kept on ice for 10 min, then centrifuged at 4 °C for 15 min at 13,000× g. Protein concentrations were determined by using a Bicinchoninic Acid (BCA) kit (Merck KGaA, Darmstadt, Germany) following the manufacturer's instructions. 20 µg of lysates were resuspended in SDS loading buffer, heated 30 min at 37 C and then separated on 4%–15% Mini-PROTEAN TGX Precast Protein Gels Bio-Rad (Bio-Rad, Hercules, CA; United States). Then, the proteins were transferred out of the gel on to the PVDF Membrane (Trans-Blot Turbo Transfer Pack, Bio-Rad, Hercules, CA; United States) with the Trans-Blot Turbo Transfer apparatus (BioRad, Hercules, CA; United States). Membranes were blocked by incubation for 1 h at room temperature in TBST (20 mM Tris, 150 mM NaCl, 0.1% Tween 20, pH 7.6) 5% BSA solution and then incubated in agitation overnight at 4 °C with rabbit anti–TRPML1 (#ACC-081, 1:200 in TBST 5% BSA 0.02% sodium azide; Alomone, Jerusalem, Israel) and anti-β-Actin-Peroxidase (#A385416, 1:1,000 in TBST 5% BSA 0.02% sodium azide; Merck KGaA, Darmstadt, Germany) antibodies. Membranes were then washed with TBST and incubated with the appropriate HPR–conjugated antibody (antirabbit HRP #31460, 1:2,000 in TBST 5% BSA; Thermo Fisher Scientific, Waltham, MA, United States). Differences in protein expression was evaluated by using Fiji (ImageJ software).

6.7 Immunofluorescence

Cells were cultured on Collagen Type I (#C3867, Merck KGaA, Darmstadt, Germany) coated glass coverslips and used after 80%– 90% confluency. Cells were washed and then incubated with LysoTracker™ Red DND-99 (#L7528, 50 nM; Thermo Fisher Scientific, Waltham, MA, United States) for 1 h. After incubation, cells were washed twice with Hanks' Balanced Salt Solution (HBSS), fixed in 4% paraformaldehyde at room temperature for 10 min and permeabilized with 0.1% Triton X-100 in PBS for 10 min. Cells were then blocked with 1% BSA in PBS and incubated overnight at 4 °C with the following primary antibodies: anti-TRPML1 (#ACC-081; Alomone Labs, Jerusalem, Israel) 1:200 in TBST 1% BSA. Bound antibodies were detected with Alexa Fluor secondary antibodies (#A11008, #A21235, 1:500, Alexa FluorTM 488; Thermo Fisher Scientific, Waltham, MA, United States). Images were collected on a Leica SP8 Confocal scanning microscope using oil immersion 60x (HC PL APO 63x/1.40 OIL CS2 UV, Leica, Wetzlar, Germany) objectives.

6.8 Statistical analysis

Regarding the second chapter of the results: following a treatment, four types of Ca^{2+} responses have been identified in hCMEC/D3 cells: (I) No Response (NR), i.e., no changes in the baseline indicating resting [Ca^{2+}]; (II) Single Ca^{2+} spike (SC), i.e., a rapid Ca^{2+} transient; (III) Slow Rising Increase (SRI), i.e., slow but sustained over the time [Ca^{2+}] increase; (IV) Oscillations (O), i.e., more than one Ca^{2+} spike.

Regarding all the Ca^{2+} and NO recordings, all the data have been obtained from at least three independent experiments on hCMEC/D3 cells and at least 80 cells, for each condition. The number of Ca^{2+} response types, was normalized to the total number of cells analysed, and the response percentages were thus derived. Data were analyzed with GraphPad Prism 7 (GraphPad Software, Inc., La Jolla, California, USA). Preliminary Shapiro-Wilk test was performed to check the normal distributions of each dataset: accordingly, statistical analysis was performed by using either the non-parametric tests (Mann-Whitney test or Kruskal-Wallis test) or parametric tests (Student's t-test or One-way ANOVA test). A *p*-value of <0.05 was considered significant.

All the electrophysiological data were obtained by using the Patch-Master software. Pooled data are given as mean ± SEM. Comparisons between two groups were done using Student's t-test, whereas multiple comparisons were performed using ANOVA with the Bonferroni post-hoc test. P-values less than 0.05 were considered statistically significant.

6.9 Chemicals

SEA0400 (Cat. #SML2054), U-73122 (Cat. #662035), 2-APB (Cat. #D9754), CPA (Ciclopiazonic acid; Cat. #C1530), Pyrilamine maleate (Cat. #P5514) and Histamine (Cat. #H7125) were purchased from Merck GKaA (Darmstadt, Germany). ML-SAI (# SML0627), ML-SI3 (GW405833 hydrochloride; BTP-2 (# 203890 CRAC channel inhibitor BTP2), Pyr6 (#SML1241), were purchased from Merck GKaA (Darmstadt, Germany). BAPTA/AM (#196419) and L-NIO (L-N^5-1-Iminoethyl ornithine, Dihydrochloride; # 400600) were purchased from Merck Millipore (Burlington, Massachusetts, United States). Nigericin sodium salt (# 4,312) was purchased from Tocris Bioscience (Bristol, United Kingdom). (Salt Lake City, United States). All other chemicals were of analytical grade and purchased from Sigma Chemical Co. (Milan, Italy).

CHAPTER 7: RESULTS

PART 1: Evaluation of biophysical properties of the membrane

7.1 Measurement of the resting V_M of hCMEC/D3 cells by using the APC technology

The resting V_M of hCMEC/D3 cells, when measured in the presence of a standard extracellular solution (PSS, Table 1) and of a K^+-based intracellular solution (Table 1, solution 1), ranged between -70 mV and +4 mV, the average value being -16.7 ± 4.5 mV (n=19) (**Figure 12A**). The C_M was 14.1 ± 1.8 pF (n=19, range 4.4-27.5 pF). The inward-rectifier K^+ channels have long been known to maintain the endothelial V_M at negative potentials ranging between -70 mV and -60 mV (Voets et al., 1996) . Cations, such as Cs^+ and Ba^{2+}, have long been known to block K^+ currents by obstructing the selectivity filter of K^+-selective channels. However, the replacement of intracellular K^+ with an equimolar amount of Cs^+ (Table 1, solution 2) did not affect the wide scattering of the V_M, which ranged between -60 mV and +3 mV, and did not significantly affect the average V_M (-8.3 ± 2.1 mV, n=38; p=0.0567) (**Figure 12A**). These findings, although preliminary, suggest that the resting V_M of hCMEC/D3 cells is not primarily maintained by a K^+ conductance. However, the resting V_M was reversibly hyperpolarized by lowering both the extracellular Na^+ concentration ($[Na^+]_o$) **(Figure 12B)** and the extracellular Cl^- concentration ($[Cl^-]_o$) (**Figure 12C**). Surprisingly, the superfusion of a hypertonic solution (100 mM mannitol) did not significantly ($p>0.05$) affect the resting V_M (**Figure 12D**), as reported in other ECs types (Nilius et al., 1994; Voets et al., 1996). Taken together, these findings confirm that the Port-a-Patch automated system is able to measure the resting V_M in hCMEC/D3 cells and to report its changes in response to ionic manipulation. Furthermore, these preliminary observations indicate that the resting V_M of hCMEC/D3 cells is primarily contributed by Na^+ and Cl^-.

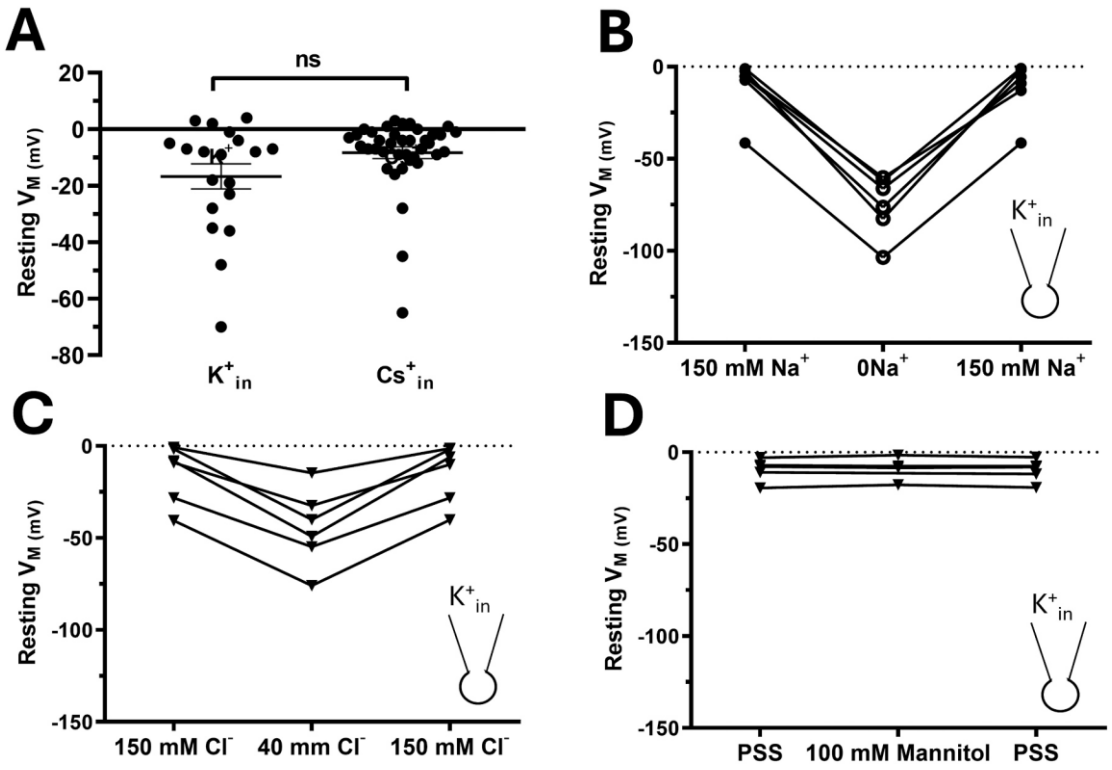

Fig 12. Measurement of the resting V_M in hCMEC/D3 cells. (**A**) Membrane potentials of the hCMEC/D3 cells measured in the current-clamp mode immediately after having obtained the whole-cell configuration in hCMEC/D3 cells perfused with a K^+-based intracellular solution (K^+_{in}) or a Cs^+-based intracellular solution (Cs^+_{in}). There is no significant difference between the two averages value. **(B)**, removal of extracellular Na^+ ($[0Na^+]_o$) caused a reversible hyperpolarization of the resting V_M. (**C**), reduction of the $[Cl^-]_o$ to 40 mM caused a reversible hyperpolarization of the resting V_M. (**D**), superfusion of a hypertonic extracellular solution enriched with 100 mM mannitol did not affect the resting V_M.

7.2 Measurement of the resting membrane currents in hCMEC/D3 cells

The resting membrane currents of hCMEC/D3 cells were measured by using the Port-a-Patch APC system by first using a K^+-based intracellular solution and a voltage-step protocol. **Figure 13A** shows that virtually no current could be measured at membrane potentials ranging from - 100 mV and -10 mV. At more positive depolarizing steps, the whole-cell recordings showed the appearance of a voltage-dependent current (**Figure 13A**), which conferred an outward rectified profile to the I-V relationship (**Figure 13B**). When intracellular K^+ was replaced by an equimolar amount of Cs^+, no inward current could still be detected at membrane potentials more negative than -10 mV (**Figure 13C**). However, depolarizations more positive than -20 mV evoked time-dependent outward currents that were significantly larger than those measured in the presence of intracellular K^+ (**Figure 13C**). Taken together, these findings confirm that the Port-a-Patch automated system is able to measure the

resting membrane currents in hCMEC/D3 cells and that K^+ channels do not play a prominent role in the control of their basal permeability.

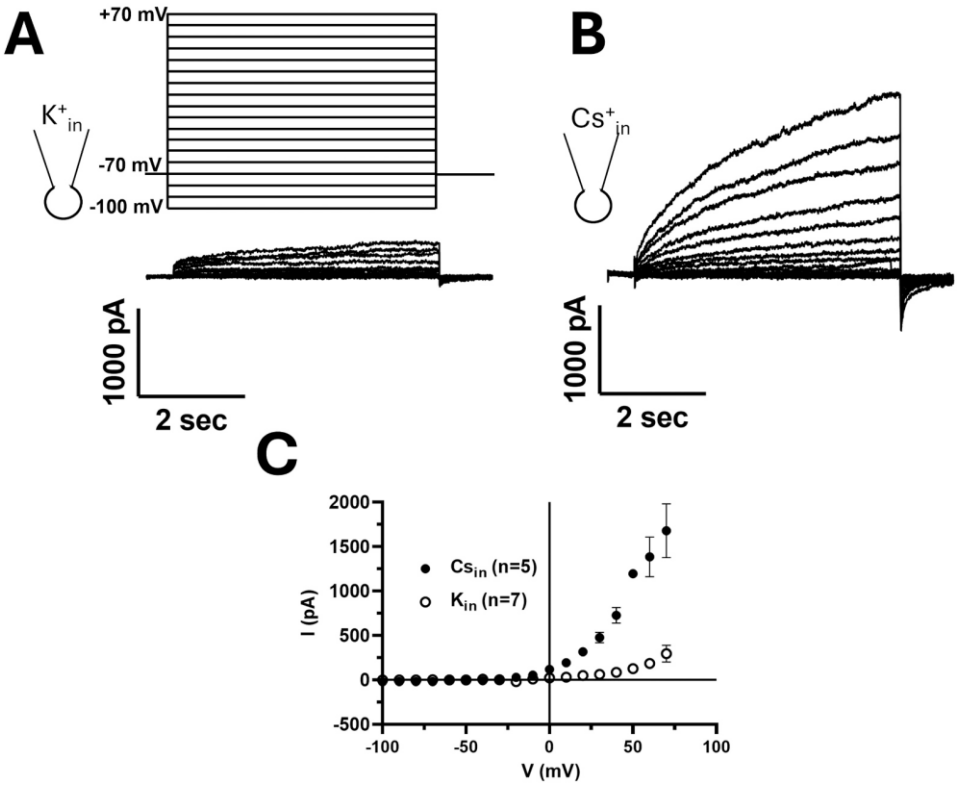

Fig. 13. Measurement of the resting membrane currents in hCMEC/D3 cells. **(A)** Whole-cell currents measured in the voltage-clamp mode after compensation of the C_M and the series resistance with a K^+-based intracellular solution. The voltage protocol has been described in the Materials and methods**. (B)** Whole-cell currents measured in the voltage-clamp mode after compensation of the C_M and the series resistance with a Cs^+-based intracellular solution. The voltage protocol has been described in the Materials and methods. (**C)** I-V relationship of the whole-cell currents measured in the presence of either a K^+- or a Cs^+-based intracellular solution.

PART 2: Evaluation of global Ca^{2+} dynamics in hCMEC/D3 cells: effects of extracellular Na^+ on NCX/H1R signaling pathway

7.3 Extracellular Na^+ reduction induces intracellular Ca^{2+} signals in hCMEC/D3 cells

The physiological $[Na^+]_o$ (150 mM) was replaced by the organic cation NMDG. Na^+ imaging in hCMEC/D3 cells loaded with the Na^+ -sensitive fluorophore, SBFI, confirmed that the removal of external Na^+ caused a reversible drop in the intracellular Na^+ concentration (**Data not shown**). The obtained Na^+-depleted solution ($0Na^+_o$) induced two main types of Ca^{2+} responses in hCMEC/D3 cells loaded with the ratiometric Ca^{2+}-sensitive fluorophore, Fura-2: a basal Ca^{2+} increase followed

by Ca^{2+} oscillations (**Figure 14A**) and a slow rising Ca^{2+} increase (SRI) sustained over the time (**Figure 14B**). The $0Na^{+}_{o}$-induced Ca^{2+} oscillations were reversible as they immediately faded upon restitution of extracellular Na^{+} (**Figure 14C**). Furthermore, they were unrelated to the specific use of NMDG, as the replacement of extracellular Na^{+} with choline chloride results in the same Ca^{2+} response (**Figure 14C**). The removal of extracellular Na^{+} activates the reverse mode of the NCX, thereby leading the extracellular Ca^{2+} entry and the intracellular Na^{+} exit from the cells. Therefore, to emphasize the contribution of NCX to these Ca^{2+} responses, we inhibited the NCX by using both a pharmacologic (SEA0400, 3 μM) and genetic (siNCX1) approach to inhibit NCX1, which is the NCX isoform expressed in hCMEC/D3 cells. (**Figure 14D-E**). Under these conditions, the SRI was abrogated in the majority of hCMEC/D3 cells (**Figure 14G**). Moreover, either in the presence of SEA0400 or of the siNCX, we still observed $0Na^{+}_{o}$-induced Ca^{2+} spikes, despite to a lesser extent compared to the control, i.e., only a single Ca^{2+} spike was observed in almost the totality of the responding hCMEC/D3 cells treated with the selective siNCX1 (**Figure 14G**). Whereas, in SEA-treated cells, up to a maximum of two Ca^{2+} spikes were observed, which therefore were considered as an oscillatory response. Nevertheless, most of the responding cells showed again only a single Ca^{2+} spike. Finally, to mimic the physiological changes in $[Na^{+}]_o$ that are likely to occur during intense neuronal activity, we conducted experiments by reducing Na^{+} out by 20 mM. We found that reducing the $[Na^{+}]_o$ from 150 mM to 135 mM evokes no Ca^{2+} response, whereas a reduction down to 130 mM is able to elicit intracellular Ca^{2+} oscillations in hCMEC/D3 cells (**Figure 14F**), as shown for $0Na^{+}_{o}$ (**Figure 14 G-H**). Taken together, these findings show that the removal of extracellular Na^{+} induces variable Ca^{2+} response in hCMEC/D3 cells that may involve different molecular mechanisms. The

SRI-type response is explained by the activity of the reverse mode NCX, while the onset of the $0Na^+_o$ -induced Ca^{2+} spikes is probably due to endogenous Ca^{2+} release.

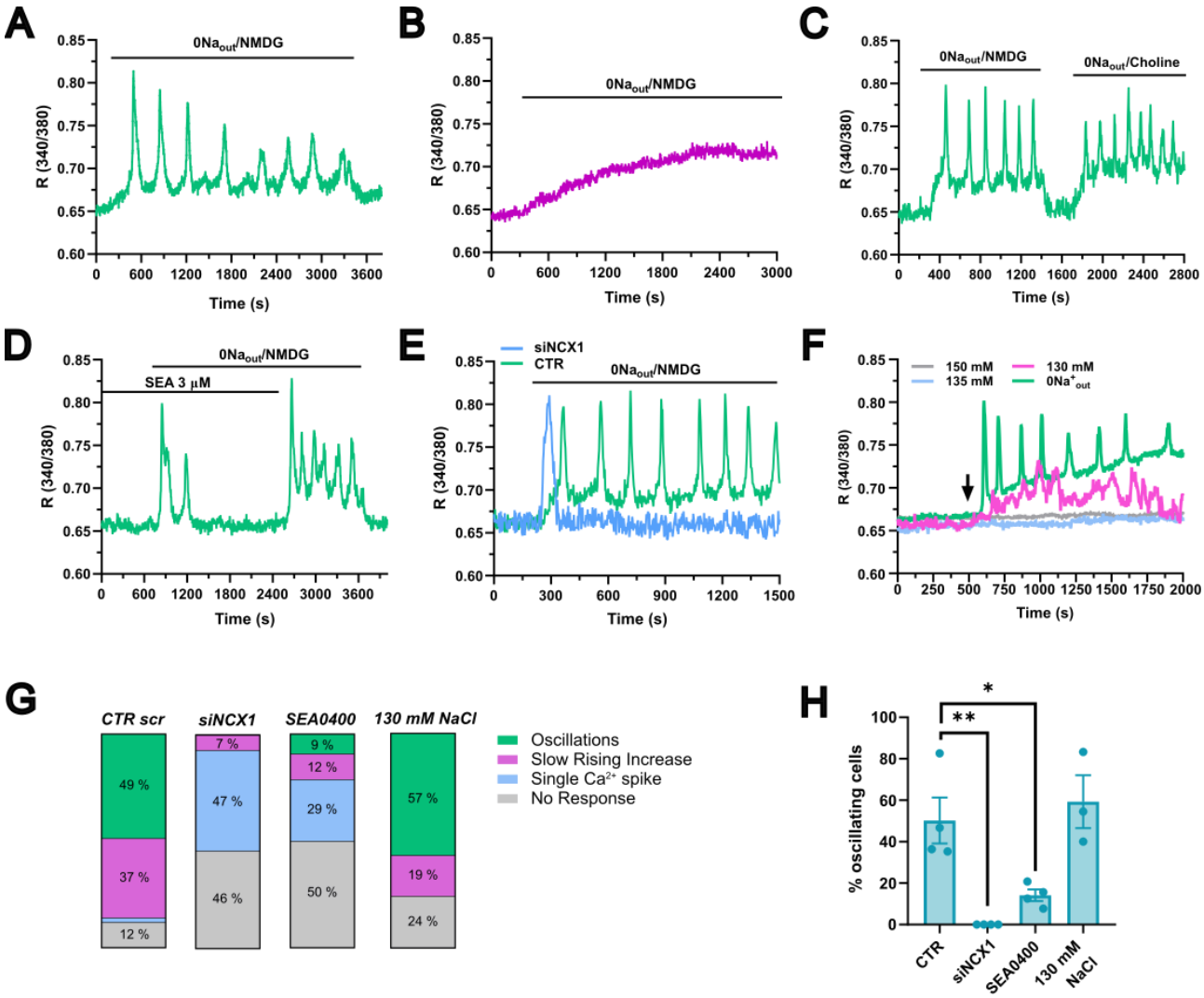

Figure 14. $0Na^+_o$ evokes an increase in $[Ca^{2+}]_i$ in hCMEC/D3 cells. ***(A)*** Representative intracellular Ca^{2+} oscillations evoked by $0Na^+_o$ perfusate. **(B)** Representative slow rising intracellular Ca^{2+}increase (SRI-type response) evoked by $0Na^+_o$ perfusate. **(C)** Representative Ca^{2+} trace showing that $0Na^+_o$-induced Ca^{2+} oscillations are independent on the base employed to replace extracellular Na^+. ***(D)*** Representative Ca^{2+} signal obtained after pharmacological inhibition (SEA 3 µM) of NCX. **(E)** Representative Ca^{2+} signals obtained after genetic inhibition of NCX (siNCX) and the corresponding control (CTR) trace. **(F)** Representative Ca^{2+} signals induced by extracellular Na^+ reduction, starting from 150 mM up to 135 mM (blue), 130 mM (pink) and $0Na^+_o$ (green) **(G)** Analysis of the response percentage obtained after $0Na^+_o$ treatment in scramble cells (CTR scr) and upon either genetic (siNCX) and pharmacological (SEA0400) blockade of NCX, and in 130 mM Na^+_o. CTR scr, n = 94 cells; siNCX, n = 110 cells; SEA0400, n = 159 cells; 130 mM NaCl, n = 97 cells. **(H)** Percentage of cells showing an oscillatory Ca^{2+} response to: $0Na^+_o$ in CTR condition (CTR) and upon either genetic

(siNCX1) and pharmacological (SEA0400) blockade of NCX; a reduction from 150 mM to 130 mM of $0Na^+_o$. ** indicates $p < 0.005$, * indicates $p < 0.05$ (one-way Anova test followed by Dunn's post hoc test).

7.4 Extracellular Ca^{2+} entry is necessary to trigger $0Na^+_o$-induced Ca^{2+} oscillations in hCMEC/D3 cells

Previous studies demonstrated that the removal of extracellular Na^+ induces intracellular Ca^{2+} release through the activation of phospholipase C (PLC) and $InsP_3Rs$ (Boitano, Woodruff, & Dirksen, 1997; Katritch et al., 2014; Koster, van Os, & Bindels, 1993). Therefore, to unveil a potential involvement of intracellular Ca^{2+} release in the $0Na^+_o$-induced Ca^{2+} oscillations in hCMEC/D3 cells, we performed experiments in the absence of extracellular Ca^{2+} ($0Ca^{2+}_{out}$). In such conditions, we did not obtain any Ca^{2+} response to the removal of extracellular Na^+ in ≈85% of hCMEC/D3 cells (**Figure 15A and Figure 15D**). The remaining cells (≈15%) displayed a single Ca^{2+} transient that was not followed by additional Ca^{2+} oscillations (**Figure 15A and Figure 15D**). Likewise, the removal of extracellular Ca^{2+} during ongoing oscillations immediately interrupt Ca^{2+} oscillations (**Figure 15B**).

The analysis of the Ca^{2+} responses revealed that although most of the examined cells did not respond to $0Na^+_o$ in absence of extracellular Ca^{2+}, a minority of cells were still able to evoke single Ca^{2+} spikes (**Figure 15C**). To further assess the role of extracellular Ca^{2+}, we pretreated the cells with 300 µM Gd^{3+}, which is a non-selective inhibitor of Ca^{2+} entry at this dose by interfering with both SOCE and TRP channels (Lodola, Laforenza, et al., 2017; Tolstykh, Cantu, Tarango, & Ibey, 2019). In the presence of 300 µM Gd^{3+}, the removal of extracellular Na^+ only induced the SRI, with a response percentage similar to that occurring in control conditions (**Figure 15F**), which was not accompanied by the spiking Ca^{2+} signal (**Figure 15C-D**), i.e., no Ca^{2+} oscillations were observed (**Figure 15E**). Taken together, these data indicate that extracellular Ca^{2+} is required for the oscillatory Ca^{2+} response to occur. However, NCX-mediated Ca^{2+} entry alone is not sufficient to trigger the Ca^{2+} spikes.

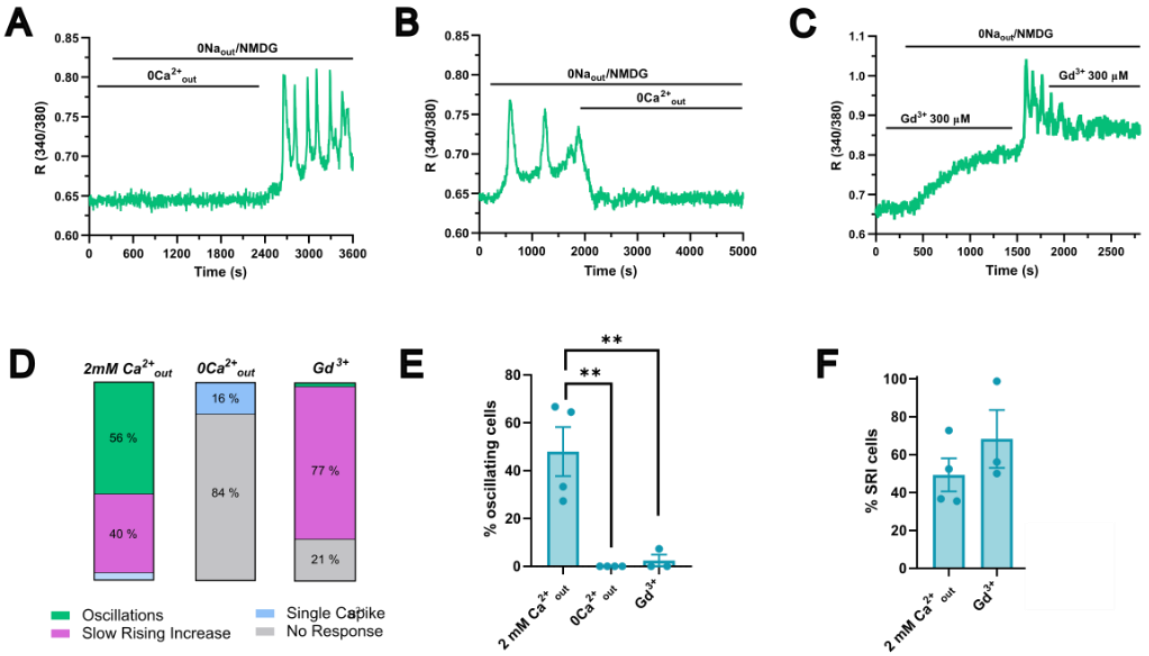

Figure 15. Extracellular Ca^{2+} entry in necessary to trigger $0Na^{+}_{o}$-induced Ca^{2+} oscillations in hCMEC/D3 cells. **(A)** Representative Ca^{2+} signal obtained in $0Na^{+}_{o}$ perfusate in absence of extracellular Ca^{2+} ($0Ca^{2+}_{out}$). **(B)** Representative Ca^{2+} trace showing that the removal of extracellular Ca^{2+} during ongoing oscillations immediately interrupt the Ca^{2+} response to $0Na^{+}_{o}$. **(C)** Representative Ca^{2+} trace showing that the pre-treatment with 300 µM Gd^{3+} prevents the $0Na^{+}_{o}$-induced Ca^{2+} oscillations. **(D)** Analysis of the response percentage obtained after $0Na^{+}_{o}$ treatment in presence (2 mM Ca^{2+}_{out}) and absence ($0Ca^{2+}_{out}$) of extracellular Ca^{2+}, and after the pre-treatment with 300 µM Gd^{3+}. 2 mM Ca^{2+}_{out}, n = 83 cells; $0Ca^{2+}_{out}$, n = 93 cells, Gd^{3+}, n = 153 cells. **(E)** Percentage of cells showing an oscillatory Ca^{2+} response to $0Na^{+}_{o}$ in presence (2 mM Ca^{2+}) and absence of extracellular Ca^{2+}, and following the pre-treatment with 300 µM Gd^{3+} (Gd^{3+}). ** indicates $p < 0.005$ (one-way Anova test followed by Dunn's *post hoc* test). **(F)** Percentage of cells showing an SRI in $[Ca^{2+}]_i$ in response to $0Na^{+}_{o}$ in control condition (2 mM Ca^{2+}) and after the following the pre-treatment with 300 µM Gd^{3+} (Gd^{3+}). The statistical Student's t-test found no significant difference between the two conditions.

7.5 $0Na^{+}_{o}$ –induced Ca^{2+} oscillations are triggered and sustained by $InsP_3$-dependent intracellular Ca^{2+} release in hCMEC/D3 cells.

The $InsP_3R/Ca^{2+}$ pathway is primarily responsible for intracellular Ca^{2+} release in many cell types including hCMEC/D3 cells (Abbott, Patabendige, Dolman, Yusof, & Begley, 2010; Berra-Romani et al., 2023; Weksler et al., 2013). Here, we treated hCMEC/D3 cells with 2-aminoethoxy diphenyl borate (2-APB; 50 µM), an $InsP_3R$ blocker and U-73122 (10 µM), a potent and selective PLC

inhibitor. In such conditions, an SRI-type Ca^{2+} response to $0Na^{+}_{o}$ was observed in all the responsive cells we analysed (**Figure 16B; Figure 16I**), whereas no Ca^{2+} response was observed in the absence of extracellular Ca^{2+} **(Figure 16C**). To further investigate the role of $InsP_3Rs$, we assessed the effect of Xestospongin C (XeC; 1 μM), which is another selective $InsP_3Rs$ inhibitor (Blatter, 2017). Similar to 2-APB, XeC converted the Ca^{2+} response to $0Na^{+}_{o}$ into an SRI (**Figure 16D; Figure 16I)**. We previously showed that U73343, an inactive structural analogue of the aminosteroid U73122, does not affect Ca^{2+} signaling in hCMEC/D3 cells (Zuccolo, Laforenza, et al., 2019). Herein, we confirm that U73343 (10 μM) does not interfere with $0Na^{+}_{o}$-induced intracellular Ca^{2+} oscillations in human cerebrovascular endothelial cells (**data not shown)**. Finally, we found that, in the presence of the G_q inhibitor, FR900359 (10 μM) (Groschner, Shrestha, & Fameli, 2017), the removal of extracellular Na^{+} induced an SRI in most hCMEC/D3 cells (**Figure 16D; Figure 16I)**. Consistent with the role of $InsP_3$-dependent ER Ca^{2+} mobilization, the treatment with the selective SERCA inhibitor, CPA (30 μM), during ongoing Ca^{2+} oscillations immediately interrupted the Ca^{2+} response to $0Na^{+}_{o}$ (**Figure 16E**), emphasizing that continuous $InsP_3R$-mediated ER Ca^{2+} release is necessary to sustain the Ca^{2+} response over time. We reasoned that, if ER Ca^{2+} mobilization is required to initiate and maintain the $0Na^{+}_{o}$-induced intracellular Ca^{2+} oscillations, the deprivation of extracellular Na^{+} was predicted to only trigger the SRI after depletion of the ER Ca^{2+} pool with CPA (Negri et al., 2022). In accord with this hypothesis, the removal of extracellular Na^{+}, immediately after the CPA-mediated ER Ca^{2+} emptying, evoked an SRI that reflects the activation of the reverse-mode NCX (**Figure 16F; Figure 16I**). Consistently, $0Na^{+}_{o}$ treatment in the presence of CPA failed to induce a detectable increase in $[Ca^{2+}]_i$ under $0Ca^{2+}$ conditions (**Figure 16G**). Overall, these data point out that $0Na^{+}_{o}$-induced oscillatory Ca^{2+} response are supported by $InsP_3$-mediated ER Ca^{2+} release.

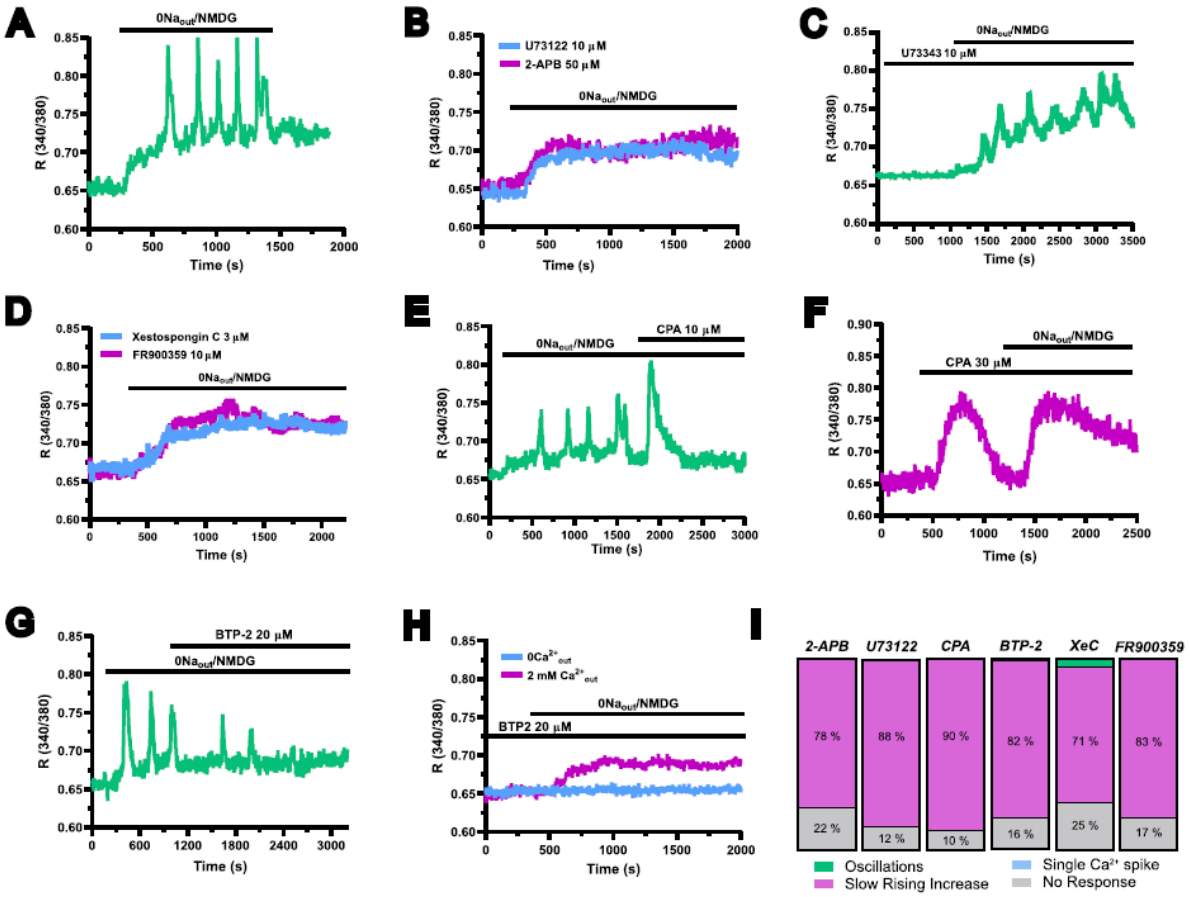

Figure 16. 0Na$^{+}_{o}$-induced Ca^{2+} oscillations in hCMEC/D3 cells are triggered and sustained by extracellular Ca^{2+} entry and intracellular Ca^{2+} release **(A)** Representative intracellular Ca^{2+} oscillations evoked by 0Na$^{+}_{o}$ perfusate. **(B)** Representative Ca^{2+} trace showing that the pre-treatment with U73122 (10 µM) and 2-APB (50 µM) prevents 0Na$^{+}_{o}$ -induced Ca^{2+} oscillations but not the SRI-type response. **(C)** Representative Ca^{2+} trace showing that the pre-treatment with U73343 (10 µM) does not affect 0Na$^{+}_{o}$ -induced Ca^{2+} oscillations. **(D)** Representative Ca^{2+} traces showing that the pre-treatment with XeC (1 µM) or FR900359 (10 µM) prevents 0Na$^{+}_{o}$ -induced Ca^{2+} oscillations but not the SRI-type response. **(E)** Representative Ca^{2+} signal showing 0Na$^{+}_{o}$ -induced Ca^{2+} oscillations interruption upon CPA (10 µM) treatment. **(F)** Representative Ca^{2+} signal showing that the pre-treatment with CPA (10 µM) prevents 0Na$^{+}_{o}$ -induced Ca^{2+} oscillations but not the SRI-type response. **(G)** Representative Ca^{2+} signal showing gradual curtailing of 0Na$^{+}_{o}$ -induced Ca^{2+} oscillations by the treatment with BTP-2 (20 µM). **(H)** Representative Ca^{2+} trace showing that the treatment with BTP-2 (20 µM) prevents 0Na$^{+}_{o}$ -induced Ca^{2+} oscillations but not the SRI-type response. **(I)** Analysis of the percentage response obtained after pre-treatment with 2-APB (n = 73 cells), or U73122 (n = 50 cells), or CPA (n = 50 cells), or-BTP-2 (n = 68 cells), or XeC (n = 50 cells), or FR900359 (n = 52 cells), to the stimulation with 0Na$^{+}_{o}$.

7.6 SOCE sustains $0Na^+_o$-induced Ca^{2+} oscillations in hCMEC/D3 cells

SOCE is the main pathway that sustains Ca^{2+} entry during ER Ca^{2+} release events through $InsP_3Rs$ in vascular ECs (Lodola, Laforenza, et al., 2017; Tolstykh et al., 2019; Zuccolo, Laforenza, et al., 2019), including hCMEC/D3 cells (Pafumi et al., 2015; Weksler et al., 2013). Orai1 serves as store-operated Ca^{2+} channel in hCMEC/D3 cells (Maione et al., 2022; Qi et al., 2023). Consistent with this, the acute application of 20 μM BTP-2 (**Figure 16H**), which is an established blocker of Orai1 (Blatter, 2017; Groschner et al., 2017; Longden et al., 2021) gradually curtailed $0Na^+_o$-induced Ca^{2+} oscillations. Likewise, pre-treatment with 20 μM BTP-2, or 10 μM Pyr6, which is another selective SOCE inhibitor (Soda et al., 2025) (**data not shown**), converted the complex Ca^{2+} signature induced by $0Na^+_o$ into an SRI in most hCMEC/D3 cells (**Figure 16I**). These data indicate that SOCE, which can be activated downstream of ER Ca^{2+} release through $InsP_3Rs$ in hCMEC/D3, is necessary to sustain $0Na^+_o$-induced Ca^{2+} oscillations over time.

7.7 $0Na^+_o$–induced Ca^{2+} oscillations are triggered by H1R in hCMEC/D3 cells

Na^+ has been described as an endogenous regulator of Class A G_qPCRs, which are responsible for the activation of the $InsP_3/Ca^{2+}$ pathway (Agasid, Sorensen, Urner, Yan, & Robinson, 2021; Ferre et al., 2023; Zarzycka, Zaidi, Roth, & Katritch, 2019). Moreover, previous studies indicate that Na^+ depletion may increase the basal G_qPCR activity in the absence of agonist, suggesting that Na^+ may act as a negative modulator of G_qPCR activation (Ferre et al., 2023; Zarzycka et al., 2019). In order to investigate the molecular identity of the Na^+ "sensor" that initiates intracellular Ca^{2+} release in hCMEC/D3, we stimulated cells with the neuromodulator histamine (10 μM), previously demonstrated to trigger Ca^{2+} oscillations in hCMEC/D3 cells through the activation of the Histamine Receptor 1 (H1R) (Kurauchi, Hisatsune, Seki, & Katsuki, 2016), in absence of extracellular Na^+. In fact, $0Na^+_o$ significantly increased the Ca^{2+} response to histamine (**Figure 17A-B**). Interestingly, pre-treatment with pyrilamine (10 μM) (**Figure 17C-D**), a selective inhibitor of H1R, as well as the genetic silencing of H1R (**Figure 17C-D, 17 E-F**), prevent the $0Na^+_o$-induced Ca^{2+} oscillations.

These data suggest that H1R participates in the intracellular Ca^{2+} release that triggers $0Na^+_o$-induced Ca^{2+} oscillations. The decrease in intracellular Na^+ concentration could influence the basal activity of H1Rs, activating them even without the presence of the agonist (Agasid et al., 2021; Ferre et al., 2023; Zarzycka et al., 2019).

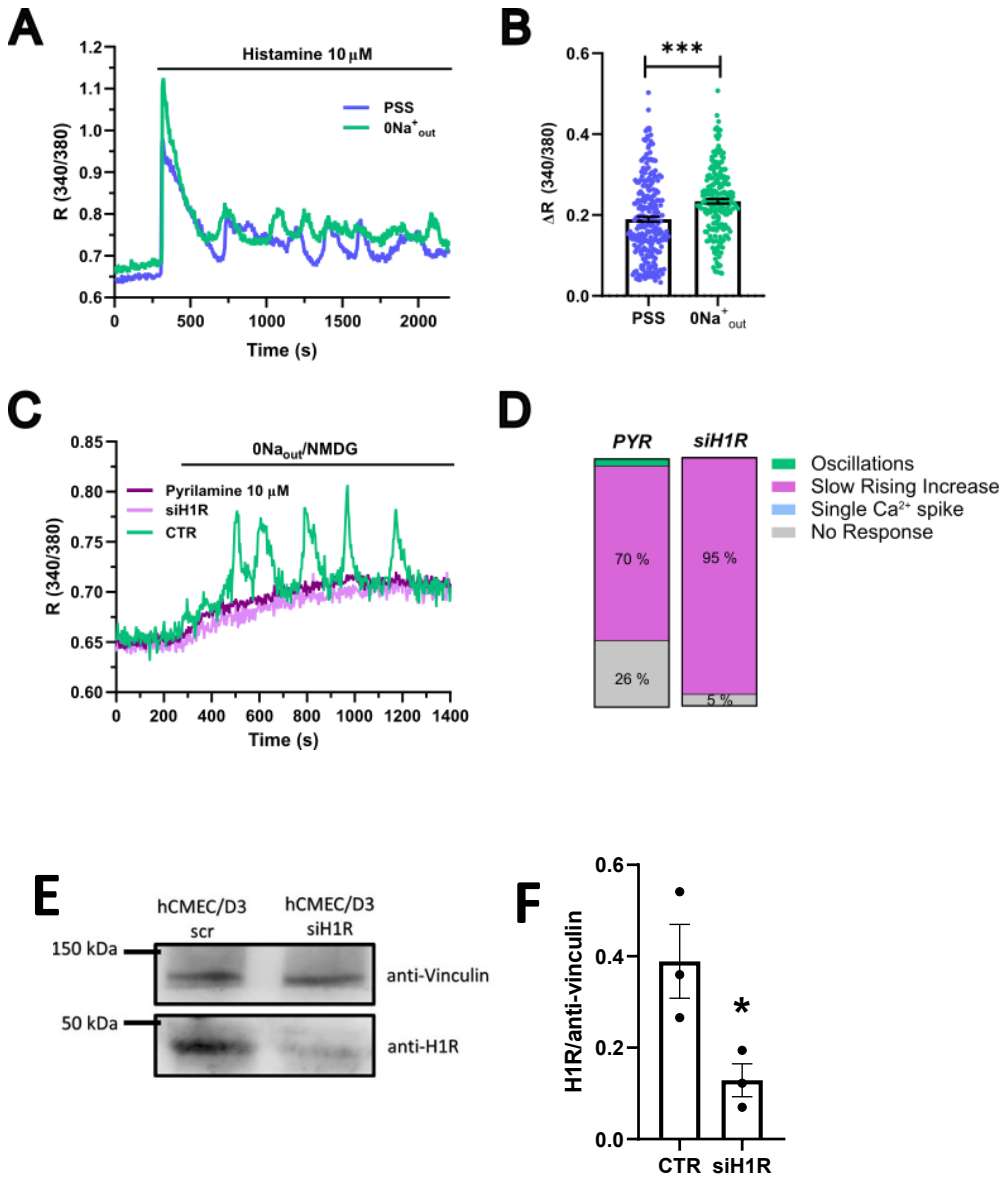

Figure 17. $0Na^+_o$-affects H1R-mediated Ca^{2+} signals in hCMEC/D3 cells. **(A)** Representative intracellular Ca^{2+} signals induced by histamine (50 µM) in presence (PSS) or absence ($0Na^+_o$) of extracellular Na^+. **(B)** Mean ± SEM of the peak amplitude of $0Na^+_o$-induced Ca^{2+} responses. *** indicates $p < 0.0001$ (Mann-Whitney test). **(C)** Representative Ca^{2+} signals obtained after genetic (siH1R) and pharmacological (pyrilamine 10 µM) blockade of H1R and control Ca^{2+} trace (CTR). **(D)** Analysis of the percentage response obtained after $0Na^+_o$ treatment in hCMEC/D3 cells subjected to genetic (siH1R) or pharmacological (PYR) inhibition of H1R. PYR, $n = 105$ cells; siH1R, $n = 43$ cells. (**E**) Representative western blotting analysis of the HR1 protein expressed in hCMEC/D3 (Ctrl) and hCMEC/D3 transfected with the specific siHR1. Major bands of the expected molecular weights (MW) for HR1 (50 kDa) and the loading control protein anti-vinculin (150 kDa) is indicated. (**F**) Mean ± SEM of the HR1/anti-vinculin ratio expression of four independent western blotting experiments. ** indicates $p < 0.005$ (Student's t-test).

7.8 $0Na^+_o$–induced Ca^{2+} oscillations lead to NO release

A series of recent studies have shown that several neurotransmitters and neuromodulators, including histamine (Berra-Romani et al., 2020), induce NO release through an increase in $[Ca^{2+}]_i$ in hCMEC/D3 cells. It is known than an increase in $[Ca^{2+}]_i$ can result in the production of the vasoactive mediator NO in hCMEC/D3 cells (Berra-Romani et al., 2023; Chauvet et al., 2016; Kurauchi et al., 2016; Pafumi et al., 2015; Verkhratsky, Trebak, Perocchi, Khananshvili, & Sekler, 2018). For these reasons, we investigated whether $0Na^+_o$-induced Ca^{2+} oscillations could also induce NO release by loading cells with the NO-sensitive fluorophore, DAF-FM. We found that $0Na^+_o$ induces a slow, but sustained increase in DAF-FM fluorescence (**Figure 18A**), indicative of NO release (Berra-Romani et al., 2023; Chauvet et al., 2016; Kurauchi et al., 2016; Pafumi et al., 2015; Verkhratsky et al., 2018), which was significantly inhibited by BAPTA-AM (20 µM; **Figure 18A-B**), a membrane permeable buffer of intracellular Ca^{2+} levels, and by L-NIO (50 µM; **Figure 18A-B**), a specific eNOS inhibitor. Therefore, the $0Na^+_o$ perfusate is able to trigger Ca^{2+}-dependent NO production in the human cerebrovascular endothelial cell line, hCMEC/D3.

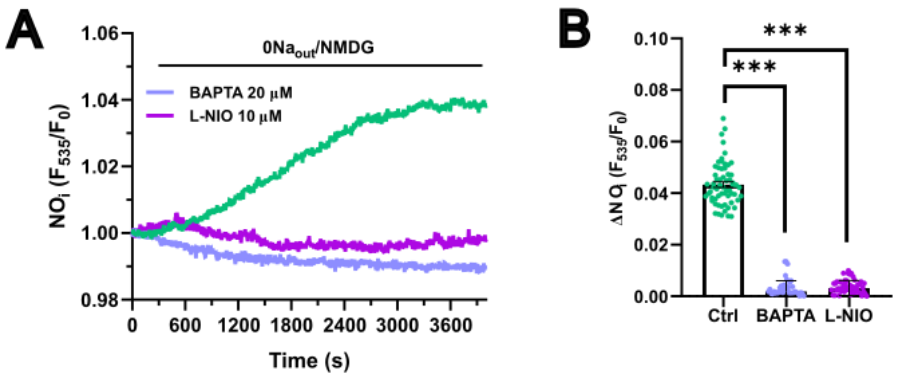

Figure 18. $0Na^+_o$-induced Ca^{2+} signals lead to NO release in hCMEC/D3 cells. **(A)** Representative $0Na^+_o$-induced increase in DAF-FM fluorescence, reflecting NO release, which was inhibited by L-NIO (10 µM, 1 h) and BAPTA-AM (20 µM, 2 h). **(B)** Mean ± SEM of the amplitude of NO responses obtained in control conditions and following the pre-treatment with L-NIO and BAPTA-AM. *** indicates $p < 0.0001$ (Mann-Whitney test).

PART 3: Evaluation of global Ca^{2+} dynamics in hCMEC/D3 cells: TRPML1

7. 9 Lysosomal TRPML1 contribution to global Ca^{2+} signaling in hCMEC/D3 cells

The synthetic agonist, ML-SAI, has been widely used to evaluate the functional expression of functional TRPML1 channels in a variety of cell lines (Boretto et al., 2023; Kilpatrick, Yates, Grimm, Schapira, & Patel, 2016; Scorza et al., 2023; Tedeschi, Sisalli, Petrozziello, Canzoniero, & Secondo, 2021; Thakore & Earley, 2019). In hCMEC/D3 cells loaded with the ratiometric Ca^{2+}-sensitive fluorophore, Fura-2, ML-SAI induced a dose-dependent increase in $[Ca^{2+}]_i$ that was evident at concentrations ≥10 μM (**Figure 19A**). At 10–50 μM, ML-SA1 caused a slow but transient increase in $[Ca^{2+}]_i$ that started with some delay after the application of the agonist (**Figure 19A**). Higher concentrations of ML-SA1 (100 μM and 200 μM) induced a biphasic Ca^{2+} signal following the slow increase in $[Ca^{2+}]_i$ and representing a rapid Ca^{2+} peak followed by a sustained plateau level (**Figure 19A**). The amplitude of the Ca^{2+} response to increasing concentrations of ML-SA1 has been reported in **Figure 19B**. Immunofluorescence showed that punctate vesicular structures could be detected in hCMEC/D3 cells stained with the lysosomal marker LAMP-1 (**Figure 19E**) and Lysotracker Red (**Figure 19F**), a red fluorescent weak base that is selective for acidic organelles (Faris et al., 2022; Scorza et al., 2023). Consistent with this, nigericin (50 μM), a H^+/K^+ ionophore that alkalinizes the lysosomal pH (Morgan & Galione, 2021; Morgan, Platt, Lloyd-Evans, & Galione, 2011) erased Lysotracker Red fluorescence (**Figure 19G**), confirming that it selectively labels lysosomal vesicles. Co-immunofluorescence analysis showed that both Lysotracker Red and a TRPML1 specific antibody exhibited a similar punctate distribution throughout the cells (**Figure 19C**). Finally, immunoblotting with a TRPML1-specific antibody detected a major band of ~75 kDa (**Figure 19D**), which is the predictive molecular weight for the TRPML1 protein (Tedeschi et al., 2021). Taken together, these findings show that the lysosomal TRPML1 is expressed and triggers global Ca^{2+} signals in hCMEC/D3 cells.

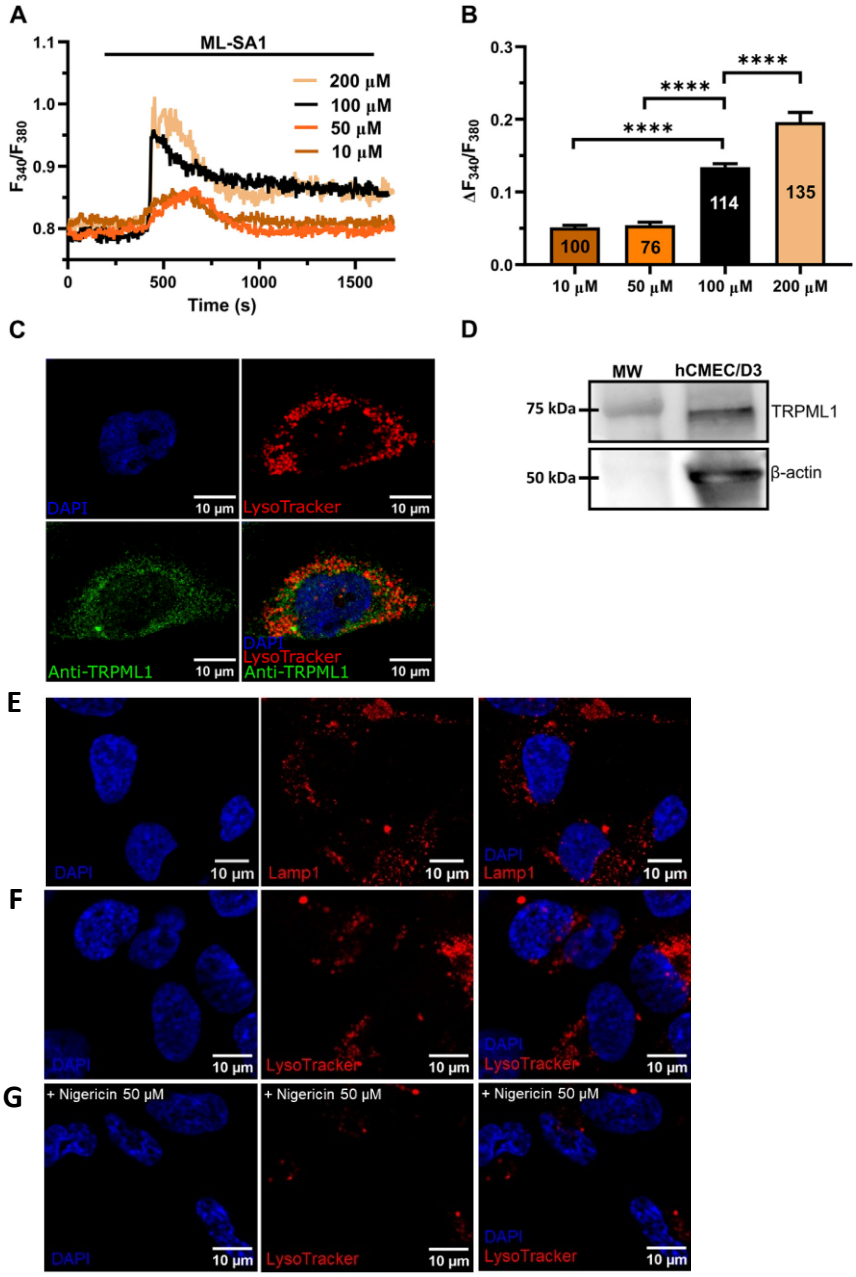

Figure 19. TRPML1 is expressed in the hCMEC/D3 cell line. ML-SA1 evokes a dose-dependent increase in $[Ca^{2+}]_i$ in hCMEC/D3 cells. (**A**) Intracellular Ca^{2+} signals evoked by increasing concentration of ML-SA1 in hCMEC/D3 cells. (**B**) Mean ± SEM of the peak amplitude of ML-SA1-induced Ca^{2+} responses in hCMEC/D3 cells at different agonist concentrations. **** indicates $p < 0.0001$ (Student's t-test and Mann-Whitney test). (**C**) Confocal fluorescence images of hCMEC/D3 cells loaded with LysoTracker-Red DND-99 (red) to mark acidic organelles and stained with an antibody against TRPML1 antibody (green). Nuclei were stained using DAP (blue). Scale bar: 10 µm. (**D**) Representative western blotting analysis of TRPML1 on hCMEC/D3 cells lysates. Major bands of the expected molecular weights (MW) for TRPML1 (75 kDa) and the loading control protein β-actin (50 kDa) is indicated. Representative confocal fluorescence image of hCMEC/D3 cells loaded with the lysosomal marker LAMP-1 and **(E)** LysoTracker-Red DND-99 **(F)** to mark acidic organelles.

Nuclei were stained using DAPI (blue). Scale bar: 10 μm. (**G**) Representative confocal fluorescence images of hCMEC/D3 cells pre-incubated with 50 μM Nigericin, reflecting the depletion of lysosomal Ca^{2+} stores. Acidic organelles were marked with LysoTracker-Red DND-99 (red) and nuclei were stained using DAPI (blue). Scale bar: 10 μm.

7.10 TRPML1-mediated global Ca^{2+} signals are sustained by lysosomal Ca^{2+} release and extracellular Ca^{2+} entry

Recent studies have shown that the global Ca^{2+} response to TRPML1 activation involves both lysosomal Ca^{2+} release and extracellular Ca^{2+} entry across the plasma membrane (Kilpatrick et al., 2016). The long-lasting plateau phase of the Ca^{2+} responses illustrated in **Figure 20A** suggests that MLSA1 at concentrations higher than 50 μM may also activate a Ca^{2+} entry pathway in hCMEC/D3 cells. Consistent with this hypothesis, in the absence of extracellular Ca^{2+} (0 Ca^{2+}) 100 μM ML-SA1 induced a transient increase in $[Ca^{2+}]_i$ whose amplitude was significantly ($p < 0.05$) smaller as compared to the amplitude of the Ca^{2+} response recorded in the presence of extracellular Ca^{2+} (**Figure 20A-B**). Restoration of extracellular Ca^{2+} 300 sec after the removal of ML-SA1 induced a prompt increase in $[Ca^{2+}]_i$ that was obviously independent of the presence of the agonist in the bath (**Figure 20C**). As discussed in (Faris et al., 2019; Garrity et al., 2016; Lloyd-Evans & Platt, 2011; Moccia, Zuccolo, et al., 2021; Morgan et al., 2011), depletion of the lysosomal Ca^{2+} pool with nigericin has long been used as a pharmacological approach to confirm that MLSA1 and NAADP mobilize the lysosomal Ca^{2+} store. Consistent with this, the application of nigericin (50 μM) under 0Ca^{2+} conditions induced a transient increase in $[Ca^{2+}]_i$ reflecting the depletion of the lysosomal Ca^{2+} content (**Figure 20D**). The subsequent application of 100 μM ML-SA1 failed to induce a discernible Ca^{2+} response in hCMEC/D3 cells (**Figure 20D-F**). In addition, ML-SA1-induced intracellular Ca^{2+} release was abolished by ML-SI3 (10μM) (**Figure 20E-F**), a specific TRPML1 antagonist (Boretto et al., 2023; Kilpatrick et al., 2016; W. Wang et al., 2015), and by the genetic deletion of TRPML1 with a selective small interfering RNA (siTRPML1) (**Figure 20E- F**). The efficacy of the siTRPML1-mediated reduction in TRPML1 protein expression has been illustrated in (**Figure 20G -H)**. Taken together, these findings show that TRPML1-mediated global Ca^{2+} signals are triggered by lysosomal Ca^{2+} release and sustained by extracellular Ca^{2+} entry.

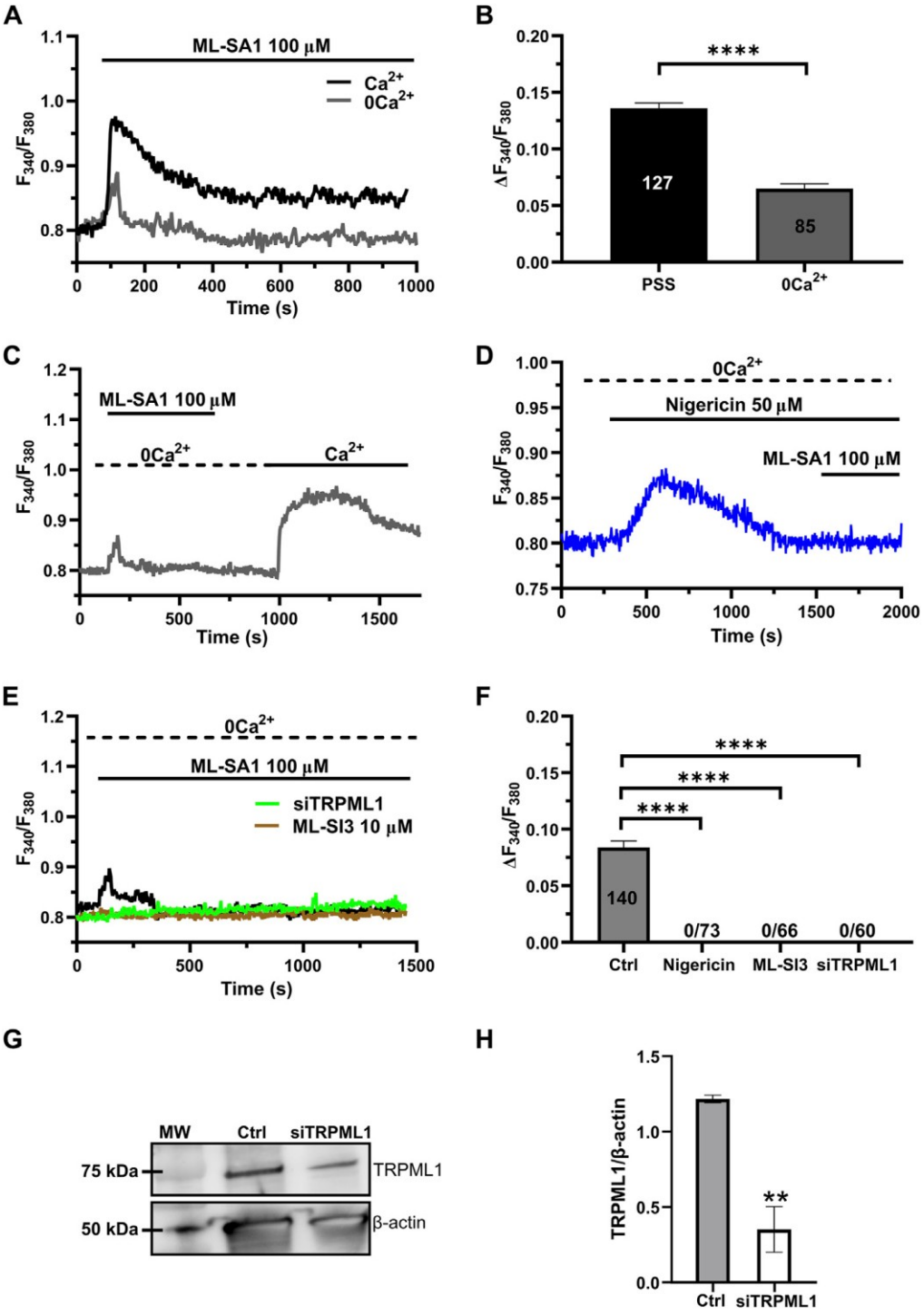

Figure 20. Lysosomal Ca^{2+} release and extracellular Ca^{2+} entry sustain TRPML1-mediated global Ca^{2+} signals. (**A**) ML-SA1 induced a small transient increase in $[Ca^{2+}]_i$ in the absence of extracellular Ca^{2+} ($0Ca^{2+}$). (**B**) Mean ± SEM of the peak amplitude of the TRPML1-induced Ca^{2+} responses in presence and absence of extracellular Ca^{2+}. **** indicates $p < 0.0001$ (Student's t-test). (**C**) Restoration of extracellular Ca^{2+} upon removal of the agonist resulted in a second bump in $[Ca^{2+}]_i$, which was indicative of SOCE. (**D**) Pre-incubation with nigericin (50 µM, 20 min) under $0Ca^{2+}$

conditions, induced a transient increase in $[Ca^{2+}]_i$, reflecting the depletion of the Ca^{2+} store. The subsequent application of ML-SA1 failed to induce a significant Ca^{2+} response in hCMEC/D3 cells. (**E**) Pharmacological (ML-SI3; 10 μM, 20 min) and genetic (siTRPML1) inhibition of TRPML1, totally abolished the Ca^{2+} response under $0Ca^{2+}$ conditions. (**F**) Mean ± SEM of the amplitude of Ca^{2+} responses in cells under the designated treatments. **** indicates $p < 0.0001$ (Kruskal–Wallis one-way Anova test followed by Dunn's post hoc test). (**G**) Representative western blotting analysis of the TRPML1 protein expressed in hCMEC/D3 (Ctrl) and hCMEC/D3 transfected with the specific siTRPML1 (siTRPML1). Major bands of the expected molecular weights (MW) for TRPML1 (75 kDa) and the loading control protein β-actin (50 kDa) is indicated. (**H**) Mean ± SEM of the TRPML1/β-actin ratio expression of four independent western blotting experiments. ** indicates $p < 0.005$ (Student's t-test).

7.11 ER Ca^{2+} release through $InsP_3Rs$ and SOCE contribute to TRPML1-mediated global Ca^{2+} signals in hCMEC/D3 cells

The ER is the major Ca^{2+} store that may amplify spatially restricted lysosomal Ca^{2+} microdomains into global increases in $[Ca^{2+}]_i$ (Galione, Davis, Martucci, & Morgan, 2023; Moccia, Brunetti, Soda, Berra-Romani, et al., 2023; Morgan, 2016). Furthermore, the evidence mentioned previously that ML-SA1- induced extracellular Ca^{2+} entry may occur even in the absence of the agonist of the bath is reminiscent of SOCE activation (Bird & Putney, 2005; Moccia, Brunetti, Soda, Faris, et al., 2023; Murata et al., 2007), further confirming the contribution of the ER Ca^{2+} store between the initial event of lysosomal Ca^{2+} release and the subsequent influx of Ca^{2+}. Consistent with this, the intracellular Ca^{2+} response to 100 μM ML-SA1 was significantly ($p < 0.05$) reduced by the prior incubation with CPA (20 μM) under $0Ca^{2+}$ conditions to deplete the ER Ca^{2+} store (**Figure 21A**) and by 2-aminoethoxy diphenyl borate (2-APB; 50 μM) (**Figure 21B**), a reliable $InsP_3R$ blocker in the absence of extracellular Ca^{2+} (Pafumi et al., 2017). The inhibitory effect of CPA and 2-APB on ML-SA1-induced intracellular Ca^{2+} release has been illustrated in (**Figure 21C).** hCMEC/D3 cells do not express RyRs (Zuccolo, Kheder, et al., 2019) and, therefore, we did not assess their contribution to ML-SA1-induced intracellular Ca^{2+} release. SOCE is the main pathway that sustains Ca^{2+} entry during ER Ca^{2+} release events through $InsP_3Rs$ in vascular endothelial cells (Blatter, 2017; Groschner et al., 2017; Moccia, Brunetti, Perna, et al., 2023), including hCMEC/D3 cells (Berra-Romani et al., 2023; Negri, Faris, et al., 2021a; Negri et al., 2020; Negri et al., 2022). Consistent with this, 100 μM ML-SA1 induced a transient and tiny Ca^{2+} response in the presence of 20 μM BTP-2 (**Figure 21D-E**) or 10 μM Pyr6 (**Figure 21D-E**), which are two established blockers of Orai1(Chauvet et al., 2016; Schleifer et al., 2012; Zhang et al., 2020; Zuccolo et al., 2016), which serves as store-operated Ca^{2+} channel in hCMEC/D3 cells (Negri et al., 2020; Zuccolo, Laforenza, et al., 2019). However, TRPML1

can directly mediate Ca^{2+} entry across the plasma membrane (Kilpatrick et al., 2016). TRPML1 is also permeable to Fe^{2+}, which causes a significant quench in Fura-2 fluorescence when it enters the cytosol. Therefore, hCMEC/D3 cells were challenged with $FeCl_2$ (1 mM) under $0Ca^{2+}$ conditions after stimulation with ML-SA1 (100 µM), as shown in (Kilpatrick et al., 2016). **Data not shown** shows that $FeCl_2$ did not induce any detectable quench in Fura-2 fluorescence, thereby suggesting TRPML1 does not directly contribute to ML-SA1-evoked Ca^{2+} entry. Taken together, these findings demonstrate that TRPML1-mediated global Ca^{2+} signals in hCMEC/D3 cells are supported by ER Ca^{2+} release through $InsP_3Rs$ and by SOCE activation.

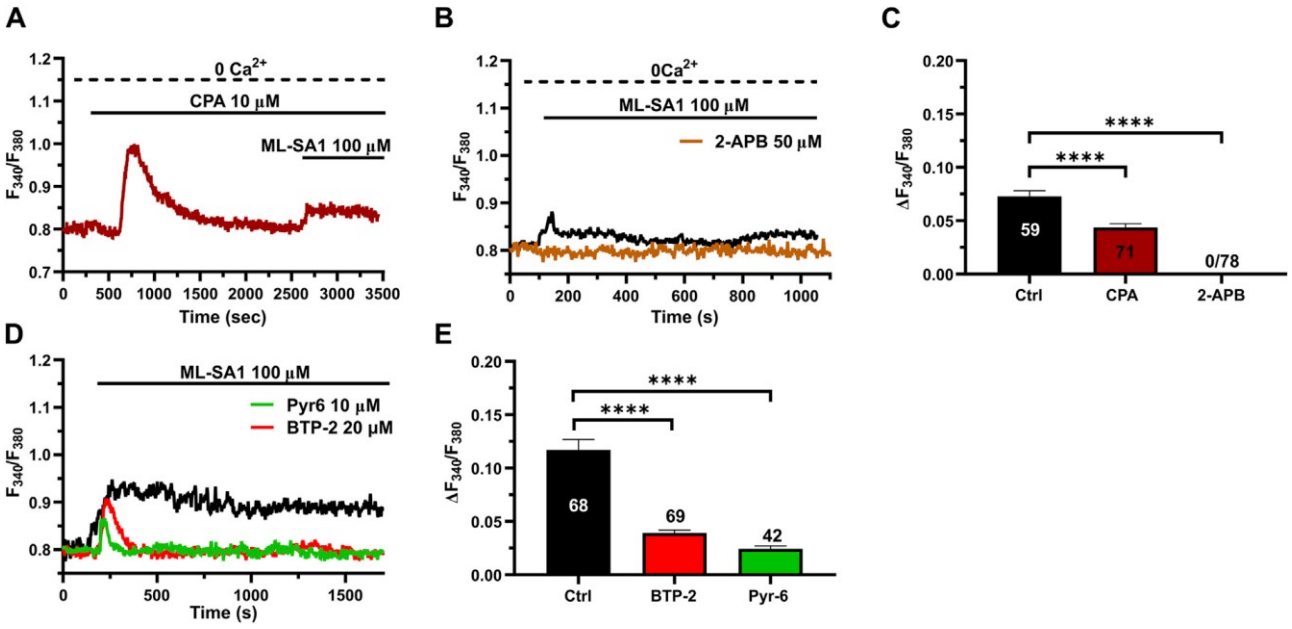

Figure 21. SOCE sustains global Ca^{2+} release. ER Ca^{2+} release and SOCE contribute to the TRPML1-mediated Ca^{2+} signals in hCMEC/D3 cells. (**A, B**) pre-incubation with CPA (10 µM, 30 min) or 2-APB (50 µM, 30 min) significantly reduced the ML-SA1-induced Ca^{2+} response under $0Ca^{2+}$ conditions. (**C**) Mean ± SEM of the amplitude of the Ca^{2+} responses in cells under the designated treatments. **** indicates $p < 0.0001$ (Kruskal–Wallis one-way Anova test followed by Dunn's post hoc test). (**D**) The Orai1 blockers, BTP-2 (20 µM, 20 min) and Pyr6 (20 µM, 20 min), reduced the ML-SA1-evoked Ca^{2+} response. (**E**) Mean ± SEM of the amplitude of Ca^{2+} responses in cells under the designated treatments. Each drug totally inhibited the Ca^{2+} response. **** indicates $p < 0.0001$ (Kruskal–Wallis one - way Anova test followed by the Dunn's post hoc test).

7.12 TRPML1 regulates ER Ca^{2+} load in hCMEC/D3 cells

TRPML1 could promote ER Ca^{2+} release by directly activating the juxtaposed $InsP_3Rs$ via CICR (Thakore, Pritchard, et al., 2020) or by loading the ER with Ca^{2+} in a SERCA-dependent manner, thereby activating $InsP_3Rs$ via the ER Ca^{2+} overload (Macgregor et al., 2007). A recent study showed that TRPML1 regulates the ER Ca^{2+} content in primary rat cortical neurons (Tedeschi et al., 2021). Therefore, we reasoned that, if TRPML1 did the same in hCMEC/D3 cells, CPA-evoked ER Ca^{2+} release would be impaired by interfering with TRPML1-mediated Ca^{2+} mobilization. In agreement with this hypothesis, the ER Ca^{2+} response to CPA (20 μM) was significantly ($p < 0.05$) reduced by blocking TRPML1 with either ML-SI3 (10 μM) (**Figure 22A**) or the specific siTRPML1 (**Figure 22A**). The statistical analysis of these experiments has been illustrated in (**Figure 22B)**. Collectively, these findings strongly suggest that TRPML1-mediated lysosomal Ca^{2+} release leads to an increase in ER Ca^{2+} content, which is decreased upon its inhibition. Therefore, we conclude that TRPML1 may mediate ER Ca^{2+} content and lead to $InsP_3$ activation upon an increase in luminal Ca^{2+} (Missiaen, Taylor, & Berridge, 1992).

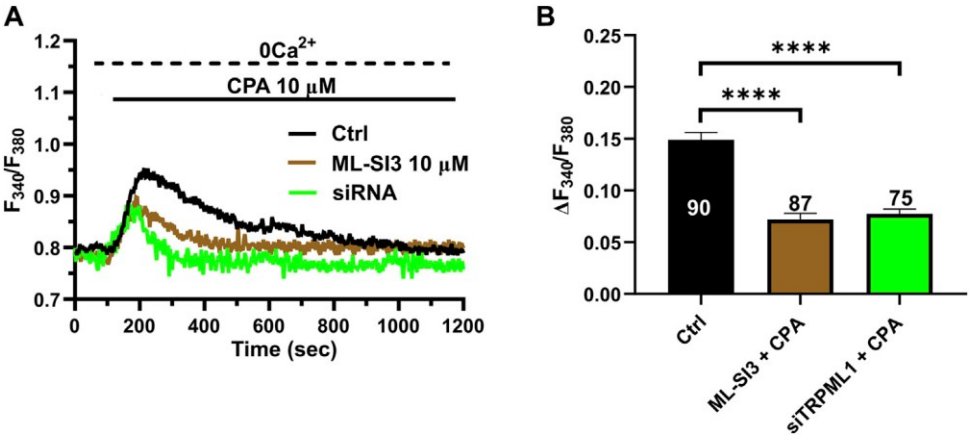

Figure 22. TRPML1 contributes to the ER Ca^{2+} loading. (**A**) The transient Ca^{2+} response induced by CPA (10 μM) under $0Ca^{2+}$ conditions is strongly reduced in the presence of ML-SI3 (10 μM, 20 min) and in hCMEC/D3 cells transfected with the selective siTRPML1. (**B**) Mean ± SEM of the amplitude of the Ca^{2+} responses in cells under the designated treatments. **** indicates $p < 0.0001$ (Kruskal–Wallis one-way Anova test followed by the Dunn's post hoc test).

7.13 TRPML1 mediates PI(3,5)P_2-evoked Ca^{2+} signals in hCMEC/D3 cells

The lysosomal phosphoinositide PI(3,5)P_2 is regarded as a putative endogenous ligand of TRPML1 (Dong et al., 2010; Zhang et al., 2012; Isobe et al., 2019; Li et al., 2019; Negri et al., 2021b). In order to assess whether PI(3,5)P_2 was also able to induce TRPML1-mediated global Ca^{2+} signals in hCMEC/D3 cells, we challenged the cells with PI(3,5)P_2 diC8, a cell-permeable analog of PI(3,5)P_2 (Tedeschi et al., 2021). 10 µM PI(3,5)P_2 diC8 induced a slowly rising, but long-lasting increase in $[Ca^{2+}]_i$ (**Figure 23A**). The Ca^{2+} add-back protocol confirmed that, under $0Ca^{2+}$ conditions, 10 µM PI(3,5)P_2 diC8 induced a transient increase in $[Ca^{2+}]_i$ that was followed by a second elevation in $[Ca^{2+}]_i$ upon restoring extracellular Ca^{2+} in the absence of the agonist (**Figure 23B**). As described above for ML-SA1, previous depletion of the lysosomal Ca^{2+} store with nigericin (50 µM) abolished PI(3,5)P_2 diC8-induced intracellular Ca^{2+} release in the absence of extracellular Ca^{2+} (**Figure 23C**). Furthermore, the intracellular Ca^{2+} response to PI(3,5)P_2 diC8 was significantly ($p < 0.05$) reduced by both ML-SI3 (10 µM; **Figure 23D**) and by the selective siTRPML1 (**Figure 23D**). The inhibitory effect of nigericin, ML-SI3, and siTRPML1 on PI(3,5)P_2 diC8-induced intracellular Ca^{2+} release has been illustrated in **Figure 23E**. Collectively, these findings provide evidence that PI(3,5)P_2 may also serve as an endogenous agonist of TRPML1 in hCMEC/D3 cells.

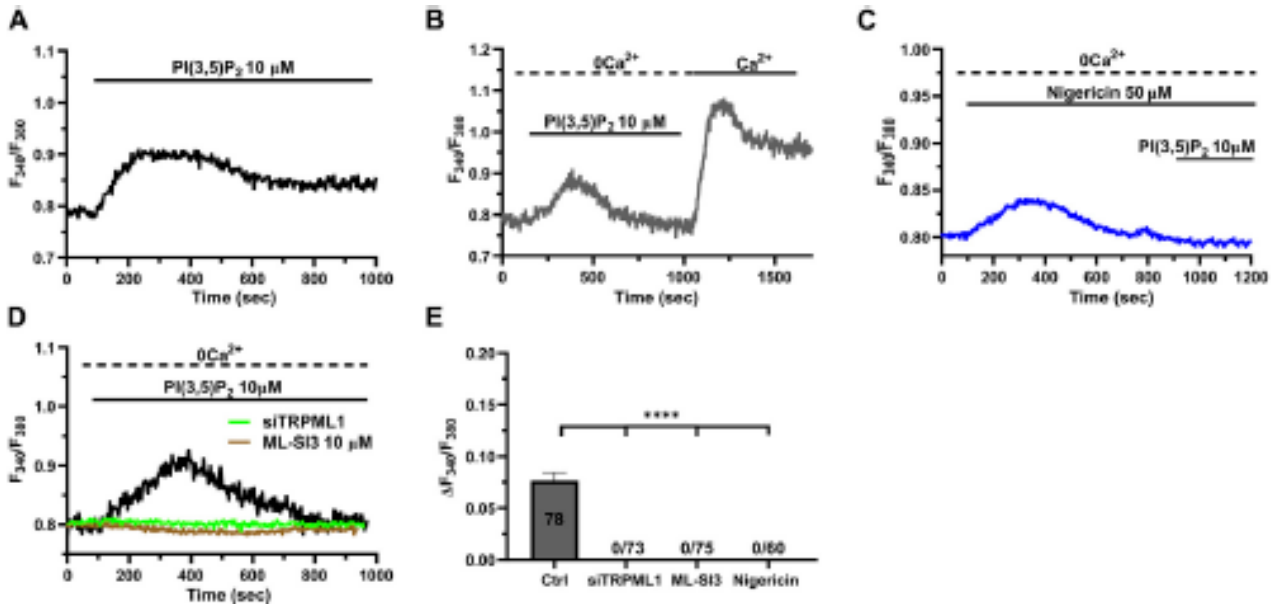

Figure 23. The endogenous ligand PI(3,5)P_2 mimics the Ca^{2+} response to ML-SA1. (**A**) 10 µM PI(3,5)P_2 induced a long-lasting increase in $[Ca^{2+}]_i$, mimicking the ML-SA1-evoked Ca^{2+} response. (**B**) Restoration of extracellular Ca^{2+} upon removal of the agonist PI(3,5)P_2 resulted in a second bump in $[Ca^{2+}]_i$, which was indicative of SOCE. (**C**) Depletion of the lysosomal Ca^{2+} stores with 50 µM nigericin abolished the PI(3,5)P_2 –induced Ca^{2+} response. (**D**). Pharmacological (ML-SI3; 10 µM, 20

min) and genetic (siTRPML1) inhibition of TRPML1 totally abolished the PI(3,5)P_2–induced Ca^{2+} response, in absence and presence of extracellular Ca^{2+}. (**E**) Mean ± SEM of the amplitude of Ca^{2+} responses in the absence of extracellular Ca^{2+} under the designated treatments. Each drug totally inhibited the Ca^{2+} response. **** indicates $p < 0.0001$ (Kruskal–Wallis one-way Anova test followed by the Dunn's post hoc test).

7.14 TRPML1-mediated global Ca^{2+} signals lead to NO release in hCMEC/D3 cells

Recent studies have shown that a global increase in $[Ca^{2+}]_i$ can result in robust NO release from hCMEC/D3 cells (Berra-Romani et al., 2023; Berra-Romani et al., 2020; Negri et al., 2020; Negri et al., 2022). In order to assess whether TRPML1-mediated global Ca^{2+} signals could also induce NO production, we loaded hCMEC/D3 cells with the NO-sensitive fluorophore, DAF-FM DA. We found that 100 µMML-SA1 induced a slow, but sustained increase in DAF-FM fluorescence (**Figure 24A**), which was indicative of NO release (Berra-Romani et al., 2023; Berra-Romani et al., 2020; Greenberg et al., 2017; Negri et al., 2020; Negri et al., 2022; Sheng & Braun, 2007; Sheng, Wang, & Braun, 2005). ML-SAI-induced NO release was significantly inhibited by BAPTA-AM (20 µM; **Figure 24A**), a membrane permeable buffer of intracellular Ca^{2+} levels, and by L-NIO (50 µM; **Figure 24A**), a specific eNOS inhibitor. The inhibitory effect of BAPTA and L-NIO on ML-SA1-induced NO release has been illustrated in **Figure 24C**. Moreover, ML-SI3 (10 µM) and siTRPML1 significantly ($p < 0.05$) inhibited ML-SA1-induced NO release (**Figure 24B-C**). Therefore, the lysosomal TRPML1 is able to trigger massive NO production in the human cerebrovascular endothelial cell line, hCMEC/D3.

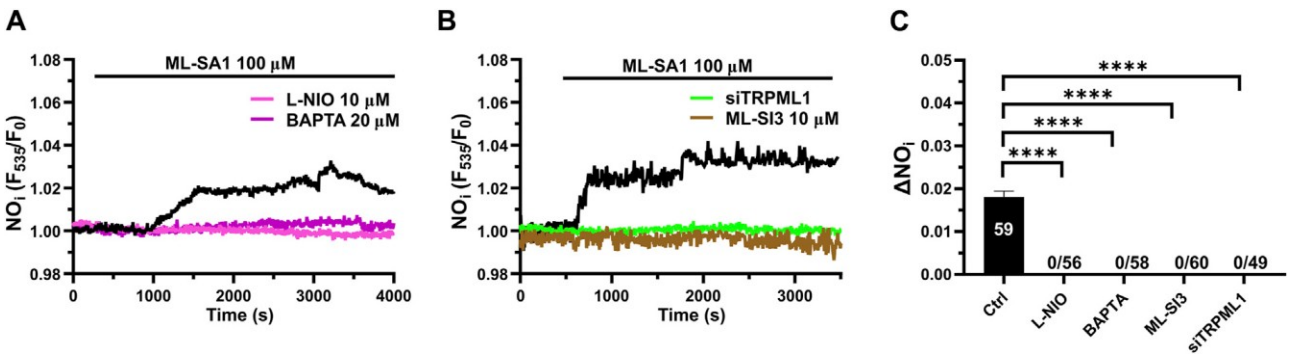

Figure 24. TRPML1 induces Ca^{2+}-dependent NO release in hCMEC/D3 cells. **(A)** 100 µM ML-SA1 evoked a slow, but sustained increase in DAF-FM fluorescence, which reflected NO release and was inhibited by L-NIO (10 µM, 1 h) and BAPTA-AM (20 µM, 2 h). **(B)** Pharmacological (ML-SI3; 10 µM, 20 min) and genetic (siTRPML1) inhibition of TRPML1, significantly abolished the ML-SA1-induced NO response. **(C)** Mean ± SEM of the amplitude of NO responses in presence of extracellular

Ca^{2+}. **** indicates $p < 0.0001$ (Kruskal–Wallis one-way Anova test followed by the Dunn's post hoc test).

7.15 TRPML1 supports ATP-induced Ca^{2+} signaling and NO release in hCMEC/D3 cells

The evidence that lysosomal Ca^{2+} release through TRPML1 controls ER Ca^{2+} release and induce $InsP_3R$-mediated Ca^{2+} signaling strongly suggests that TRPML1 may support agonist-induced Ca^{2+} signals and NO release in hCMEC/D3 cells. ATP has long been the most widely exploited agonist to stimulate endothelial Ca^{2+} signals along the vascular tree (Lisec et al., 2024; Scarpellino et al., 2019; Scarpellino et al., 2022). ATP activates the G_q-coupled $P2Y_2$ receptors to elicit $InsP_3$-induced ER Ca^{2+} release in hCMEC/D3 cells (Bintig et al., 2012; Forcaia et al., 2021). A recent study showed that ATP-induced Ca^{2+} signaling is primarily mediated by intracellular Ca^{2+} release in hCMEC/D3 cells (Bintig et al., 2012). Herein, we found that ATP (100 μM) evoked a transient increase in $[Ca^{2+}]_i$ that was significantly ($p < 0.05$) reduced by ML-SI3 (10 μM) (**Figure 25A**) and siTRPML1 (**Figure 25A**). We then assessed whether the pharmacological blockade of PYKfive, which is part of the lipid kinase complex that synthetizes $PI(3,5)P_2$, with the selective inhibitor, apilimod (Somogyi et al., 2023), affected ATP-induced ER Ca^{2+} release. Apilimod (100 nM) significantly ($p < 0.05$) reduced ATP-induced ER Ca^{2+} release in hCMEC/D3 cells (**Figure 25A**), while it did not activate per se any increase in $[Ca^{2+}]_i$, as reported in (Hou, He, Ma, & Zhou, 2023). The inhibitory effect of ML-SI3, siTRPML1, and apilimod on the intracellular Ca^{2+} response to ATP has been illustrated in **Figure 25B**. Furthermore, both the pharmacological and genetic blockade of TRPML1-mediated lysosomal Ca^{2+} release with, respectively, ML-SI3 (10 μM) (**Figure 25C-D**) and the siTRPML1 (**Figure 25C-D**), significantly reduced ATP-induced NO release in hCMEC/D3 cells loaded with DAF-DM. Overall, these findings indicate that TRPML1, either indirectly (by refilling the ER Ca^{2+} pool) or directly (by activating the ER-embedded $InsP_3Rs$ via the luminal Ca^{2+} overload) can support agonist-induced endothelial Ca^{2+} signaling at the neurovascular unit.

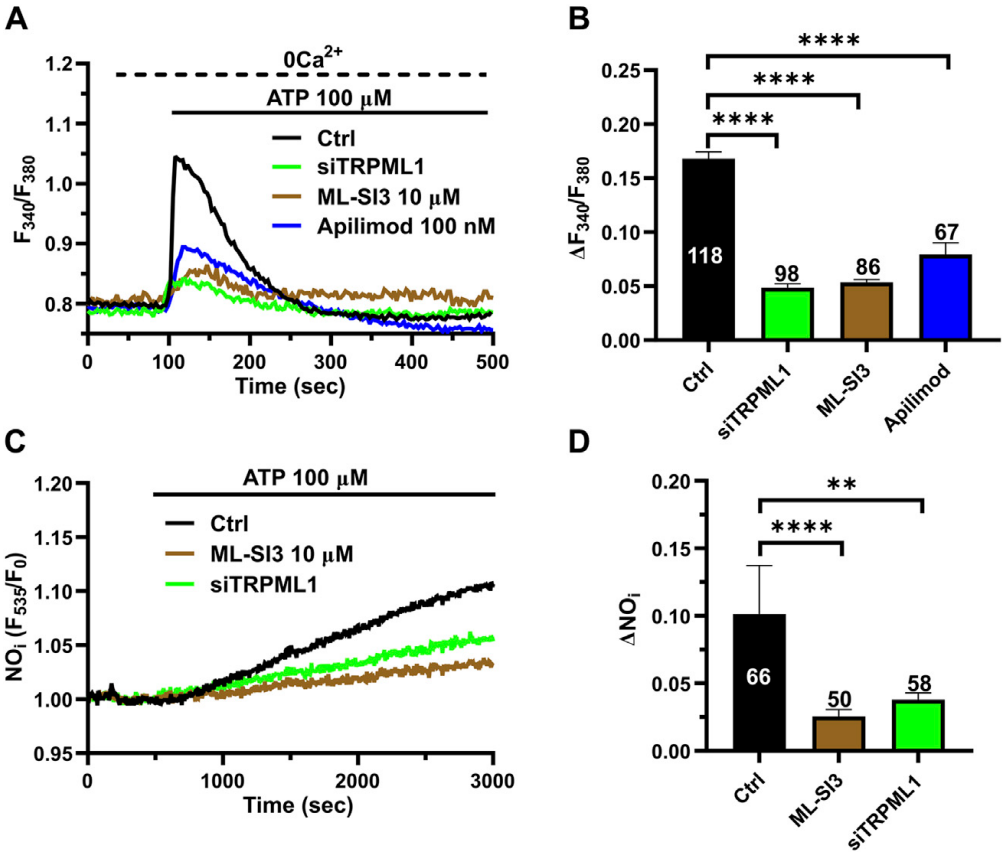

Figure 25. TRPML1 mediates ATP-induced intracellular Ca^{2+} release and NO production. **(A)** The Ca^{2+} response to ATP (100 µM) under $0Ca^{2+}$ conditions was strongly reduced in the presence of ML-SI3 (10 µM, 20 min) or apilimod (100 nM, 20 min) and in hCMEC/D3 cells transfected with the selective siTRPML1. **(B)** Mean ± SEM of the amplitude of the Ca^{2+} responses in cells under the designated treatments. **** indicates $p < 0.0001$ (Kruskal–Wallis one-way Anova test followed by Dunn's post hoc test). **(C)**. ATP (100 µM) induced a sustained increase in DAF-DM fluorescence, which was significantly inhibited by the pharmacological (ML-SI3) and genetic (siTRPML1) inhibition of TRPML1 activity. **** indicates $p < 0.0001$ (Kruskal–Wallis one-way Anova test followed by the Dunn's post hoc test). (**D**) Mean±SEM of the amplitude of the Ca^{2+} responses in cells under the designated treatments. **** indicates $p<0.0001$ (Kruskal-Wallis one-way Anova test followed by the Dunn's post-hoc test).

CHAPTER 8: DISCUSSION

PART 1: Evaluation of the biophysical properties of hCMEC/D3 cells

Vascular ECs are gaining momentum as crucial regulators of cardiovascular physiology due to their ability to sense changes in the extracellular microenvironment and to adjust the vascular function to the local tissue requirements (Jackson, 2022; Moccia et al., 2022). Furthermore, the endothelial monolayer is able to finely tune the activity of resident cells throughout the vascular bed, including the brain microcirculation (Brunetti et al., 2024; Soda, Brunetti, Berra-Romani, & Moccia, 2023), in response to blood-borne or parenchymal signals. Recently, high throughput sequencing and proteomics have begun to unveil the molecular architecture and heterogeneity of organ-specific ECs, including those lining the brain microcirculation (Walchli et al., 2024). The V_M, as well as the underlying ionic conductances, is instrumental to the endothelium-dependent regulation of both vascular and parenchymal cells (Brunetti et al., 2024; Jackson, 2022; Moccia et al., 2022; Soda et al., 2023). In the present work, we unveiled, using the Port-a-Patch APC system by Nanion Technologies (Obergrussberger, Friis, Bruggemann, & Fertig, 2021), the basic electrophysiological properties of hCMEC/D3 cells. As discussed in (Weksler et al., 2013), the hCMEC/D3 cell line is the gold standard for the investigation of human cerebrovascular ECs when human brain samples cannot be obtained and the access to naïve cerebral endothelium is not permitted. We found that the average resting V_M of hCMEC/D3 in the presence of physiological extra- and intracellular solutions is in the same range as that measured in other ECs types (Moccia et al., 2002; Nilius & Droogmans, 2001; Voets et al., 1996). Intriguingly, the average value of the resting V_M, i.e., - 16.7 ± 4.5 mV, is within the same range as that measured by using the conventional whole-cell recording technique, i.e., - 20.5 ± 6.0 mV (Negri, Faris, Soda, & Moccia, 2021). Interestingly, the average value of the resting V_M we measured with the Port-a-Patch planar patch-clamp system is within the same range as that reported for mouse cerebral microvascular ECs (-15.5 ± 10.8 mV) (Celentano et al., 2024) and for isolated endothelial cells from other vascular beds, such as rat coronary microcirculation (-33.3 ± 1.8 mV) (Moccia et al., 2002), mouse aorta (-19 ± 3 mV) and calf pulmonary artery ECs (-26.3 ± 3 mV) (Voets et al., 1996). The average value of C_M is also within the same range as that typically measured in microvascular endothelial cells (Moccia, Frost, Berra-Romani, Tanzi, & Adams, 2004), including mouse brain capillary ECs. The highly variable resting V_M has already been described in the ECs from other vascular districts (Suh et al., 1999; Voets et al., 1996) and reflects the different contribution to endothelial electrogenesis of resting K^+, Cl- and Na^+ conductances (Nilius & Droogmans, 2001). The rapid perfusion system of the Port-a-Patch system enabled us to obtain a preliminary characterization of the ion membrane conductances that underlie such a rather depolarized V_M. Two pieces of evidence

suggest that K^+ channels do not play a major role in determining the resting V_M. First, the replacement of intracellular K^+ with an equimolar amount of Cs^+ did not significantly affect either the scattering or the average value of the resting V_M. It should, however, be noted that we observed a tendency to a slight ($p = 0.056$) depolarization of the resting V_M in the presence of intracellular Cs^+. Second, voltage clamp recordings clearly showed the appearance of a time-dependent outward current at positive potentials in the presence of intracellular Cs^+, while there was no detectable sign of inward rectification at potentials more negative than - 70 mV, i.e., the equilibrium potential for K^+, in the presence of either cytosolic K^+ or Cs^+. Future work might explore the possibility that the inwardly-rectifying K^+ current could be unmasked by increasing the extracellular concentration of K^+, as described in (Longden et al., 2017; Voets et al., 1996). The major candidates to mediate the time-dependent outward current are the Cl^- channels, such as the Ca^{2+}-activated Cl- channel, TMEM16A (Moccia et al., 2002), and the volume-sensitive Cl channel (Voets et al., 1996), and the non-selective cation pathway that represents a ubiquitous feature of ECs electrophysiology (Moccia et al., 2002; Voets et al., 1996). Our preliminary recordings showed that the superfusion of a hypertonic solution did not affect the resting V_M of hCMEC/D3 cells. Therefore, volume-sensitive Cl^- channels are unlikely to be activated under resting conditions. On the other hand, the voltage-dependent behavior of the outward current measured in the presence of intracellular Cs^+, which is a feature of TMEM16A, suggests that Ca^{2+}-activated Cl^- channels are the main determinants of the basal Cl^- permeability in hCMEC/D3 cells. Furthermore, the larger outward current measured with Cs^+ internal solution could also reflect the contribution of a basal non-selective cation conductance that is more permeable to Cs^+ than to K^+, as observed for the Eisenman sequence I or II (Eisenman, 1962). Intriguingly, the non-selective cation channel, TRPV1 is featured by an Eisenman sequence of type I (Garcia-Avila et al., 2024) and is expressed in hCMEC/D3 cells (Luo et al., 2019). The contribution of Na^+ and Cl^- to the resting V_M is highlighted by the reversible hyperpolarization observed upon removal of extracellular Na^+ and upon reduction in the $[Cl^-]_o$, as commonly reported in vascular ECs (Moccia et al., 2002). Interestingly, the hyperpolarization observed upon reduction in the $[Cl^-]_o$ is unlikely to be ascribed to a prevalence of the Ba^{2+}-sensitive inward-rectifier K^+ channels under these conditions, as reported in calf pulmonary artery endothelial cells (Nilius & Droogmans, 2001; Voets et al., 1996). Indeed, negative V_M can also be measured in the presence of a Cs^+ internal solution, which blocks all K^+ conductances. On the other hand, a reduction in the $[Cl^-]_o$ results in a more positive Cl^- equilibrium potential (E_{Cl}), while this maneuver causes the reversible hyperpolarization of hCMEC/D3 cells. A plausible explanation, which obviously requires more experiments, is that the reduction in the $[Cl^-]_o$ also causes a rapid decrease in the intracellular Cl^- concentration, which may cause endothelial hyperpolarization by activating the Cl^- sensitive With-No-Lysine (WNK) kinase. WNK, in turn,

phosphorylates the SPS-1-related proline/alanine-rich kinase (SPAK) and the oxidative-stress responsive kinase-1 (OSR1), which activate Ca^{2+} entry through TRPV4 followed by the activation of small- and intermediate-conductance K^+ channels. If this hypothesis is correct, one of the main determinants of the resting V_M of hCMEC/D3 cells is the intracellular chloride concentration, which is mainly driven by the $Na^+/K^+/2Cl^-$ cotransporter, NKCC1 (Lu et al.,2023). Notably, the NKCC1 protein in expressed in hCMEC/D3 cells (Luo et al., 2018), as well as TRPV4 (Berra-Romani, Faris, Negri, et al., 2019) and small and intermediate-conductance K^+ channels (Berra-Romani et al., 2023), and a recent investigation demonstrated that changes in $[Cl^-]_o$ also lead to rapid changes in the intracellular Cl^- concentration (Lu et al., 2023). Moreover, reducing Cl^- entry has long been known to hyperpolarize VSMCs (Garneau et al., 2020). It is likely that rather negative V_M that can sometimes be measured in the presence of the Cs^+ internal solution reflects the lower activation of the NKCC1 transporter and a decrease in the intracellular Cl^- concentration. Future work will have to assess whether and how synaptically released neurotransmitters and neuromodulators influence the resting V_M and whether these alterations are associated with changes in driving-force supporting Ca^{2+} entry in hCMEC/D3 cells.

PART 2: Evaluation of global Ca^{2+} dynamics in hCMEC/D3 cells: NCX1 AND HR1

It has long been known that a reduction in the $[Na^+]_o$ causes an increase in $[Ca^{2+}]_i$ by switching the NCX into the reverse mode in mammalian cells (Rose, Ziemens, & Verkhratsky, 2020; Verkhratsky et al., 2018), including vascular ECs (Berra-Romani et al., 2012; Lillo et al., 2017). Sporadic evidence showed that the removal of extracellular Na^+ may also lead to ER Ca^{2+} release by stimulating PLC activity through a yet to be elucidated mechanism (Boitano et al., 1997). Na^+-depletion has recently been shown to stimulate PLC activity and thereby induce $InsP_3$-dependent Ca^{2+} release in invasive breast cancer cells (James et al., 2023). Similarly, a reduction in $[Na^+]_o$ induced a Ca^{2+} signal, which strongly resembled the $InsP_3$-mediated Ca^{2+} response to bradykinin, in canine coronary artery ECs. However, the mechanism(s) by which fluctuations in $[Na^+]_o$ may increase PLC activity and lead to ER Ca^{2+} mobilization are still unclear. Herein, we showed that reverse NCX interacts with the Na^+-sensitive H1Rs to trigger complex intracellular Ca^{2+} signatures in human brain microvascular endothelial cells. This is the first evidence that the removal of extracellular Na^+ could increase PLC activity by activating H1Rs.

Perfusing a monolayer of hCMEC/D3 cells with an extracellular solution in which Na^+ was replaced with an equimolar amount of NMDG elicited a slow increase in $[Ca^{2+}]_i$, which then returned to the

baseline without displaying any further increase in $[Ca^{2+}]_i$, in a minority of hCMEC/D3 cells. This SRI is the typical Ca^{2+} response mediated by the NCX operating in the reverse mode (Rose et al., 2020; Verkhratsky et al., 2018), as also reported in ECs from multiple vascular districts (Andrikopoulos, Eccles, & Yaqoob, 2017; Berra-Romani et al., 2012; Lillo et al., 2017). In accord, the SRI was strongly inhibited by selectively blocking the reverse mode NCX with SEA0400 and by a specific siNCX1. However, in most hCMEC/D3 cells, the slowly rising increase in $[Ca^{2+}]_i$ was followed by intracellular Ca^{2+} oscillations that resembled those triggered by $InsP_3Rs$ (Berra-Romani et al., 2020) and were inhibited upon restoration of the $[Na^+]_o$. This complex Ca^{2+} signature was independent on the base employed to replace extracellular Na^+ as it could also be observed when Na^+ was substituted by choline chloride. The pharmacological or genetic blockade of the reverse mode NCX inhibited the initial, slow increase in $[Ca^{2+}]_i$ in ~93 % of hCMEC/D3 cells. However, 1‑2 Ca^{2+} transients still occurred in around half of the cells, while the remaining half did not display any detectable increase in $[Ca^{2+}]_i$. These findings demonstrate that Na^+ removal does not only switch the NCX into the reverse mode, thereby promoting Ca^{2+} entry, but may also engage a more complex Ca^{2+} signaling machinery in hCMEC/D3 cells.

Endothelial Ca^{2+} oscillations, including those previously recorded in hCMEC/D3 cells (Berra-Romani et al., 2020), are shaped by the rhythmic ER Ca^{2+} release through $InsP_3Rs$ and maintained over time by SOCE (Longden et al., 2021; Moccia, Brunetti, Soda, Berra-Romani, et al., 2023). Removal of extracellular Ca^{2+} abolished the complex intracellular Ca^{2+} activity evoked by the $0Na^+_o$ perfusate in most hCMEC/D3 cells. This finding suggests that, when extracellular Ca^{2+} is absent and the NCX cannot operate in reverse mode, neither the sporadic Ca^{2+} transients nor the prolonged Ca^{2+} oscillations may easily take place. The residual Ca^{2+} spikes recorded upon the pharmacological and genetic blockade of NCX are likely to reflect the uncomplete inhibition exerted by SEA0400 and the selective siNCX on NCX activity and expression, respectively. Therefore, under such conditions, some Ca^{2+} entry may still occur, although it does not lead to an evident SRI. Nevertheless, this tiny Ca^{2+} influx may silently trigger 1‑2 Ca^{2+} oscillations in a fraction of hCMEC/D3 cells. It should, however, be pointed out that, under $0Ca^{2+}$conditions, the removal of external Na^+ induced a single Ca^{2+} transient in less than 20 % of hCMEC/D3 cells. This evidence suggests that NCX-mediated Ca^{2+} entry is required to effectively boost the recruitment of $InsP_3$ signaling, which is otherwise not so efficient at triggering single Ca^{2+} spikes or intracellular Ca^{2+} oscillations. Pharmacological manipulation revealed that, blocking PLC activity with the selective inhibitor, U73122 (Berra-Romani et al., 2020; Bintig et al., 2012; Leo et al., 2019), converted the $0Na^+_o$-induced complex Ca^{2+} signals into an SRI. Similar findings were obtained in the presence of FR900359, which selectively blocks G_q signaling (Longden et al., 2021). Therefore, removal of extracellular Na^+ must activate

PLC-dependent $InsP_3$ production to trigger the complex Ca^{2+} signature recorded in hCMEC/D3 cells. Likewise, 2-APB, which may also block $InsP_3Rs$ in the presence of extracellular Ca^{2+} (Berra-Romani et al., 2020; Bintig et al., 2012; Leo et al., 2019), and XeC abolished the Ca^{2+} spiking response to the $0Na^+_o$ perfusate but did not inhibit the SRI in most hCMEC/D3 cells. The same effect was mimicked by BTP-2 and Pyr6, which selectively block SOCE through Orai1 channels in vascular endothelial cells (Gandhirajan et al., 2013; Moccia, Brunetti, Perna, et al., 2023), including hCMEC/D3 cells (Negri, Faris, Maniezzi, et al., 2021; Negri et al., 2020). Overall, these observations are consistent with the following model: 1) removal of extracellular Na^+ leads to Ca^{2+} entry through the reverse mode of NCX, which is responsible for the SRI, and to the stimulation of PLC activity; 2) PLC produces $InsP_3$, thereby inducing the rhythmic activation of $InsP_3R_3$, the only $InsP_3R$ isoform expressed in hCMEC/D3 cells (Zuccolo, Laforenza, et al., 2019), and progressive depletion of the ER Ca^{2+} pool; 3) the fall in the ER Ca^{2+} concentration leads to quick SOCE activation, which maintains the intracellular Ca^{2+} oscillations by rapidly refilling the ER Ca^{2+} store (Zuccolo, Laforenza, et al., 2019); 4) the reverse mode of NCX contributes to prolonging the intracellular Ca^{2+} oscillations as they rapidly fade when NCX activity is pharmacologically or genetically inhibited. The absolute requirement for Ca^{2+} entry to effectively trigger the complex Ca^{2+} signature suggests that the reverse mode of NCX, which is the first mechanism to be engaged by the removal of extracellular Na^+, supports $InsP_3$-induced ER Ca^{2+} spikes (Di Giuro et al., 2017). In the absence of extracellular Ca^{2+}, it is significantly less likely that the removal of external Na^+ results in one-two Ca^{2+} spikes. This hypothesis is consistent with the ability of extracellular Ca^{2+} entry to induce ER Ca^{2+} release via the stimulation of $InsP_3Rs$ through the process of CICR (Heathcote et al., 2019; Mughal et al., 2024). Of course, we cannot rule out the possibility that the requirement for Ca^{2+} entry also reflects the rapid activation of SOCE, which can be enhanced by the $0Na^+_o$-induced membrane hyperpolarization (Soda et al., 2024) and may boost $InsP_3R3$ signaling by rapidly increasing the intraluminal Ca^{2+} concentration (Morgan & Jacob, 1996). Consistently, Morgan and Jacob showed that H1R with histamine can fail to produce $InsP_3Rs$-mediated intracellular Ca^{2+} oscillations even when the ER Ca^{2+} pool is not depleted in the absence of Ca^{2+} entry, which maintains sensitivity to $InsP_3$ by probably preventing a drop in the ER Ca^{2+} concentration (Bootman, Berridge, & Taylor, 1992). In this setting, the question raises as to what molecular mechanism is responsible for PLC activation.

Although this notion is yet to be fully recognized by cell physiologists, extracellular Na^+ depletion may result in PLC activation and $InsP_3$ generation (Boitano et al., 1997). A recent investigation showed that exposing invasive breast cancer cells to a $0Na^+_o$ perfusate induced intracellular Ca^{2+} signals that required $InsP_3$-dependent ER Ca^{2+} mobilization and were coupled with the activation of a G_qPCR (Boitano et al., 1997). As highlighted by the authors of this investigation, extracellular Na^+

serves as an allosteric modulator of many Class A G_qPCR that can increase their basal activity upon a reduction in $[Na^+]_o$ (Katritch et al., 2014; Seifert & Wenzel-Seifert, 2001). In accord, extracellular Na^+ can serve as a negative allosteric modulator that stabilizes the inactive state and primarily suppresses the basal activity of several Class A G_qPCRs, such as D4 dopamine receptor , μ-type opioid receptors (Costa, Lang, Gless, & Herz, 1990; Selley, Cao, Liu, & Childers, 2000), ghrelin receptor (Ferre et al., 2023), and chemokine receptor type 4 (CXCR4) . Several neurotransmitters and neuromodulators induce Ca^{2+} signals in hCMEC/D3 cells, including acetylcholine (Zuccolo, Laforenza, et al., 2019), glutamate (Negri, Faris, Pellavio, et al., 2019), and ATP (Bintig et al., 2012; Soda et al., 2025). However, only histamine has been shown to trigger intracellular Ca^{2+} oscillations via the H1R (Berra-Romani et al., 2020). Histamine-induced repetitive Ca^{2+} transients in hCMEC/D3 cells are driven by $InsP_3$-induced ER Ca^{2+} mobilization and SOCE (Berra-Romani, Faris, Pellavio, et al., 2019). Molecular simulation dynamics and quantitative structure-activity relationship (QSAR) analysis revealed that H1R also contains an allosteric Na^+-binding site that is close to the highly conserved aspartate residue D2.50 located in the transmembrane α-helix II. Extracellular Na^+ may compete with agonist binding to the human H1R, thereby reducing G_qPCR signaling activity in the presence of the agonist. However, H1R also displays a high constitutive signaling capacity that is unmasked when the H1R protein is overexpressed in heterologous cell lines but may also be detected in naïve cells (Arrang & Armand, 2024). Herein, we found that both pyrilamine, a selective H1R antagonist, and a selective siH1R (Berra-Romani et al., 2020) inhibited the $0Na^+_o$-induced intracellular Ca^{2+} oscillations while sparing the SRI. In agreement with this observation, the oscillatory Ca^{2+} response to histamine was enhanced in the absence of extracellular Na^+. These findings suggest that extracellular Na^+ depletion enhances the basal activity of H1R in hCMEC/D3 cells, thereby initiating the signal transduction pathway that leads to PLCβ activation, $InsP_3$-induced ER Ca^{2+} discharge, and SOCE activation. It must be pointed out that, while a reduction in $[Na^+]_o$ increases H1R affinity to agonist binding, it is still unclear whether extracellular Na^+ also regulates its constitutive activity. However, the basal signaling of the G_i Protein Coupled receptor, H3R, can be strongly reduced by increasing the extracellular concentration of NaCl (Schnell, Burleigh, Trick, & Seifert, 2010; Schnell & Seifert, 2010). Moreover, there is no evidence that hCMEC/D3 cells release histamine into the extracellular milieu. Therefore, we suggest that $0Na^+_o$-induced intracellular Ca^{2+} oscillations are driven by an increase in H1R-mediated constitutive signaling. In this context, an additional mechanism by which Ca^{2+} entry contributes to regulate the onset of the Ca^{2+} oscillations is by boosting PLCβ activity as shown earlier in HeLa cells (Bootman, Young, Young, Moreton, & Berridge, 1996). Indeed, if $0Na^+_o$ -induced increase in spontaneous H1R signaling is weak, Ca^{2+} entry could further stimulate PLCβ activation.

It has long been known that an increase in $[Ca^{2+}]_i$ is crucial to the regulation of many BBB functions, including the production of NO (E. Brailoiu, Shipsky, Yan, Abood, & Brailoiu, 2017; Negri, Faris, Soda, et al., 2021), which is the main vasorelaxing mediator in the human microcirculation and has also been shown to drive the haemodynamic response in the mouse somatosensory cortex (Longden et al., 2021). In addition, endothelial-derived NO may modulate neuronal excitability and long-term plasticity, as reviewed in (Scarpellino et al., 2024). A recent series of studies showed that multiple neurotransmitters and neuromodulators (Negri, Faris, Pellavio, et al., 2019; Negri et al., 2022; Soda et al., 2025; Zuccolo, Laforenza, et al., 2019), including histamine (Berra-Romani, Faris, Pellavio, et al., 2019), induce NO release through an increase in $[Ca^{2+}]_i$ in hCMEC/D3 cells. Our findings confirm that a long-lasting increase in endothelial $[Ca^{2+}]_i$ recruit eNOS to produce NO and influence NO-dependent signaling pathways at the NVU (Scarpellino et al., 2024).

As mentioned above, it has long been known that the total removal of extracellular Na^+ can induce $InsP_3$-dependent ER Ca^{2+} release events that are associated with the switch of NCX into the reverse, i.e., Ca^{2+} entry, mode (Boitano et al., 1997; James et al., 2023). The findings illustrated in the present investigation demonstrate for the first time that H1R is the G_qPCR that can be activated under $0Na^+_o$ conditions to recruit the PLCβ signaling pathway. We do believe that this information could be helpful to understand the complex Ca^{2+} signature that can be recorded when external Na^+ is fully replaced to investigate Na^+-dependent signaling pathways, e.g., cytosolic Ca^{2+} clearance through the NCX (Berra-Romani et al., 2010), cell migration, glycolysis and mitochondrial Ca^{2+}efflux. But obviously the question arises as to whether the complex Na^+ dependence of intracellular Ca^{2+} dynamics in human cerebrovascular endothelial cells has any physiological and/or pathological relevance (Larsen, Stoica, & MacAulay, 2016). Measuring changes in $[Na^+]_o$ in the brain milieu poses several technical challenges because of the size of Na^+-selective electrodes and the low signal-to-noise ratio. It has been estimated that the $[Na^+]_o$ may fall up to 20 mM during intense neuronal activity, although it is likely to reach even lower values in the synaptic cleft between nerve terminals and brain capillary endothelial cells (Paternain, Cohen, Stern-Bach, & Lerma, 2003). We found that a reduction in $[Na^+]_o$ from 150 mM to 130 mM was still able to reverse NCX into the reverse-mode and elicit intracellular Ca^{2+} oscillations in hCMEC/D3 cells. A reduction in the $[Na^+]_o$ may affect H1R signaling from the extracellular site of the receptor, i.e., the conserved Asp2.50. Therefore, H1Rs may be able to sense small fluctuations in $[Na^+]_o$, as reported for H3R. On the other hand, the resting V_M of hCMEC/D3 cells is rather depolarized (~ - 16 mV), as is commonly reported in microvascular ECs (Nilius & Droogmans, 2001), due to background Na^+ conductance and the lack of a detectable inwardly-rectifying K^+ current (Soda et al., 2024). For extracellular concentrations of 150 mM Na^+ and 1.8 mM Ca^{2+}, and at baseline intracellular concentrations of ~15 mM Na^+ and ~126 nM Ca^{2+} (Laskey, Adams,

Cannell, & van Breemen, 1992), the reversal potential for NCX is: ENCX = $3E_{Na}$ - $2E_{Ca}$ = - 68.1 mV (Blaustein & Lederer, 1999). Therefore, the NCX is likely to already operate in the reverse-mode under basal conditions to prevent intracellular Na^+ accumulation (Rose et al., 2020). Furthermore, NCX in the vascular cells is known to be expressed in restricted plasma membrane-ER junctional complexes, in which Na^+ entry - such as through TRP or background channels - may lead to local Na^+ nanodomains. In VSMCs, as well as in vascular ECs (Di Giuro et al., 2017), these plasma membrane-ER nanojunctions may present vertical pillars that strongly limit Na^+ diffusion into the bulk cytosol (Poburko, Fameli, Kuo, & van Breemen, 2008). Therefore, it is likely that, upon a reduction in $[Na^+]_o$ by 20 mM, the transmembrane Na^+ gradient driving Na^+ efflux through NCX is initially increased, thereby boosting Ca^{2+} entry and initiating the functional interplay with H1Rs. Additionally, even considering a small hyperpolarization of ~5 mV, ENCX would be ~ -79 mV with a $[Na^+]_o$ of 130 mM and, therefore, still in favor of Ca^{2+} entry. The lower strength of extracellular Na^+ signaling, however, will result in a less robust intracellular Ca^{2+} activity. Intriguingly, a reduction in $[Na^+]_o$ by 23 mM was recently shown to switch the NCX into the reverse-mode, thereby inducing Ca^{2+} entry and NO release in endothelial cells of the rat middle cerebral artery (Klapczynska et al., 2023). This data fully concurs with our findings that brain cerebrovascular ECs are able to sense even small fluctuations in $[Na^+]_o$ through NCX and H1R. In addition, it should be pointed out that: 1) iontophoretic application of glutamate and N-methyl-D-aspartate in rat CA1 hippocampal slices, respectively, caused a drop in $[Na^+]_o$ of more than 45 mM and 60 mM and 2) mathematical modeling demonstrated that the external Na^+ concentration at the center of the synaptic cleft may be depleted by ≈100 mM at the cat neuromuscular junction (Attwell & Iles, 1979) . Therefore, we cannot rule out the possibility that brain capillary endothelial cells sense intense neuronal firing through an increase in $[Ca^{2+}]_i$ that can ultimately lead to NO production. Furthermore, a dramatic reduction in $[Na^+]_o$ down to 40-60 mM has been recorded during cortical spreading depression (Herreras & Somjen, 1993). Intriguingly, endothelial-derived NO has been shown to modulate the threshold for spreading depolarization in eNOS-deficient mice (Petzold et al., 2008). Future work is mandatory to assess the physio-pathological role of $0Na^+_o$-induced intracellular Ca^{2+} oscillations, but this signaling pathway may constitute an unexpected signaling pathway to modulate the BBB during intense neuronal activity.

PART 3: Evaluation of global Ca^{2+} dynamics in hCMEC/D3 cells: TRPML1

In the present investigation, we showed that the lysosomal TRPML1 can trigger global Ca^{2+} signals, involving both Ca^{2+} release and Ca^{2+} entry, in human cerebrovascular ECs, as recently shown for HeLa cells and primary cultured human skin fibroblasts (Kilpatrick et al., 2016), rat primary cortical neurons (Tedeschi et al., 2021), and MDA-MB-231 breast cancer cells (Boretto et al., 2023). We further showed that TRPML1-mediated global Ca^{2+} signals lead to robust NO production, which is not only a recognized proxy for endothelial Ca^{2+} signaling, but also a critical vasorelaxing pathway in brain microcirculation. Therefore, the endothelial TRPML1 channel stands out as a novel component of the Ca^{2+} toolkit at the NVU that could be involved in the regulation of CBF during neuronal activity (Longden et al., 2021; Moccia et al., 2022; Mughal et al., 2024; Negri, Faris, Soda, et al., 2021). In agreement with this hypothesis, we showed that TRPML1 supports ATP-induced intracellular Ca^{2+} release and NO production in hCMEC/D3 cells. Lysosomal Ca^{2+} signaling though TPCs is emerging as an additional regulator of endothelial Ca^{2+} dynamics (Moccia, Negri, et al., 2021; Negri, Faris, et al., 2021a), but the endothelial role of TRPML1 is less known. A recent study has shown that TRPML1 can increase the interaction between lysosomes and multivesicular bodies in mouse coronary artery ECs, which results in reduced exosome release (Li et al., 2022). The application of low concentrations of ML-SA1 (10 μM), a TRPML1 synthetic agonist, induced a spatially-restricted lysosomal Ca^{2+} signal, as revealed by a GCaMP3-ML1 construct that was designed by expressing the genetic Ca^{2+}-indicator, GCaMP3, on the cytoplasmic NH2-tail of TRPML1 (Li et al., 2022). Herein, we assessed whether TRPML1 was expressed and able to induce global Ca^{2+} signals in hCMEC/D3 cells, as cytosolic Ca^{2+} signals are believed to play a crucial role in endothelium dependent NO release and CBF regulation at the neurovascular unit (Negri, Faris, Soda, et al., 2021). ML-SA1 induced a dose-dependent global Ca^{2+} signal consisting of a slow rise in $[Ca^{2+}]_i$ that leads to rapid Ca^{2+} upstroke followed by a plateau-like phase slightly above the baseline. This long-lasting increase in $[Ca^{2+}]_i$ was evident at concentrations of ML-SA1 ≥ 50 μM. Immunofluorescence and immunoblotting confirmed that the TRPML1 protein was expressed in acidic lysosomal vesicles that were widely distributed throughout the cytosol. These findings demonstrate that the endothelial TRPML1 channel is not only expressed in coronary, but also in brain circulation. Lysosomal derived Ca^{2+} signals can be amplified into a global increase in $[Ca^{2+}]_i$ by the recruitment of ER-embedded $InsP_3Rs$ via the CICR process (Galione et al., 2023; Kilpatrick, Eden, Schapira, Futter, & Patel, 2013; Kilpatrick et al., 2016; Penny, Kilpatrick, Han, Sneyd, & Patel, 2014). An additional pathway that could be activated upon the NAADP-triggered depletion of the $InsP_3$-sensitive ER Ca^{2+} store is SOCE, as reported in human cardiac mesenchymal stromal cells (Faris et

al., 2022) and MDA-MB-231 cells (Boretto et al., 2023), but not endothelial colony forming cells (Moccia, Negri, et al., 2021) and metastatic colorectal cancer cells (Faris et al., 2019). Furthermore, extracellular Ca^{2+} entry through TRPML1 channels that are located on the plasma membrane can support lysosomal Ca^{2+} mobilization (Kilpatrick et al., 2016). Consistently, in the absence of extracellular Ca^{2+}, ML-SA1 evoked a tiny and transient increase in $[Ca^{2+}]_i$ in hCMEC/D3 cells, which is similar to that recorded under the same conditions in HeLa cells (Kilpatrick et al., 2016). This finding supports the emerging notion that ML-SA1 can induce both intracellular Ca^{2+} release and extracellular Ca^{2+} entry (Kilpatrick et al., 2016; Tedeschi et al., 2021). The intracellular Ca^{2+} response to ML-SA1 was abolished by depleting the lysosomal Ca^{2+} pool and by the pharmacological or genetic blockade of TRPML1. These findings confirm that TRPML1 activation can also result in lysosomal Ca^{2+} mobilization in human cerebrovascular endothelial cells. We must point out that the tiny Ca^{2+} response evoked by ML-SA1 under $0Ca^{2+}$ conditions was almost suppressed despite the 60% reduction in TRPML1 protein expression achieved by the specific siTRPML1 used in the present study. The following mechanisms could explain these seemingly contradictory results. First, the remaining TRPML1 protein (≈40%) is not expressed in the acidic vesicle membranes and, therefore, cannot contribute to the Ca^{2+} signal. Second, our epifluorescence imaging system does not detect subcellular Ca^{2+} signals, as already reported in (Moccia, Negri, Shekha, Faris, & Guerra, 2019). Thus, we cannot rule out that some TRPML1-mediated local Ca^{2+} release events still occurred but were not detected. This hypothesis would be further consistent with the evidence that, although lysosomes contain ≈500 μM free Ca^{2+}, they occupy ≈3% of the total endothelial cell volume and are sparse throughout the cytoplasm. Thus, reducing TRPML1 protein expression by 60% could result in discrete subcellular Ca^{2+} signals that can be recorded only with confocal or 2-photon microscopy (Kinnear et al., 2008), especially if they are uncoupled from the ER, as further discussed below. For instance, Kinnear et al. revealed that NAADP elicited subcellular Ca^{2+} signals that did not significantly increase Fura-2 fluorescence until they led to ER Ca^{2+} release in rat pulmonary artery vascular smooth muscle cells (Kinnear et al., 2008). In agreement with these hypotheses, we have recently shown that the lysosomal Ca^{2+} response to NAADP is virtually abolished in circulating endothelial colony forming cells transfected with a siRNA selectively targeting TPC1 despite the fact the TPC1 protein expression is downregulated by ≈ 60% (Moccia, Negri, et al., 2021). Therefore, we are confident that the overall evidence based upon the pharmacological and genetic blockade of TRPML1 supports its primary role in the Ca^{2+}-response to ML-SA1. ML-SA1-induced intracellular Ca^{2+} mobilization was also attenuated or virtually abolished by depleting the ER Ca^{2+} store and by blocking $InsP_3Rs$. These findings are consistent with those reported in HeLa cells (Kilpatrick et al., 2016) and indicate that $InsP_3Rs$ sustain the lysosomal Ca^{2+} signal in hCMEC/D3 cells. Therefore, the

absence of a regenerative Ca^{2+} response at low concentrations of ML-SA1 (<50 μM) can be explained by the failure of spatially-restricted lysosomal Ca^{2+} nanodomains to fully recruit the juxtaposed $InsP_3Rs$ (Davis, Morgan, & Galione, 2023; Medina et al., 2015). On the other hand, an increase in the amount of lysosomal Ca^{2+} mobilized by higher concentrations of ML-SA1 (>50 μM) could successfully trigger ER Ca^{2+} release through $InsP_3Rs$. Lysosomal Ca^{2+} release could mobilize the ER Ca^{2+} pool by either triggering CICR through RyRs/$InsP_3Rs$ (Yuan et al., 2024) or by refilling the ER in a SERCA-dependent manner, thereby leading to luminal Ca^{2+} overload and $InsP_3R$/RyR opening (Macgregor et al., 2007). A recent investigation revealed that TRPML1-mediated lysosomal Ca^{2+} release tonically regulates the ER Ca^{2+} content in primary rat cortical neurons (Tedeschi et al., 2021). Herein, we found that CPA-evoked ER Ca^{2+} release, which can be used as a proxy for the free ER Ca^{2+} concentration (Brandman, Liou, Park, & Meyer, 2007; Lodola, Martino, Tullii, Lanzani, & Antognazza, 2017), was significantly reduced upon the pharmacological (with ML-SI3) or genetic (with the specific siTRPML1) blockade of TRPML1. This finding strongly suggests that local TRPML1-mediated Ca^{2+} signals are rerouted into the ER in a SERCA-dependent manner, thereby controlling the free ER Ca^{2+} concentration that is available to be released through the ER leakage channels and/or the $InsP_3R$. Therefore, it is reasonable to conclude that ML-SA1 gates TRPML1, which is likely to lead to ER Ca^{2+} overload and $InsP_3R$ activation from the luminal side. Consistent with this hypothesis, the pharmacological blockade of SOCE with two distinct pyrazole derivatives, Pyr6 and BTP-2, converted the global increase in $[Ca^{2+}]_i$ induced by ML-SA1 into a tiny Ca^{2+} transient that strongly resembled that measured under $0Ca^{2+}$ conditions. In addition, the "Ca^{2+} add-back" protocol revealed that TRPML1-dependent Ca^{2+} entry did not require the presence of the extracellular agonist to occur, while it was only associated with the previous depletion of the intracellular Ca^{2+} pool. This feature is a hallmark of SOCE activation, which confirms that TRPML1 leads to ER Ca^{2+} depletion (Bird, DeHaven, Smyth, & Putney, 2008; Murata et al., 2007). A recent study showed that TRPML1 may physically interact with STIM1 (Tedeschi et al., 2021), which could facilitate the assembly of the SOCE machinery. Collectively, these findings strongly suggest that TRPML1-mediated lysosomal Ca^{2+} release can trigger ER Ca^{2+} release through the Ca^{2+}-dependent luminal recruitment of $InsP_3Rs$, thereby leading to SOCE activation. Nevertheless, a direct measurement of the ER Ca^{2+} concentration is necessary to provide the clear-cut evidence that TRPML1 contributes to ER Ca^{2+} refilling.

A further hint at the physiological role played by TRPML1-mediated global Ca^{2+} signals arises from NO measurements. Single-cell imaging of DAF-FM DA fluorescence showed that ML-SA1 induced robust NO release via the Ca^{2+}-dependent recruitment of eNOS. As reported by single-cell Fura-2 imaging, ML-SA1-induced NO production was abolished by preventing lysosomal Ca^{2+} release

through TRPML1 and the Ca^{2+}-dependent eNOS activation. These findings provide the first evidence that, in addition to NAADP-gated TPCs (G. C. Brailoiu et al., 2016), the lysosomal Ca^{2+} pool could also lead to endothelium-dependent NO release via TRPML1. A recent study has shown that TRPML1-mediated Ca^{2+} release can trigger Ca^{2+} sparks via CICR through juxtaposed RyRs in VSMCs from mouse cerebral arteries (Thakore, Ali, & Earley, 2020). Ca^{2+} sparks, in turn, induce vasodilation and increase local CBF by activating big conductance Ca^{2+}-dependent K^+ channels (Thakore, Ali, et al., 2020). However, these data collectively suggest that TRPML1 could be critical to regulate vascular reactivity in brain microcirculation, in both VSMCs and ECs. In addition, TRPML1 could also regulate other functions in human cerebrovascular endothelial cells, including lysosome size and trafficking, autophagy (Yang, Zhao, Gu, Feng, & Xu, 2019), and membrane repair. TRPML1 could also be physiologically regulated by ROS (Zhang et al., 2016), which are emerging as crucial regulators of the endothelial Ca^{2+} signals at the NVU (Berra-Romani et al., 2023). Future work might assess whether ROS modulate TRPML1 activation in human cerebrovascular endothelial cells. In order to confirm that TRPML1 is involved in agonist-evoked Ca^{2+} signaling in hCMEC/D3 cells, we assessed whether TRPML1 modulates the Ca^{2+} response to ATP, which is one of the most widespread endothelial agonists (Scarpellino et al., 2019). ATP has been shown to elicit $InsP_3$-induced ER Ca^{2+} release in hCMEC/D3 cells (Bintig et al., 2012; Forcaia et al., 2021). Herein, we found that ATP-induced Ca^{2+} signals and NO release were both impaired by blocking TRPML1 with ML-SI3 or the specific siTRPML1 or by inhibiting $PI(3,5)P_2$ production with apilimod. The most plausible hypothesis to explain these findings is that TRPML1 is gated by $PI(3,5)P_2$ to maintain ER Ca^{2+} levels, thereby enabling the proper Ca^{2+} response to ATP.

CHAPTER 9: CONCLUSIONS

This study has highlighted the importance of studying Ca^{2+} dynamics in the human cerebral endothelium. By examining membrane biophysical properties, we were able to identify the main ionic species, i.e., Na^+ and Cl^-, that govern the resting V_M of hCMEC/D3 cells. Furthermore, we investigated the global Ca^{2+} dynamics in hCMEC/D3 cells, focusing on the role of reverse mode NCX and H1R in the complex Ca^{2+} signatures and NO production elicited by the reduction in $[Na^+]_o$. Finally, analysis of the TRPML1 further highlighted the critical role of lysosomes, alongside the ER, as key organelles supporting Ca^{2+}-mediated signaling pathways in human cerebrovascular ECs. These data emphasize the need to shed further light on endothelial signaling pathways to better understand how ECs contribute to the regulation of CBF and NVC.

CHAPTER 10: BIBLIOGRAPHY

Abbott, N. J., Patabendige, A. A., Dolman, D. E., Yusof, S. R., & Begley, D. J. (2010). Structure and function of the blood-brain barrier. *Neurobiology of Disease, 37*(1), 13-25. doi:10.1016/j.nbd.2009.07.030

Agasid, M. T., Sorensen, L., Urner, L. H., Yan, J., & Robinson, C. V. (2021). The Effects of Sodium Ions on Ligand Binding and Conformational States of G Protein-Coupled Receptors-Insights from Mass Spectrometry. *J Am Chem Soc, 143*(11), 4085-4089. doi:10.1021/jacs.0c11837

Agrud, A., Subburaju, S., Goel, P., Ren, J., Kumar, A. S., Caldarone, B. J., . . . Vasudevan, A. (2022). Gabrb3 endothelial cell-specific knockout mice display abnormal blood flow, hypertension, and behavioral dysfunction. *Sci Rep, 12*(1), 4922. doi:10.1038/s41598-022-08806-9

Andrikopoulos, P., Baba, A., Matsuda, T., Djamgoz, M. B., Yaqoob, M. M., & Eccles, S. A. (2011). Ca2+ influx through reverse mode Na+/Ca2+ exchange is critical for vascular endothelial growth factor-mediated extracellular signal-regulated kinase (ERK) 1/2 activation and angiogenic functions of human endothelial cells. *J Biol Chem, 286*(44), 37919-37931. doi:10.1074/jbc.M111.251777

Andrikopoulos, P., Eccles, S. A., & Yaqoob, M. M. (2017). Coupling between the TRPC3 ion channel and the NCX1 transporter contributed to VEGF-induced ERK1/2 activation and angiogenesis in human primary endothelial cells. *Cell Signal, 37*, 12-30. doi:10.1016/j.cellsig.2017.05.013

Andrikopoulos, P., Kieswich, J., Harwood, S. M., Baba, A., Matsuda, T., Barbeau, O., . . . Yaqoob, M. M. (2015). Endothelial Angiogenesis and Barrier Function in Response to Thrombin Require Ca2+ Influx through the Na+/Ca2+ Exchanger. *J Biol Chem, 290*(30), 18412-18428. doi:10.1074/jbc.M114.628156

Arrang, J. M., & Armand, V. (2024). Histamine H(1)-receptor-mediated modulation of NMDA receptors signaling responses. *Pharmacol Res Perspect, 12*(5), e1216. doi:10.1002/prp2.1216

Attwell, D., Buchan, A. M., Charpak, S., Lauritzen, M., Macvicar, B. A., & Newman, E. A. (2010). Glial and neuronal control of brain blood flow. *Nature, 468*(7321), 232-243. doi:10.1038/nature09613

Attwell, D., & Iles, J. F. (1979). Synaptic transmission: ion concentration changes in the synaptic cleft. *Proc R Soc Lond B Biol Sci, 206*(1162), 115-131. doi:10.1098/rspb.1979.0095

Baker, M. R., Fan, G., Arige, V., Yule, D. I., & Serysheva, II. (2023). Understanding IP(3)R channels: From structural underpinnings to ligand-dependent conformational landscape. *Cell Calcium, 114*, 102770. doi:10.1016/j.ceca.2023.102770

Berra-Romani, R., Brunetti, V., Pellavio, G., Soda, T., Laforenza, U., Scarpellino, G., & Moccia, F. (2023). Allyl Isothiocianate Induces Ca(2+) Signals and Nitric Oxide Release by Inducing Reactive Oxygen Species Production in the Human Cerebrovascular Endothelial Cell Line hCMEC/D3. *Cells, 12*(13). doi:10.3390/cells12131732

Berra-Romani, R., Faris, P., Negri, S., Botta, L., Genova, T., & Moccia, F. (2019). Arachidonic Acid Evokes an Increase in Intracellular Ca(2+) Concentration and Nitric Oxide Production in Endothelial Cells from Human Brain Microcirculation. *Cells, 8*(7). doi:10.3390/cells8070689

Berra-Romani, R., Faris, P., Pellavio, G., Orgiu, M., Negri, S., Forcaia, G., . . . Moccia, F. (2019). Histamine induces intracellular Ca(2+) oscillations and nitric oxide release in endothelial cells from brain microvascular circulation. *Journal of Cellular Physiology*. doi:10.1002/jcp.29071

Berra-Romani, R., Faris, P., Pellavio, G., Orgiu, M., Negri, S., Forcaia, G., . . . Moccia, F. (2020). Histamine induces intracellular Ca(2+) oscillations and nitric oxide release in endothelial

cells from brain microvascular circulation. *Journal of Cellular Physiology, 235*(2), 1515-1530. doi:10.1002/jcp.29071

Berra-Romani, R., Raqeeb, A., Guzman-Silva, A., Torres-Jacome, J., Tanzi, F., & Moccia, F. (2010). Na+-Ca2+ exchanger contributes to Ca2+ extrusion in ATP-stimulated endothelium of intact rat aorta. *Biochem Biophys Res Commun, 395*(1), 126-130. doi:10.1016/j.bbrc.2010.03.153

Berra-Romani, R., Raqeeb, A., Torres-Jácome, J., Guzman-Silva, A., Guerra, G., Tanzi, F., & Moccia, F. (2012). The mechanism of injury-induced intracellular calcium concentration oscillations in the endothelium of excised rat aorta. *J Vasc Res, 49*(1), 65-76. doi:10.1159/000329618

Bintig, W., Begandt, D., Schlingmann, B., Gerhard, L., Pangalos, M., Dreyer, L., . . . Ngezahayo, A. (2012). Purine receptors and Ca(2+) signalling in the human blood-brain barrier endothelial cell line hCMEC/D3. *Purinergic Signal, 8*(1), 71-80. doi:10.1007/s11302-011-9262-7

Bird, G. S., DeHaven, W. I., Smyth, J. T., & Putney, J. W., Jr. (2008). Methods for studying store-operated calcium entry. *Methods, 46*(3), 204-212. doi:10.1016/j.ymeth.2008.09.009

Bird, G. S., & Putney, J. W., Jr. (2005). Capacitative calcium entry supports calcium oscillations in human embryonic kidney cells. *J Physiol, 562*(Pt 3), 697-706. doi:10.1113/jphysiol.2004.077289

Birnbaumer, L. (2009). The TRPC class of ion channels: a critical review of their roles in slow, sustained increases in intracellular Ca(2+) concentrations. *Annu Rev Pharmacol Toxicol, 49*, 395-426. doi:10.1146/annurev.pharmtox.48.113006.094928

Blatter, L. A. (2017). Tissue Specificity: SOCE: Implications for Ca2+ Handling in Endothelial Cells. *Adv Exp Med Biol, 993*, 343-361. doi:10.1007/978-3-319-57732-6_18

Blaustein, M. P., & Lederer, W. J. (1999). Sodium/calcium exchange: its physiological implications. *Physiol Rev, 79*(3), 763-854. doi:10.1152/physrev.1999.79.3.763

Boitano, S., Woodruff, M. L., & Dirksen, E. R. (1997). Reduction of extracellular Na+ causes a release of Ca2+ from internal stores in airway epithelial cells. *Am J Physiol, 272*(6 Pt 1), L1189-1197. doi:10.1152/ajplung.1997.272.6.L1189

Boittin, F. X., Alonso, F., Le Gal, L., Allagnat, F., Beny, J. L., & Haefliger, J. A. (2013). Connexins and M3 muscarinic receptors contribute to heterogeneous Ca(2+) signaling in mouse aortic endothelium. *Cell Physiol Biochem, 31*(1), 166-178. doi:10.1159/000343358

Bootman, M. D., Berridge, M. J., & Taylor, C. W. (1992). All-or-nothing Ca2+ mobilization from the intracellular stores of single histamine-stimulated HeLa cells. *J Physiol, 450*, 163-178. doi:10.1113/jphysiol.1992.sp019121

Bootman, M. D., Young, K. W., Young, J. M., Moreton, R. B., & Berridge, M. J. (1996). Extracellular calcium concentration controls the frequency of intracellular calcium spiking independently of inositol 1,4,5-trisphosphate production in HeLa cells. *Biochemical Journal, 314 (Pt 1)*, 347-354. doi:10.1042/bj3140347

Boretto, C., Actis, C., Faris, P., Cordero, F., Beccuti, M., Ferrero, G., . . . Autelli, R. (2023). Tamoxifen Activates Transcription Factor EB and Triggers Protective Autophagy in Breast Cancer Cells by Inducing Lysosomal Calcium Release: A Gateway to the Onset of Endocrine Resistance. *Int J Mol Sci, 25*(1). doi:10.3390/ijms25010458

Brailoiu, E., Shipsky, M. M., Yan, G., Abood, M. E., & Brailoiu, G. C. (2017). Mechanisms of modulation of brain microvascular endothelial cells function by thrombin. *Brain Res, 1657*, 167-175. doi:10.1016/j.brainres.2016.12.011

Brailoiu, G. C., Deliu, E., Console-Bram, L. M., Soboloff, J., Abood, M. E., Unterwald, E. M., & Brailoiu, E. (2016). Cocaine inhibits store-operated Ca2+ entry in brain microvascular endothelial cells: critical role for sigma-1 receptors. *Biochemical Journal, 473*(1), 1-5. doi:10.1042/BJ20150934

Brandman, O., Liou, J., Park, W. S., & Meyer, T. (2007). STIM2 is a feedback regulator that stabilizes basal cytosolic and endoplasmic reticulum Ca2+ levels. *Cell, 131*(7), 1327-1339. doi:10.1016/j.cell.2007.11.039

Brunetti, V., Soda, T., Berra-Romani, R., De Sarro, G., Guerra, G., Scarpellino, G., & Moccia, F. (2024). Two Signaling Modes Are Better than One: Flux-Independent Signaling by Ionotropic Glutamate Receptors Is Coming of Age. *Biomedicines, 12*(4). doi:10.3390/biomedicines12040880

Celentano, C., Carotenuto, L., Miceli, F., Carleo, G., Corrado, B., Baroli, G., . . . Barrese, V. (2024). Kv7 channel activation reduces brain endothelial cell permeability and prevents kainic acid-induced blood-brain barrier damage. *Am J Physiol Cell Physiol, 326*(3), C893-C904. doi:10.1152/ajpcell.00709.2023

Cerneckis, J., Cai, H., & Shi, Y. (2024). Induced pluripotent stem cells (iPSCs): molecular mechanisms of induction and applications. *Signal Transduct Target Ther, 9*(1), 112. doi:10.1038/s41392-024-01809-0

Chauvet, S., Jarvis, L., Chevallet, M., Shrestha, N., Groschner, K., & Bouron, A. (2016). Pharmacological Characterization of the Native Store-Operated Calcium Channels of Cortical Neurons from Embryonic Mouse Brain. *Front Pharmacol, 7*, 486. doi:10.3389/fphar.2016.00486

Chebib, M., & Johnston, G. A. (1999). The 'ABC' of GABA receptors: a brief review. *Clin Exp Pharmacol Physiol, 26*(11), 937-940. doi:10.1046/j.1440-1681.1999.03151.x

Chen, Q., She, J., Zeng, W., Guo, J., Xu, H., Bai, X. C., & Jiang, Y. (2017). Structure of mammalian endolysosomal TRPML1 channel in nanodiscs. *Nature, 550*(7676), 415-418. doi:10.1038/nature24035

Chen, Y. L., & Sonkusare, S. K. (2020). Endothelial TRPV4 channels and vasodilator reactivity. *Curr Top Membr, 85*, 89-117. doi:10.1016/bs.ctm.2020.01.007

Cheng, W., Yang, F., Takanishi, C. L., & Zheng, J. (2007). Thermosensitive TRPV channel subunits coassemble into heteromeric channels with intermediate conductance and gating properties. *Journal of General Physiology, 129*(3), 191-207. doi:10.1085/jgp.200709731

Choi, Y. K., & Vasudevan, A. (2018). Endothelial GABA signaling: a phoenix awakened. *Aging (Albany NY), 10*(5), 859-860. doi:10.18632/aging.101457

Cosens, D. J., & Manning, A. (1969). Abnormal electroretinogram from a Drosophila mutant. *Nature, 224*(5216), 285-287. doi:10.1038/224285a0

Costa, T., Lang, J., Gless, C., & Herz, A. (1990). Spontaneous association between opioid receptors and GTP-binding regulatory proteins in native membranes: specific regulation by antagonists and sodium ions. *Mol Pharmacol, 37*(3), 383-394.

Daneman, R., & Prat, A. (2015). The blood-brain barrier. *Cold Spring Harb Perspect Biol, 7*(1), a020412. doi:10.1101/cshperspect.a020412

Davis, L. C., Morgan, A. J., & Galione, A. (2023). Optical profiling of autonomous Ca(2+) nanodomains generated by lysosomal TPC2 and TRPML1. *Cell Calcium, 116*, 102801. doi:10.1016/j.ceca.2023.102801

De Bock, M., Wang, N., Decrock, E., Bol, M., Gadicherla, A. K., Culot, M., . . . Leybaert, L. (2013). Endothelial calcium dynamics, connexin channels and blood-brain barrier function. *Prog Neurobiol, 108*, 1-20. doi:10.1016/j.pneurobio.2013.06.001

Di Giuro, C. M. L., Shrestha, N., Malli, R., Groschner, K., van Breemen, C., & Fameli, N. (2017). Na (+)/Ca(2+) exchangers and Orai channels jointly refill endoplasmic reticulum (ER) Ca(2+) via ER nanojunctions in vascular endothelial cells. *Pflugers Arch, 469*(10), 1287-1299. doi:10.1007/s00424-017-1989-8

Di Paola, S., Scotto-Rosato, A., & Medina, D. L. (2018). TRPML1: The Ca((2+))retaker of the lysosome. *Cell Calcium, 69*, 112-121. doi:10.1016/j.ceca.2017.06.006

Ding, L., Kshirsagar, P., Agrawal, P., & Murry, D. J. (2025). Crossing the Blood-Brain Barrier: Innovations in Receptor- and Transporter-Mediated Transcytosis Strategies. *Pharmaceutics, 17*(6). doi:10.3390/pharmaceutics17060706

Dong, X. P., Cheng, X., Mills, E., Delling, M., Wang, F., Kurz, T., & Xu, H. (2008). The type IV mucolipidosis-associated protein TRPML1 is an endolysosomal iron release channel. *Nature, 455*(7215), 992-996. doi:10.1038/nature07311

Dong, X. P., Shen, D., Wang, X., Dawson, T., Li, X., Zhang, Q., . . . Xu, H. (2010). PI(3,5)P(2) controls membrane trafficking by direct activation of mucolipin Ca(2+) release channels in the endolysosome. *Nat Commun, 1*, 38. doi:10.1038/ncomms1037

Du, J., Xie, J., & Yue, L. (2009). Intracellular calcium activates TRPM2 and its alternative spliced isoforms. *Proc Natl Acad Sci U S A, 106*(17), 7239-7244. doi:10.1073/pnas.0811725106

Earley, S. (2011). Endothelium-dependent cerebral artery dilation mediated by transient receptor potential and Ca2+-activated K+ channels. *J Cardiovasc Pharmacol, 57*(2), 148-153. doi:10.1097/FJC.0b013e3181f580d9

Earley, S., & Brayden, J. E. (2015). Transient receptor potential channels in the vasculature. *Physiol Rev, 95*(2), 645-690. doi:10.1152/physrev.00026.2014

Eisenman, G. (1962). Cation selective glass electrodes and their mode of operation. *Biophys J, 2*(2 Pt 2), 259-323. doi:10.1016/s0006-3495(62)86959-8

Elhusseiny, A., & Hamel, E. (2000). Muscarinic--but not nicotinic--acetylcholine receptors mediate a nitric oxide-dependent dilation in brain cortical arterioles: a possible role for the M5 receptor subtype. *J Cereb Blood Flow Metab, 20*(2), 298-305. doi:10.1097/00004647-200002000-00011

Faris, P., Casali, C., Negri, S., Iengo, L., Biggiogera, M., Maione, A. S., & Moccia, F. (2022). Nicotinic Acid Adenine Dinucleotide Phosphate Induces Intracellular Ca(2+) Signalling and Stimulates Proliferation in Human Cardiac Mesenchymal Stromal Cells. *Front Cell Dev Biol, 10*, 874043. doi:10.3389/fcell.2022.874043

Faris, P., Pellavio, G., Ferulli, F., Di Nezza, F., Shekha, M., Lim, D., . . . Moccia, F. (2019). Nicotinic Acid Adenine Dinucleotide Phosphate (NAADP) Induces Intracellular Ca(2+) Release through the Two-Pore Channel TPC1 in Metastatic Colorectal Cancer Cells. *Cancers (Basel), 11*(4), pii: E542. doi:10.3390/cancers11040542

Faris, P., Shekha, M., Montagna, D., Guerra, G., & Moccia, F. (2018). Endolysosomal Ca(2+) Signalling and Cancer Hallmarks: Two-Pore Channels on the Move, TRPML1 Lags Behind! *Cancers (Basel), 11*(1). doi:10.3390/cancers11010027

Ferre, G., Gomes, A. A. S., Louet, M., Damian, M., Bisch, P. M., Saurel, O., . . . Baneres, J. L. (2023). Sodium is a negative allosteric regulator of the ghrelin receptor. *Cell Rep, 42*(4), 112320. doi:10.1016/j.celrep.2023.112320

Forcaia, G., Formicola, B., Terribile, G., Negri, S., Lim, D., Biella, G., . . . Sancini, G. (2021). Multifunctional Liposomes Modulate Purinergic Receptor-Induced Calcium Wave in Cerebral Microvascular Endothelial Cells and Astrocytes: New Insights for Alzheimer's disease. *Mol Neurobiol, 58*(6), 2824-2835. doi:10.1007/s12035-021-02299-9

Forstermann, U., & Sessa, W. C. (2012). Nitric oxide synthases: regulation and function. *Eur Heart J, 33*(7), 829-837, 837a-837d. doi:10.1093/eurheartj/ehr304

Galione, A., Davis, L. C., Martucci, L. L., & Morgan, A. J. (2023). NAADP-Mediated Ca(2+) Signalling. *Handb Exp Pharmacol, 278*, 3-34. doi:10.1007/164_2022_607

Gandhirajan, R. K., Meng, S., Chandramoorthy, H. C., Mallilankaraman, K., Mancarella, S., Gao, H., . . . Madesh, M. (2013). Blockade of NOX2 and STIM1 signaling limits lipopolysaccharide-induced vascular inflammation. *J Clin Invest, 123*(2), 887-902. doi:10.1172/JCI65647

Garcia, D. C. G., & Longden, T. A. (2020). Ion channels in capillary endothelium. *Curr Top Membr, 85*, 261-300. doi:10.1016/bs.ctm.2020.01.005

Garland, C. J., & Dora, K. A. (2017). EDH: endothelium-dependent hyperpolarization and microvascular signalling. *Acta Physiol (Oxf), 219*(1), 152-161. doi:10.1111/apha.12649

Garrity, A. G., Wang, W., Collier, C. M., Levey, S. A., Gao, Q., & Xu, H. (2016). The endoplasmic reticulum, not the pH gradient, drives calcium refilling of lysosomes. *Elife, 5*. doi:10.7554/eLife.15887

Gascoigne, D. A., Serdyukova, N. A., & Aksenov, D. P. (2021). Early Development of the GABAergic System and the Associated Risks of Neonatal Anesthesia. *Int J Mol Sci, 22*(23). doi:10.3390/ijms222312951

Gaynullina, D. K., Tarasova, O. S., Shvetsova, A. A., Borzykh, A. A., & Schubert, R. (2022). The Effects of Acidosis on eNOS in the Systemic Vasculature: A Focus on Early Postnatal Ontogenesis. *Int J Mol Sci, 23*(11). doi:10.3390/ijms23115987

Gees, M., Colsoul, B., & Nilius, B. (2010). The role of transient receptor potential cation channels in Ca2+ signaling. *Cold Spring Harb Perspect Biol, 2*(10), a003962. doi:10.1101/cshperspect.a003962

Greenberg, H. Z. E., Carlton-Carew, S. R. E., Khan, D. M., Zargaran, A. K., Jahan, K. S., Vanessa Ho, W. S., & Albert, A. P. (2017). Heteromeric TRPV4/TRPC1 channels mediate calcium-sensing receptor-induced nitric oxide production and vasorelaxation in rabbit mesenteric arteries. *Vascul Pharmacol, 96-98*, 53-62. doi:10.1016/j.vph.2017.08.005

Groschner, K., Shrestha, N., & Fameli, N. (2017). Cardiovascular and Hemostatic Disorders: SOCE in Cardiovascular Cells: Emerging Targets for Therapeutic Intervention. *Adv Exp Med Biol, 993*, 473-503. doi:10.1007/978-3-319-57732-6_24

Guerra, G., Lucariello, A., Perna, A., Botta, L., De Luca, A., & Moccia, F. (2018). The Role of Endothelial Ca(2+) Signaling in Neurovascular Coupling: A View from the Lumen. *Int J Mol Sci, 19*(4), pii: E938. doi:10.3390/ijms19040938

Hamel, E. (2004). Cholinergic modulation of the cortical microvascular bed. *Prog Brain Res, 145*, 171-178. doi:10.1016/S0079-6123(03)45012-7

Hamel, E. (2006). Perivascular nerves and the regulation of cerebrovascular tone. *J Appl Physiol (1985), 100*(3), 1059-1064. doi:10.1152/japplphysiol.00954.2005

Harraz, O. F., Longden, T. A., Hill-Eubanks, D., & Nelson, M. T. (2018). PIP2 depletion promotes TRPV4 channel activity in mouse brain capillary endothelial cells. *Elife, 7*. doi:10.7554/eLife.38689

Hartz, A. M. S., Schulz, J. A., Sokola, B. S., Edelmann, S. E., Shen, A. N., Rempe, R. G., . . . Bauer, B. (2018). Isolation of Cerebral Capillaries from Fresh Human Brain Tissue. *J Vis Exp*(139). doi:10.3791/57346

Heathcote, H. R., Lee, M. D., Zhang, X., Saunter, C. D., Wilson, C., & McCarron, J. G. (2019). Endothelial TRPV4 channels modulate vascular tone by Ca(2+) -induced Ca(2+) release at inositol 1,4,5-trisphosphate receptors. *Br J Pharmacol, 176*(17), 3297-3317. doi:10.1111/bph.14762

Helms, H. C., Abbott, N. J., Burek, M., Cecchelli, R., Couraud, P. O., Deli, M. A., . . . Brodin, B. (2016). In vitro models of the blood-brain barrier: An overview of commonly used brain endothelial cell culture models and guidelines for their use. *J Cereb Blood Flow Metab, 36*(5), 862-890. doi:10.1177/0271678X16630991

Herreras, O., & Somjen, G. G. (1993). Analysis of potential shifts associated with recurrent spreading depression and prolonged unstable spreading depression induced by microdialysis of elevated K+ in hippocampus of anesthetized rats. *Brain Res, 610*(2), 283-294. doi:10.1016/0006-8993(93)91412-l

Hogan-Cann, A. D., & Anderson, C. M. (2016). Physiological Roles of Non-Neuronal NMDA Receptors. *Trends Pharmacol Sci, 37*(9), 750-767. doi:10.1016/j.tips.2016.05.012

Hou, Y., He, H., Ma, M., & Zhou, R. (2023). Apilimod activates the NLRP3 inflammasome through lysosome-mediated mitochondrial damage. *Front Immunol, 14*, 1128700. doi:10.3389/fimmu.2023.1128700

Iadecola, C. (2017). The Neurovascular Unit Coming of Age: A Journey through Neurovascular Coupling in Health and Disease. *Neuron, 96*(1), 17-42. doi:10.1016/j.neuron.2017.07.030

Jackson, W. F. (2017). Boosting the signal: Endothelial inward rectifier K(+) channels. *Microcirculation, 24*(3). doi:10.1111/micc.12319
Jackson, W. F. (2022). Endothelial Ion Channels and Cell-Cell Communication in the Microcirculation. *Front Physiol, 13*, 805149. doi:10.3389/fphys.2022.805149
James, A. D., Unthank, K. P., Jones, I., Sajjaboontawee, N., Sizer, R. E., Chawla, S., . . . Brackenbury, W. J. (2023). Sodium regulates PLC and IP(3) R-mediated calcium signaling in invasive breast cancer cells. *Physiol Rep, 11*(7), e15663. doi:10.14814/phy2.15663
Katritch, V., Fenalti, G., Abola, E. E., Roth, B. L., Cherezov, V., & Stevens, R. C. (2014). Allosteric sodium in class A GPCR signaling. *Trends Biochem Sci, 39*(5), 233-244. doi:10.1016/j.tibs.2014.03.002
Keaney, J., & Campbell, M. (2015). The dynamic blood-brain barrier. *FEBS J, 282*(21), 4067-4079. doi:10.1111/febs.13412
Kilpatrick, B. S., Eden, E. R., Schapira, A. H., Futter, C. E., & Patel, S. (2013). Direct mobilisation of lysosomal Ca2+ triggers complex Ca2+ signals. *Journal of Cell Science, 126*(Pt 1), 60-66. doi:10.1242/jcs.118836
Kilpatrick, B. S., Yates, E., Grimm, C., Schapira, A. H., & Patel, S. (2016). Endo-lysosomal TRP mucolipin-1 channels trigger global ER Ca2+ release and Ca2+ influx. *Journal of Cell Science, 129*(20), 3859-3867. doi:10.1242/jcs.190322
Kim, K. J., Iddings, J. A., Stern, J. E., Blanco, V. M., Croom, D., Kirov, S. A., & Filosa, J. A. (2015). Astrocyte contributions to flow/pressure-evoked parenchymal arteriole vasoconstriction. *J Neurosci, 35*(21), 8245-8257. doi:10.1523/JNEUROSCI.4486-14.2015
Kinnear, N. P., Wyatt, C. N., Clark, J. H., Calcraft, P. J., Fleischer, S., Jeyakumar, L. H., . . . Evans, A. M. (2008). Lysosomes co-localize with ryanodine receptor subtype 3 to form a trigger zone for calcium signalling by NAADP in rat pulmonary arterial smooth muscle. *Cell Calcium, 44*(2), 190-201. doi:10.1016/j.ceca.2007.11.003
Kisler, K., Nelson, A. R., Montagne, A., & Zlokovic, B. V. (2017). Cerebral blood flow regulation and neurovascular dysfunction in Alzheimer disease. *Nat Rev Neurosci, 18*(7), 419-434. doi:10.1038/nrn.2017.48
Klapczynska, K., Aleksandrowicz, M., & Kozniewska, E. (2023). Role of the endothelial reverse mode sodium-calcium exchanger in the dilation of the rat middle cerebral artery during hypoosmotic hyponatremia. *Pflugers Arch, 475*(3), 381-390. doi:10.1007/s00424-022-02770-z
Kocharyan, A., Fernandes, P., Tong, X. K., Vaucher, E., & Hamel, E. (2008). Specific subtypes of cortical GABA interneurons contribute to the neurovascular coupling response to basal forebrain stimulation. *J Cereb Blood Flow Metab, 28*(2), 221-231. doi:10.1038/sj.jcbfm.9600558
Koster, H. P., van Os, C. H., & Bindels, R. J. (1993). Ca2+ oscillations in the rabbit renal cortical collecting system induced by Na+ free solutions. *Kidney Int, 43*(4), 828-836. doi:10.1038/ki.1993.117
Kumabe, H., Masuda, T., Ito, S., Furihata, T., Toda, A., Mogi, M., . . . Ohtsuki, S. (2025). Proteome profile differences among human, monkey, and mouse brain microvessels and cultured brain microvascular endothelial cells. *Fluids Barriers CNS, 22*(1), 53. doi:10.1186/s12987-025-00650-z
Kurauchi, Y., Hisatsune, A., Seki, T., & Katsuki, H. (2016). Na(+), K(+)-ATPase dysfunction causes cerebrovascular endothelial cell degeneration in rat prefrontal cortex slice cultures. *Brain Res, 1644*, 249-257. doi:10.1016/j.brainres.2016.05.025
Larsen, B. R., Stoica, A., & MacAulay, N. (2016). Managing Brain Extracellular K(+) during Neuronal Activity: The Physiological Role of the Na(+)/K(+)-ATPase Subunit Isoforms. *Front Physiol, 7*, 141. doi:10.3389/fphys.2016.00141

Laskey, R. E., Adams, D. J., Cannell, M., & van Breemen, C. (1992). Calcium entry-dependent oscillations of cytoplasmic calcium concentration in cultured endothelial cell monolayers. *Proc Natl Acad Sci U S A, 89*(5), 1690-1694.

Launay, P., Fleig, A., Perraud, A. L., Scharenberg, A. M., Penner, R., & Kinet, J. P. (2002). TRPM4 is a Ca2+-activated nonselective cation channel mediating cell membrane depolarization. *Cell, 109*(3), 397-407. doi:10.1016/s0092-8674(02)00719-5

Lecrux, C., & Hamel, E. (2016). Neuronal networks and mediators of cortical neurovascular coupling responses in normal and altered brain states. *Philos Trans R Soc Lond B Biol Sci, 371*(1705). doi:10.1098/rstb.2015.0350

Lecrux, C., Toussay, X., Kocharyan, A., Fernandes, P., Neupane, S., Levesque, M., . . . Hamel, E. (2011). Pyramidal neurons are "neurogenic hubs" in the neurovascular coupling response to whisker stimulation. *J Neurosci, 31*(27), 9836-9847. doi:10.1523/JNEUROSCI.4943-10.2011

Lee, K. P., Choi, S., Hong, J. H., Ahuja, M., Graham, S., Ma, R., . . . Yuan, J. P. (2014). Molecular determinants mediating gating of Transient Receptor Potential Canonical (TRPC) channels by stromal interaction molecule 1 (STIM1). *J Biol Chem, 289*(10), 6372-6382. doi:10.1074/jbc.M113.546556

Leo, L. M., Familusi, B., Hoang, M., Smith, R., Lindenau, K., Sporici, K. T., . . . Brailoiu, G. C. (2019). GPR55-mediated effects on brain microvascular endothelial cells and the blood-brain barrier. *Neuroscience, 414*, 88-98. doi:10.1016/j.neuroscience.2019.06.039

Li, S., Kumar, T. P., Joshee, S., Kirschstein, T., Subburaju, S., Khalili, J. S., . . . Vasudevan, A. (2018). Endothelial cell-derived GABA signaling modulates neuronal migration and postnatal behavior. *Cell Res, 28*(2), 221-248. doi:10.1038/cr.2017.135

Li, Z., Matsuoka, S., Hryshko, L. V., Nicoll, D. A., Bersohn, M. M., Burke, E. P., . . . Philipson, K. D. (1994). Cloning of the NCX2 isoform of the plasma membrane Na(+)-Ca2+ exchanger. *J Biol Chem, 269*(26), 17434-17439.

Lia, A., Di Spiezio, A., Speggiorin, M., & Zonta, M. (2023). Two decades of astrocytes in neurovascular coupling. *Front Netw Physiol, 3*, 1162757. doi:10.3389/fnetp.2023.1162757

Lillo, M. A., Gaete, P. S., Puebla, M., Ardiles, N. M., Poblete, I., Becerra, A., . . . Figueroa, X. F. (2017). Critical contribution of Na(+)-Ca(2+) exchanger to the Ca(2+)-mediated vasodilation activated in endothelial cells of resistance arteries. *Faseb Journal*. doi:10.1096/fj.201700365RR

Lim, X. R., & Harraz, O. F. (2024). Mechanosensing by Vascular Endothelium. *Annu Rev Physiol, 86*, 71-97. doi:10.1146/annurev-physiol-042022-030946

Lisec, B., Bozic, T., Santek, I., Markelc, B., Vrecl, M., Frangez, R., & Cemazar, M. (2024). Characterization of two distinct immortalized endothelial cell lines, EA.hy926 and HMEC-1, for in vitro studies: exploring the impact of calcium electroporation, Ca(2+) signaling and transcriptomic profiles. *Cell Communication and Signaling, 22*(1), 118. doi:10.1186/s12964-024-01503-2

Liu, D., & Liman, E. R. (2003). Intracellular Ca2+ and the phospholipid PIP2 regulate the taste transduction ion channel TRPM5. *Proc Natl Acad Sci U S A, 100*(25), 15160-15165. doi:10.1073/pnas.2334159100

Lloyd-Evans, E., & Platt, F. M. (2011). Lysosomal Ca(2+) homeostasis: role in pathogenesis of lysosomal storage diseases. *Cell Calcium, 50*(2), 200-205. doi:10.1016/j.ceca.2011.03.010

Lodola, F., Laforenza, U., Cattaneo, F., Ruffinatti, F. A., Poletto, V., Massa, M., . . . Moccia, A. (2017). VEGF-induced intracellular Ca^{2+} oscillations are down-regulated and do not stimulate angiogenesis in breast cancer-derived endothelial colony forming cells. *Oncotarget, 8*, 95223-95246. doi:https://doi.org/10.18632/oncotarget.20255

Lodola, F., Martino, N., Tullii, G., Lanzani, G., & Antognazza, M. R. (2017). Conjugated polymers mediate effective activation of the Mammalian Ion Channel Transient Receptor Potential Vanilloid 1. *Sci Rep, 7*(1), 8477. doi:10.1038/s41598-017-08541-6

Longden, T. A., Dabertrand, F., Koide, M., Gonzales, A. L., Tykocki, N. R., Brayden, J. E., . . . Nelson, M. T. (2017). Capillary K(+)-sensing initiates retrograde hyperpolarization to increase local cerebral blood flow. *Nat Neurosci, 20*(5), 717-726. doi:10.1038/nn.4533

Longden, T. A., Hill-Eubanks, D. C., & Nelson, M. T. (2016). Ion channel networks in the control of cerebral blood flow. *J Cereb Blood Flow Metab, 36*(3), 492-512. doi:10.1177/0271678X15616138

Longden, T. A., Mughal, A., Hennig, G. W., Harraz, O. F., Shui, B., Lee, F. K., . . . Nelson, M. T. (2021). Local IP(3) receptor-mediated Ca(2+) signals compound to direct blood flow in brain capillaries. *Sci Adv, 7*(30). doi:10.1126/sciadv.abh0101

Longden, T. A., & Nelson, M. T. (2015). Vascular inward rectifier K+ channels as external K+ sensors in the control of cerebral blood flow. *Microcirculation, 22*(3), 183-196. doi:10.1111/micc.12190

Lu, L., Hogan-Cann, A. D., Globa, A. K., Lu, P., Nagy, J. I., Bamji, S. X., & Anderson, C. M. (2017). Astrocytes drive cortical vasodilatory signaling by activating endothelial NMDA receptors. *J Cereb Blood Flow Metab*, 271678X17734100. doi:10.1177/0271678X17734100

Lu, L., Hogan-Cann, A. D., Globa, A. K., Lu, P., Nagy, J. I., Bamji, S. X., & Anderson, C. M. (2019). Astrocytes drive cortical vasodilatory signaling by activating endothelial NMDA receptors. *J Cereb Blood Flow Metab, 39*(3), 481-496. doi:10.1177/0271678X17734100

Macgregor, A., Yamasaki, M., Rakovic, S., Sanders, L., Parkesh, R., Churchill, G. C., . . . Terrar, D. A. (2007). NAADP controls cross-talk between distinct Ca2+ stores in the heart. *J Biol Chem, 282*(20), 15302-15311. doi:10.1074/jbc.M611167200

Maione, A. S., Faris, P., Iengo, L., Catto, V., Bisonni, L., Lodola, F., . . . Moccia, F. (2022). Ca(2+) dysregulation in cardiac stromal cells sustains fibro-adipose remodeling in Arrhythmogenic Cardiomyopathy and can be modulated by flecainide. *J Transl Med, 20*(1), 522. doi:10.1186/s12967-022-03742-8

Mapelli, L., Gagliano, G., Soda, T., Laforenza, U., Moccia, F., & D'Angelo, E. U. (2017). Granular Layer Neurons Control Cerebellar Neurovascular Coupling Through an NMDA Receptor/NO-Dependent System. *J Neurosci, 37*(5), 1340-1351. doi:10.1523/JNEUROSCI.2025-16.2016

Mariotti, L., Losi, G., Sessolo, M., Marcon, I., & Carmignoto, G. (2016). The inhibitory neurotransmitter GABA evokes long-lasting Ca(2+) oscillations in cortical astrocytes. *Glia, 64*(3), 363-373. doi:10.1002/glia.22933

Medina, D. L., Di Paola, S., Peluso, I., Armani, A., De Stefani, D., Venditti, R., . . . Ballabio, A. (2015). Lysosomal calcium signalling regulates autophagy through calcineurin and TFEB. *Nat Cell Biol, 17*(3), 288-299. doi:10.1038/ncb3114

Mikoshiba, K. (2007). IP3 receptor/Ca2+ channel: from discovery to new signaling concepts. *Journal of Neurochemistry, 102*(5), 1426-1446. doi:10.1111/j.1471-4159.2007.04825.x

Mishra, A., Reynolds, J. P., Chen, Y., Gourine, A. V., Rusakov, D. A., & Attwell, D. (2016). Astrocytes mediate neurovascular signaling to capillary pericytes but not to arterioles. *Nat Neurosci, 19*(12), 1619-1627. doi:10.1038/nn.4428

Missiaen, L., Taylor, C. W., & Berridge, M. J. (1992). Luminal Ca2+ promoting spontaneous Ca2+ release from inositol trisphosphate-sensitive stores in rat hepatocytes. *J Physiol, 455*, 623-640. doi:10.1113/jphysiol.1992.sp019319

Moccia, F., Berra-Romani, R., Baruffi, S., Spaggiari, S., Adams, D. J., Taglietti, V., & Tanzi, F. (2002). Basal nonselective cation permeability in rat cardiac microvascular endothelial cells. *Microvasc Res, 64*(2), 187-197.

Moccia, F., Bertoni, G., Pla, A. F., Dragoni, S., Pupo, E., Merlino, A., . . . Tanzi, F. (2011). Hydrogen sulfide regulates intracellular Ca2+ concentration in endothelial cells from excised rat aorta. *Curr Pharm Biotechnol, 12*(9), 1416-1426.

Moccia, F., Brunetti, V., Perna, A., Guerra, G., Soda, T., & Berra-Romani, R. (2023). The Molecular Heterogeneity of Store-Operated Ca(2+) Entry in Vascular Endothelial Cells: The Different

roles of Orai1 and TRPC1/TRPC4 Channels in the Transition from Ca(2+)-Selective to Non-Selective Cation Currents. *Int J Mol Sci, 24*(4). doi:10.3390/ijms24043259

Moccia, F., Brunetti, V., Soda, T., Berra-Romani, R., & Scarpellino, G. (2023). Cracking the Endothelial Calcium (Ca(2+)) Code: A Matter of Timing and Spacing. *Int J Mol Sci, 24*(23). doi:10.3390/ijms242316765

Moccia, F., Brunetti, V., Soda, T., Faris, P., Scarpellino, G., & Berra-Romani, R. (2023). Store-Operated Ca(2+) Entry as a Putative Target of Flecainide for the Treatment of Arrhythmogenic Cardiomyopathy. *J Clin Med, 12*(16). doi:10.3390/jcm12165295

Moccia, F., Frost, C., Berra-Romani, R., Tanzi, F., & Adams, D. J. (2004). Expression and function of neuronal nicotinic ACh receptors in rat microvascular endothelial cells. *Am J Physiol Heart Circ Physiol, 286*(2), H486-491. doi:10.1152/ajpheart.00620.2003

Moccia, F., Negri, S., Faris, P., & Angelone, T. (2022). Targeting endothelial ion signalling to rescue cerebral blood flow in cerebral disorders. *Vascul Pharmacol, 145*, 106997. doi:10.1016/j.vph.2022.106997

Moccia, F., Negri, S., Faris, P., Perna, A., De Luca, A., Soda, T., . . . Guerra, G. (2021). Targeting Endolysosomal Two-Pore Channels to Treat Cardiovascular Disorders in the Novel COronaVIrus Disease 2019. *Front Physiol, 12*, 629119. doi:10.3389/fphys.2021.629119

Moccia, F., Negri, S., Shekha, M., Faris, P., & Guerra, G. (2019). Endothelial Ca(2+) Signaling, Angiogenesis and Vasculogenesis: just What It Takes to Make a Blood Vessel. *Int J Mol Sci, 20*(16). doi:10.3390/ijms20163962

Moccia, F., Zuccolo, E., Di Nezza, F., Pellavio, G., Faris, P. S., Negri, S., . . . Guerra, G. (2021). Nicotinic acid adenine dinucleotide phosphate activates two-pore channel TPC1 to mediate lysosomal Ca(2+) release in endothelial colony-forming cells. *Journal of Cellular Physiology, 236*(1), 688-705. doi:10.1002/jcp.29896

Montell, C., & Rubin, G. M. (1989). Molecular characterization of the Drosophila trp locus: a putative integral membrane protein required for phototransduction. *Neuron, 2*(4), 1313-1323. doi:10.1016/0896-6273(89)90069-x

Moreno-Salgado, A., Coyotl-Santiago, N., Moreno-Vazquez, R., Lopez-Teyssier, M., Garcia-Carrasco, M., Moccia, F., & Berra-Romani, R. (2023). Alterations of the Ca(2+) clearing mechanisms by type 2 diabetes in aortic smooth muscle cells of Zucker diabetic fatty rat. *Front Physiol, 14*, 1200115. doi:10.3389/fphys.2023.1200115

Morgan, A. J. (2016). Ca2+ dialogue between acidic vesicles and ER. *Biochem Soc Trans, 44*(2), 546-553. doi:10.1042/BST20150290

Morgan, A. J., & Galione, A. (2021). Lysosomal agents inhibit store-operated Ca(2+) entry. *Journal of Cell Science, 134*(2). doi:10.1242/jcs.248658

Morgan, A. J., & Jacob, R. (1996). Ca2+ influx does more than provide releasable Ca2+ to maintain repetitive spiking in human umbilical vein endothelial cells. *Biochemical Journal, 320 (Pt 2)*, 505-517.

Morgan, A. J., Platt, F. M., Lloyd-Evans, E., & Galione, A. (2011). Molecular mechanisms of endolysosomal Ca2+ signalling in health and disease. *Biochemical Journal, 439*(3), 349-374. doi:10.1042/BJ20110949

Mughal, A., Hennig, G. W., Heppner, T., Tsoukias, N. M., Hill-Eubanks, D., & Nelson, M. T. (2024). Electrocalcium coupling in brain capillaries: Rapidly traveling electrical signals ignite local calcium signals. *Proc Natl Acad Sci U S A, 121*(51), e2415047121. doi:10.1073/pnas.2415047121

Mulligan, S. J., & MacVicar, B. A. (2004). Calcium transients in astrocyte endfeet cause cerebrovascular constrictions. *Nature, 431*(7005), 195-199. doi:10.1038/nature02827

Murata, T., Lin, M. I., Stan, R. V., Bauer, P. M., Yu, J., & Sessa, W. C. (2007). Genetic evidence supporting caveolae microdomain regulation of calcium entry in endothelial cells. *J Biol Chem, 282*(22), 16631-16643. doi:10.1074/jbc.M607948200

Negri, S., Faris, P., Berra-Romani, R., Guerra, G., & Moccia, F. (2019). Endothelial Transient Receptor Potential Channels and Vascular Remodeling: Extracellular Ca(2 +) Entry for Angiogenesis, Arteriogenesis and Vasculogenesis. *Front Physiol, 10*, 1618. doi:10.3389/fphys.2019.01618

Negri, S., Faris, P., Maniezzi, C., Pellavio, G., Spaiardi, P., Botta, L., . . . Moccia, D. F. (2021). NMDA receptors elicit flux-independent intracellular Ca(2+) signals via metabotropic glutamate receptors and flux-dependent nitric oxide release in human brain microvascular endothelial cells. *Cell Calcium, 99*, 102454. doi:10.1016/j.ceca.2021.102454

Negri, S., Faris, P., & Moccia, F. (2021a). Endolysosomal Ca(2+) signaling in cardiovascular health and disease. *Int Rev Cell Mol Biol, 363*, 203-269. doi:10.1016/bs.ircmb.2021.03.001

Negri, S., Faris, P., & Moccia, F. (2021b). Reactive Oxygen Species and Endothelial Ca(2+) Signaling: Brothers in Arms or Partners in Crime? *Int J Mol Sci, 22*(18). doi:10.3390/ijms22189821

Negri, S., Faris, P., Pellavio, G., Botta, L., Orgiu, M., Forcaia, G., . . . Moccia, F. (2019). Group 1 metabotropic glutamate receptors trigger glutamate-induced intracellular Ca(2+) signals and nitric oxide release in human brain microvascular endothelial cells. *Cell Mol Life Sci*. doi:10.1007/s00018-019-03284-1

Negri, S., Faris, P., Pellavio, G., Botta, L., Orgiu, M., Forcaia, G., . . . Moccia, F. (2020). Group 1 metabotropic glutamate receptors trigger glutamate-induced intracellular Ca(2+) signals and nitric oxide release in human brain microvascular endothelial cells. *Cell Mol Life Sci, 77*(11), 2235-2253. doi:10.1007/s00018-019-03284-1

Negri, S., Faris, P., Soda, T., & Moccia, F. (2021). Endothelial signaling at the core of neurovascular coupling: The emerging role of endothelial inward-rectifier K(+) (Kir2.1) channels and N-methyl-d-aspartate receptors in the regulation of cerebral blood flow. *Int J Biochem Cell Biol, 135*, 105983. doi:10.1016/j.biocel.2021.105983

Negri, S., Scolari, F., Vismara, M., Brunetti, V., Faris, P., Terribile, G., . . . Moccia, F. (2022). GABA(A) and GABA(B) Receptors Mediate GABA-Induced Intracellular Ca(2+) Signals in Human Brain Microvascular Endothelial Cells. *Cells, 11*(23). doi:10.3390/cells11233860

Nicoll, D. A., Ottolia, M., Goldhaber, J. I., & Philipson, K. D. (2013). 20 years from NCX purification and cloning: milestones. *Adv Exp Med Biol, 961*, 17-23. doi:10.1007/978-1-4614-4756-6_2

Nicoll, D. A., Quednau, B. D., Qui, Z., Xia, Y. R., Lusis, A. J., & Philipson, K. D. (1996). Cloning of a third mammalian Na+-Ca2+ exchanger, NCX3. *J Biol Chem, 271*(40), 24914-24921. doi:10.1074/jbc.271.40.24914

Nilius, B., & Droogmans, G. (2001). Ion channels and their functional role in vascular endothelium. *Physiol Rev, 81*(4), 1415-1459. doi:10.1152/physrev.2001.81.4.1415

Nilius, B., Sehrer, J., Viana, F., De Greef, C., Raeymaekers, L., Eggermont, J., & Droogmans, G. (1994). Volume-activated Cl- currents in different mammalian non-excitable cell types. *Pflugers Arch, 428*(3-4), 364-371. doi:10.1007/BF00724520

Nilius, B., & Voets, T. (2007). Neurophysiology: channelling cold reception. *Nature, 448*(7150), 147-148. doi:10.1038/448147a

Niwa, K., Araki, E., Morham, S. G., Ross, M. E., & Iadecola, C. (2000). Cyclooxygenase-2 contributes to functional hyperemia in whisker-barrel cortex. *J Neurosci, 20*(2), 763-770.

Obergrussberger, A., Friis, S., Bruggemann, A., & Fertig, N. (2021). Automated patch clamp in drug discovery: major breakthroughs and innovation in the last decade. *Expert Opin Drug Discov, 16*(1), 1-5. doi:10.1080/17460441.2020.1791079

Olschewski, A., Olschewski, H., Brau, M. E., Hempelmann, G., Vogel, W., & Safronov, B. V. (2001). Basic electrical properties of in situ endothelial cells of small pulmonary arteries during postnatal development. *Am J Respir Cell Mol Biol, 25*(3), 285-290. doi:10.1165/ajrcmb.25.3.4373

Pafumi, I., Favia, A., Gambara, G., Papacci, F., Ziparo, E., Palombi, F., & Filippini, A. (2015). Regulation of Angiogenic Functions by Angiopoietins through Calcium-Dependent Signaling Pathways. *Biomed Res Int, 2015*, 965271. doi:10.1155/2015/965271

Pafumi, I., Festa, M., Papacci, F., Lagostena, L., Giunta, C., Gutla, V., . . . Carpaneto, A. (2017). Naringenin Impairs Two-Pore Channel 2 Activity And Inhibits VEGF-Induced Angiogenesis. *Sci Rep, 7*(1), 5121. doi:10.1038/s41598-017-04974-1

Panula, P. (2021). Histamine receptors, agonists, and antagonists in health and disease. *Handb Clin Neurol, 180*, 377-387. doi:10.1016/B978-0-12-820107-7.00023-9

Park, D. K., Stein, I. S., & Zito, K. (2022). Ion flux-independent NMDA receptor signaling. *Neuropharmacology, 210*, 109019. doi:10.1016/j.neuropharm.2022.109019

Paternain, A. V., Cohen, A., Stern-Bach, Y., & Lerma, J. (2003). A role for extracellular Na+ in the channel gating of native and recombinant kainate receptors. *J Neurosci, 23*(25), 8641-8648. doi:10.1523/JNEUROSCI.23-25-08641.2003

Penny, C. J., Kilpatrick, B. S., Han, J. M., Sneyd, J., & Patel, S. (2014). A computational model of lysosome-ER Ca2+ microdomains. *Journal of Cell Science, 127*(Pt 13), 2934-2943. doi:10.1242/jcs.149047

Petzold, G. C., Haack, S., von Bohlen Und Halbach, O., Priller, J., Lehmann, T. N., Heinemann, U., . . . Dreier, J. P. (2008). Nitric oxide modulates spreading depolarization threshold in the human and rodent cortex. *Stroke, 39*(4), 1292-1299. doi:10.1161/STROKEAHA.107.500710

Poburko, D., Fameli, N., Kuo, K. H., & van Breemen, C. (2008). Ca2+ signaling in smooth muscle: TRPC6, NCX and LNats in nanodomains. *Channels (Austin), 2*(1), 10-12.

Qi, D., Lin, H., Hu, B., & Wei, Y. (2023). A review on in vitro model of the blood-brain barrier (BBB) based on hCMEC/D3 cells. *J Control Release, 358*, 78-97. doi:10.1016/j.jconrel.2023.04.020

Roggendorf, W., & Cervos-Navarro, J. (1977). Ultrastructure of arterioles in the cat brain. *Cell Tissue Res, 178*(4), 495-515. doi:10.1007/BF00219571

Rose, C. R., Ziemens, D., & Verkhratsky, A. (2020). On the special role of NCX in astrocytes: Translating Na(+)-transients into intracellular Ca(2+) signals. *Cell Calcium, 86*, 102154. doi:10.1016/j.ceca.2019.102154

Scarpellino, G., Brunetti, V., Berra-Romani, R., De Sarro, G., Guerra, G., Soda, T., & Moccia, F. (2024). The Unexpected Role of the Endothelial Nitric Oxide Synthase at the Neurovascular Unit: Beyond the Regulation of Cerebral Blood Flow. *Int J Mol Sci, 25*(16). doi:10.3390/ijms25169071

Scarpellino, G., Genova, T., Avanzato, D., Bernardini, M., Bianco, S., Petrillo, S., . . . Munaron, L. (2019). Purinergic Calcium Signals in Tumor-Derived Endothelium. *Cancers (Basel), 11*(6). doi:10.3390/cancers11060766

Scarpellino, G., Genova, T., Quarta, E., Distasi, C., Dionisi, M., Fiorio Pla, A., & Munaron, L. (2022). P2X Purinergic Receptors Are Multisensory Detectors for Micro-Environmental Stimuli That Control Migration of Tumoral Endothelium. *Cancers (Basel), 14*(11). doi:10.3390/cancers14112743

Schaeffer, S., & Iadecola, C. (2021). Revisiting the neurovascular unit. *Nat Neurosci, 24*(9), 1198-1209. doi:10.1038/s41593-021-00904-7

Schleifer, H., Doleschal, B., Lichtenegger, M., Oppenrieder, R., Derler, I., Frischauf, I., . . . Groschner, K. (2012). Novel pyrazole compounds for pharmacological discrimination between receptor-operated and store-operated Ca(2+) entry pathways. *Br J Pharmacol, 167*(8), 1712-1722. doi:10.1111/j.1476-5381.2012.02126.x

Schneider, J. C., El Kebir, D., Chereau, C., Mercier, J. C., Dall'Ava-Santucci, J., & Dinh-Xuan, A. T. (2002). Involvement of Na(+)/Ca(2+) exchanger in endothelial NO production and endothelium-dependent relaxation. *Am J Physiol Heart Circ Physiol, 283*(2), H837-844. doi:10.1152/ajpheart.00789.2001

Schnell, D., Burleigh, K., Trick, J., & Seifert, R. (2010). No evidence for functional selectivity of proxyfan at the human histamine H3 receptor coupled to defined Gi/Go protein heterotrimers. *J Pharmacol Exp Ther, 332*(3), 996-1005. doi:10.1124/jpet.109.162339

Schnell, D., & Seifert, R. (2010). Modulation of histamine H(3) receptor function by monovalent ions. *Neuroscience Letters, 472*(2), 114-118. doi:10.1016/j.neulet.2010.01.065

Scorza, S. I., Milano, S., Saponara, I., Certini, M., De Zio, R., Mola, M. G., . . . Gerbino, A. (2023). TRPML1-Induced Lysosomal Ca(2+) Signals Activate AQP2 Translocation and Water Flux in Renal Collecting Duct Cells. *Int J Mol Sci, 24*(2). doi:10.3390/ijms24021647

Seifert, R., & Wenzel-Seifert, K. (2001). Unmasking different constitutive activity of four chemoattractant receptors using Na+ as universal stabilizer of the inactive (R) state. *Recept Channels, 7*(5), 357-369.

Selley, D. E., Cao, C. C., Liu, Q., & Childers, S. R. (2000). Effects of sodium on agonist efficacy for G-protein activation in mu-opioid receptor-transfected CHO cells and rat thalamus. *Br J Pharmacol, 130*(5), 987-996. doi:10.1038/sj.bjp.0703382

Shastry, S., Moning, L., Tyagi, N., Steed, M., & Tyagi, S. C. (2005). GABA receptors and nitric oxide ameliorate constrictive collagen remodeling in hyperhomocysteinemia. *Journal of Cellular Physiology, 205*(3), 422-427. doi:10.1002/jcp.20416

Sheng, J. Z., & Braun, A. P. (2007). Small- and intermediate-conductance Ca2+-activated K+ channels directly control agonist-evoked nitric oxide synthesis in human vascular endothelial cells. *Am J Physiol Cell Physiol, 293*(1), C458-467. doi:10.1152/ajpcell.00036.2007

Sheng, J. Z., Wang, D., & Braun, A. P. (2005). DAF-FM (4-amino-5-methylamino-2',7'-difluorofluorescein) diacetate detects impairment of agonist-stimulated nitric oxide synthesis by elevated glucose in human vascular endothelial cells: reversal by vitamin C and L-sepiapterin. *J Pharmacol Exp Ther, 315*(2), 931-940. doi:10.1124/jpet.105.087932

Smani, T., Gomez, L. J., Regodon, S., Woodard, G. E., Siegfried, G., Khatib, A. M., & Rosado, J. A. (2018). TRP Channels in Angiogenesis and Other Endothelial Functions. *Front Physiol, 9*, 1731. doi:10.3389/fphys.2018.01731

Soda, T., Brunetti, V., Berra-Romani, R., & Moccia, F. (2023). The Emerging Role of N-Methyl-D-Aspartate (NMDA) Receptors in the Cardiovascular System: Physiological Implications, Pathological Consequences, and Therapeutic Perspectives. *Int J Mol Sci, 24*(4). doi:10.3390/ijms24043914

Soda, T., Brunetti, V., De Sarro, G., Biella, G., Moccia, F., Berra-Romani, R., & Scarpellino, G. (2025). Transient Receptor Potential Ankyrin 1 (TRPA1) Mediates Hydrogen Sulfide-induced Ca(2+) Entry and Nitric Oxide Production in Human Cerebrovascular Endothelium. *Curr Neuropharmacol, 23*(9), 1119-1133. doi:10.2174/011570159X349872250124124612

Soda, T., Negri, S., Scarpellino, G., Berra-Romani, R., De Sarro, G., Moccia, F., & Brunetti, V. (2024). An automated planar patch-clamp approach to measure the membrane potential and resting membrane currents in a human cerebrovascular endothelial cell line. *J Neurosci Methods, 410*, 110248. doi:10.1016/j.jneumeth.2024.110248

Somogyi, A., Kirkham, E. D., Lloyd-Evans, E., Winston, J., Allen, N. D., Mackrill, J. J., . . . O'Neill, C. (2023). The synthetic TRPML1 agonist ML-SA1 rescues Alzheimer-related alterations of the endosomal-autophagic-lysosomal system. *Journal of Cell Science, 136*(6). doi:10.1242/jcs.259875

Sonkusare, S. K., Bonev, A. D., Ledoux, J., Liedtke, W., Kotlikoff, M. I., Heppner, T. J., . . . Nelson, M. T. (2012). Elementary Ca2+ signals through endothelial TRPV4 channels regulate vascular function. *Science, 336*(6081), 597-601. doi:10.1126/science.1216283

Suh, S. H., Vennekens, R., Manolopoulos, V. G., Freichel, M., Schweig, U., Prenen, J., . . . Nilius, B. (1999). Characterisation of explanted endothelial cells from mouse aorta: electrophysiology and Ca2+ signalling. *Pflugers Arch, 438*(5), 612-620. doi:10.1007/s004249900085

Sullivan, M. N., Gonzales, A. L., Pires, P. W., Bruhl, A., Leo, M. D., Li, W., . . . Earley, S. (2015). Localized TRPA1 channel Ca2+ signals stimulated by reactive oxygen species promote cerebral artery dilation. *Sci Signal, 8*(358), ra2. doi:10.1126/scisignal.2005659

Tedeschi, V., Sisalli, M. J., Petrozziello, T., Canzoniero, L. M. T., & Secondo, A. (2021). Lysosomal calcium is modulated by STIM1/TRPML1 interaction which participates to neuronal survival during ischemic preconditioning. *Faseb Journal, 35*(2), e21277. doi:10.1096/fj.202001886R

Thakore, P., Ali, S., & Earley, S. (2020). Regulation of vascular tone by transient receptor potential ankyrin 1 channels. *Curr Top Membr, 85*, 119-150. doi:10.1016/bs.ctm.2020.01.009

Thakore, P., & Earley, S. (2019). Transient Receptor Potential Channels and Endothelial Cell Calcium Signaling. *Compr Physiol, 9*(3), 1249-1277. doi:10.1002/cphy.c180034

Thakore, P., Pritchard, H. A. T., Griffin, C. S., Yamasaki, E., Drumm, B. T., Lane, C., . . . Earley, S. (2020). TRPML1 channels initiate Ca(2+) sparks in vascular smooth muscle cells. *Sci Signal, 13*(637). doi:10.1126/scisignal.aba1015

Tolstykh, G. P., Cantu, J. C., Tarango, M., & Ibey, B. L. (2019). Receptor- and store-operated mechanisms of calcium entry during the nanosecond electric pulse-induced cellular response. *Biochim Biophys Acta Biomembr, 1861*(3), 685-696. doi:10.1016/j.bbamem.2018.12.007

Tran, C. H. T. (2022). Toolbox for studying neurovascular coupling in vivo, with a focus on vascular activity and calcium dynamics in astrocytes. *Neurophotonics, 9*(2), 021909. doi:10.1117/1.NPh.9.2.021909

Venkatachalam, K., & Montell, C. (2007). TRP channels. *Annu Rev Biochem, 76*, 387-417. doi:10.1146/annurev.biochem.75.103004.142819

Verkhratsky, A., Trebak, M., Perocchi, F., Khananshvili, D., & Sekler, I. (2018). Crosslink between calcium and sodium signalling. *Exp Physiol, 103*(2), 157-169. doi:10.1113/EP086534

Voets, T., Droogmans, G., & Nilius, B. (1996). Membrane currents and the resting membrane potential in cultured bovine pulmonary artery endothelial cells. *J Physiol, 497 (Pt 1)*, 95-107. doi:10.1113/jphysiol.1996.sp021752

Voets, T., Droogmans, G., Wissenbach, U., Janssens, A., Flockerzi, V., & Nilius, B. (2004). The principle of temperature-dependent gating in cold- and heat-sensitive TRP channels. *Nature, 430*(7001), 748-754. doi:10.1038/nature02732

von Beckerath, N., Dittrich, M., Klieber, H. G., & Daut, J. (1996). Inwardly rectifying K+ channels in freshly dissociated coronary endothelial cells from guinea-pig heart. *J Physiol, 491 (Pt 2)*(Pt 2), 357-365. doi:10.1113/jphysiol.1996.sp021221

Walchli, T., Ghobrial, M., Schwab, M., Takada, S., Zhong, H., Suntharalingham, S., . . . Radovanovic, I. (2024). Single-cell atlas of the human brain vasculature across development, adulthood and disease. *Nature, 632*(8025), 603-613. doi:10.1038/s41586-024-07493-y

Wang, M., Preckel, B., Zuurbier, C. J., & Weber, N. C. (2025). Effects of SGLT2 inhibitors on ion channels in heart failure: focus on the endothelium. *Basic Res Cardiol, 120*(4), 779-798. doi:10.1007/s00395-025-01115-y

Wang, W., Gao, Q., Yang, M., Zhang, X., Yu, L., Lawas, M., . . . Xu, H. (2015). Up-regulation of lysosomal TRPML1 channels is essential for lysosomal adaptation to nutrient starvation. *Proc Natl Acad Sci U S A, 112*(11), E1373-1381. doi:10.1073/pnas.1419669112

Weksler, B., Romero, I. A., & Couraud, P. O. (2013). The hCMEC/D3 cell line as a model of the human blood brain barrier. *Fluids Barriers CNS, 10*(1), 16. doi:10.1186/2045-8118-10-16

Wyllie, D. J., Livesey, M. R., & Hardingham, G. E. (2013). Influence of GluN2 subunit identity on NMDA receptor function. *Neuropharmacology, 74*, 4-17. doi:10.1016/j.neuropharm.2013.01.016

Yang, J., Zhao, Z., Gu, M., Feng, X., & Xu, H. (2019). Release and uptake mechanisms of vesicular Ca(2+) stores. *Protein Cell, 10*(1), 8-19. doi:10.1007/s13238-018-0523-x

Yuan, Y., Arige, V., Saito, R., Mu, Q., Brailoiu, G. C., Pereira, G. J. S., . . . Patel, S. (2024). Two-pore channel-2 and inositol trisphosphate receptors coordinate Ca(2+) signals between lysosomes and the endoplasmic reticulum. *Cell Rep, 43*(1), 113628. doi:10.1016/j.celrep.2023.113628

Zarzycka, B., Zaidi, S. A., Roth, B. L., & Katritch, V. (2019). Harnessing Ion-Binding Sites for GPCR Pharmacology. *Pharmacol Rev, 71*(4), 571-595. doi:10.1124/pr.119.017863

Zhang, X., Cheng, X., Yu, L., Yang, J., Calvo, R., Patnaik, S., . . . Xu, H. (2016). MCOLN1 is a ROS sensor in lysosomes that regulates autophagy. *Nat Commun, 7*, 12109. doi:10.1038/ncomms12109

Zhang, X., Xin, P., Yoast, R. E., Emrich, S. M., Johnson, M. T., Pathak, T., . . . Trebak, M. (2020). Distinct pharmacological profiles of ORAI1, ORAI2, and ORAI3 channels. *Cell Calcium, 91*, 102281. doi:10.1016/j.ceca.2020.102281

Zimmermann, K., Lennerz, J. K., Hein, A., Link, A. S., Kaczmarek, J. S., Delling, M., . . . Clapham, D. E. (2011). Transient receptor potential cation channel, subfamily C, member 5 (TRPC5) is a cold-transducer in the peripheral nervous system. *Proc Natl Acad Sci U S A, 108*(44), 18114-18119. doi:10.1073/pnas.1115387108

Zlokovic, B. V. (2011). Neurovascular pathways to neurodegeneration in Alzheimer's disease and other disorders. *Nat Rev Neurosci, 12*(12), 723-738. doi:10.1038/nrn3114

Zuccolo, E., Bottino, C., Diofano, F., Poletto, V., Codazzi, A. C., Mannarino, S., . . . Moccia, F. (2016). Constitutive Store-Operated Ca(2+) Entry Leads to Enhanced Nitric Oxide Production and Proliferation in Infantile Hemangioma-Derived Endothelial Colony-Forming Cells. *Stem Cells Dev, 25*(4), 301-319. doi:10.1089/scd.2015.0240

Zuccolo, E., Kheder, D. A., Lim, D., Perna, A., Nezza, F. D., Botta, L., . . . Moccia, F. (2019). Glutamate triggers intracellular Ca(2+) oscillations and nitric oxide release by inducing NAADP- and InsP3 -dependent Ca(2+) release in mouse brain endothelial cells. *Journal of Cellular Physiology, 234*(4), 3538-3554. doi:10.1002/jcp.26953

Zuccolo, E., Laforenza, U., Negri, S., Botta, L., Berra-Romani, R., Faris, P., . . . Moccia, F. (2019). Muscarinic M5 receptors trigger acetylcholine-induced Ca(2+) signals and nitric oxide release in human brain microvascular endothelial cells. *Journal of Cellular Physiology, 234*(4), 4540-4562. doi:10.1002/jcp.27234

Zuccolo, E., Lim, D., Kheder, D. A., Perna, A., Catarsi, P., Botta, L., . . . Moccia, F. (2017). Acetylcholine induces intracellular Ca2+ oscillations and nitric oxide release in mouse brain endothelial cells. *Cell Calcium, 66*, 33-47. doi:10.1016/j.ceca.2017.06.003

Zuccolo, E., Negri, S., Pellavio, G., Scarpellino, G., Laforenza, U., Sancini, G., . . . Moccia, F. (2018). Acetylcholine induces Ca2+ signals and nitric oxide release from human brain microvascular endothelial cells. *Vascular Pharmacology, 103-105*, 65. doi:10.1016/j.vph.2017.12.049

Zurborg, S., Yurgionas, B., Jira, J. A., Caspani, O., & Heppenstall, P. A. (2007). Direct activation of the ion channel TRPA1 by Ca2+. *Nat Neurosci, 10*(3), 277-279. doi:10.1038/nn1843